Alma Mater Studiorum – Università di Bologna

DOTTORATO DI RICERCA IN

BIOLOGIA CELLULARE E MOLECOLARE

Ciclo 34

Settore Concorsuale: 05/E2 - BIOLOGIA MOLECOLARE

Settore Scientifico Disciplinare: BIO/11 - BIOLOGIA MOLECOLARE

Unbalanced R-loops and micronuclei induced by DNA topoisomerase I poisons in cancer cells

Presentata da: Renée Concetta Duardo

Coordinatore Dottorato   **Supervisore**

Vincenzo Scarlato   Giovanni Capranico

Esame finale anno 2022

INDEX

ABSTRACT

Cancer is at the moment the principal cause of death in western countries. Among the several approaches commonly used to deal with cancer, immunotherapy has progressed considerably in recent years and has become an important treatment for human cancers either alone or in combination with other therapeutic interventions. At the same time, the success of classical antitumor chemotherapy has recently been shown to be due to the stimulation of innate and adaptive immunity against tumors. However, the relevant mechanisms have not been fully clarified yet. Topoisomerase I (Top1) poisons are among the most clinically-effective drugs for colon, ovary and lung cancers. Top1 is a key enzyme that resolves topological stress accumulated during transcription, replication and chromatin remodeling by allowing strand rotation through a transient single-strand break introduced by the enzyme into the DNA duplex substrate. Anticancer Top1 poisons trap DNA-enzyme intermediates and can lead to irreversible DNA double-strand breaks (DSBs), cell death and genome instability. We have results showing that structurally different Top1 poisons, Camptothecin (CPT) and Indimitecan (LMP776), induce the formation of micronuclei (MNi) in human cancer cells. MNi can be a source of cytoplasmic DNAs that can activate STING-dependent pathways leading to an innate immune gene activation and production of type I interferons and other cytokines in cancer cells. As the mechanisms of MNi formation are not fully established, the main aim of this PhD project is to establish the mechanism of MNi induction by Top1 poisons in human cancer cells. Using immunofluorescence assays and EdU labelling of nascent DNAs, our results show that, after 24 hours of recovery, short treatment with sub-cytotoxic doses of Top1 poisons induces the formation of MNi that do not contain newly synthetized (EdU-labelled) DNA in human cancer HeLa and U2OS cells. Under similar experimental conditions, the drugs were able to produce significant levels of γH2AX and p53BP1, markers of DSBs, in replicating cells but much lower levels in non-replicating cells. In line with published data, we also saw that Top1 poisons delay replication machinery reducing EdU incorporation. This data, together with EdU-negative (EdU-) MNi formation, suggest that under-replication may be a cause of MNi production. Further results show that

EdU- MNi formation is not dependent on transcription while being dependent on R-loops, as overexpression of RNaseH1 markedly reduces Top1 induced MNi. Genome-wide mapping of R-loops by DRIP-seq technique revealed that R-loop levels are both decreased and increased by CPT depending on the specific genomic regions. In particular, increased R-loops are mainly found at active genes and always overlapped with Top1cc sites, as defined by (Baranello et al., 2016). Additionally, we found that increased R-loops overlap with lamina associated domains while decreased R-loops correlate with replication origin sites, as reported by (M. M. Martin et al., 2011). Overall, our data are consistent with Top1ccs causing an increase of R-loop levels and then irreversible DNA cleavage at selected genomic regions. The data altogether are consistent with the formation of MNi due to R-loop increase and under-replication at specific regions caused by Top1 poisons. Finally, we found that Top1 poison treatments lead to an asymmetric distribution of newly synthesized DNA at mitosis, which may suggest, together with published data, that MNi are formed through an active process to preserve genome integrity at least in one daughter cell in relation to a non-random chromatid segregation at mitosis. These results will eventually help in developing new strategies for effective personalized interventions by using Top1-targeted compounds as immuno-modulators in cancer patients.

INTRODUCTION

Cancer, together with cardiovascular diseases, is the primary cause of death in western countries. In ancient times, its incidence was negligible mainly because of short life expectancy, which was also due to the wide diffusion of infectious diseases. It was in the second half of the 20th century that, with increased life expectancy (also thanks to antibiotics and vaccines which dealt with infectious diseases), cancer became a serious problem to be faced. Nowadays, cancer is among the top two principal causes of death in 112 of 183 counties (Sung et al., 2021). With reference to estimates reported by the International Agency for Research on Cancer (IARC), new cases of cancer increased worldwide from 18.1 million in 2018 to 19.3 million in 2020, while death caused by cancer during the same period raised from 9.5 to 10 million (Bray et al., 2018; Sung et al., 2021). On the other side infectious diseases and other important pathologies such as stroke and coronary heart disease registered an evident decline in mortality rate (Bray et al., 2021).

To cope with cancer, different strategies have been developed over the years. To date, the most conventional approaches are chemotherapy, surgery and radiation therapy even if the more recent development and success of strategies involving the immune system resulted in immunotherapy as a new pillar of cancer treatment. Although mono-immunotherapy produced striking results in some patients, it has been shown that combination immunotherapy maximizes antitumor activity (Barbari et al., 2020; Drake, 2012). Of particular interest is the combination of immunotherapy and chemotherapy and their ability to mutually potentiate their action against cancer (Bailly et al., 2020; Q. Liu et al., 2021; S. Zhu et al., 2021). The positive action of chemotherapy on immunotherapy efficacy is given by the fact that, despite old believes, chemotherapy can stimulate the immune system with consequent antitumor effects (Emens & Middleton, 2015; Galluzzi et al., 2020; Saxena et al., 2020). Among the most important chemotherapeutic drugs, DNA topoisomerase poisons can have immunomodulant activity, as already described (Bracci et al., 2014; Haggerty et al., 2011; Hannesdóttir et al., 2013; Wan et al., 2012). However, how these poisons can activate the innate immunity is still under evaluation and its understanding will probably

open to the development of innovative, safer and more effective use of these established antitumor agents.

1. Topoisomerases 1B poisons as chemotherapeutic agents

1.1 DNA Topoisomerases

DNA topoisomerases are fundamental enzymes which regulate local and long-range genome structure by packing it into nuclear chromatin and resolving topological stresses generated during replication, transcription, DNA recombination and chromatin remodeling. Besides Spo11, a topoisomerase II-related enzyme expressed only in germ cells, six topoisomerases are encoded in the mammalian genome, classified into three main sub-families: Topoisomerase IA (TOP3α and TOP3β), Topoisomerase IB (TOP1 and TOP1mt) and Topoisomerase II (TOP2α, TOP2β) (Capranico et al., 2017; James J Champoux, 2001; Pommier et al., 2016; Wang, 2002).

TYPE-1 TOPOISOMERASES cleave only one of the two DNA strands. Type 1A enzymes relax only hyper-negative supercoiling using Mg2+ as a metal cofactor. More specifically, they cut the DNA and covalently link to the 5'-phosphate (5'-P) end (Fig.1). Then, they allow the passage of a duplex through the previously-produced strand break (**strand-passage mechanism**). On the other end, the molecular mechanism of Type 1B enzyme is different as they relax, without using any energy cofactor, both negative and positive supercoils by rotating the cut strand around the intact one (**controlled-rotation mechanism**) and becoming transiently linked to the 3'-phosphate (3'-P) end of the cut strand (Fig.1). Type I topoisomerases are usually monomeric enzyme.

TYPE-2 TOPOISOMERASES cut both DNA strands of a duplex, and become linked to the 5'-P ends of cut strands. These enzymes are composed of two or four subunits and use a strand-passage mechanism to change the topology of DNA substrates. By multiple protein

conformational changes, they allow a duplex DNA to pass through the double-strand break of another duplex DNA (Fig.1). They resolve negative and positive supercoils, catenates and DNA knots by using ATP molecules and Mg2+ as a cofactor.
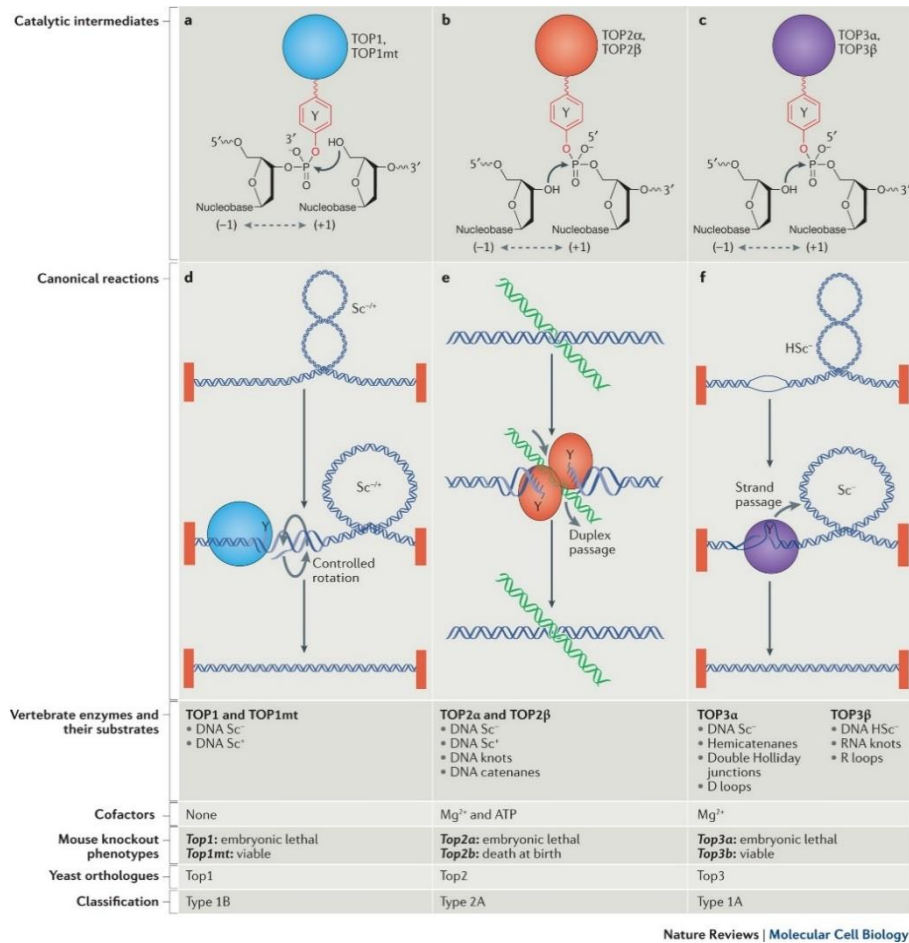
Fig.1 Human topoisomerases. Figure from Pommier, Y., Sun, Y., Shar-yin, N. H., & Nitiss, J. L. (2016). Roles of eukaryotic topoisomerases in transcription, replication and genomic stability. Nature reviews Molecular cell biology, 17(11), 703-721. Image licensed by Springer Nature and Copyright Clearance Center's RightsLink® service (License n. 5236000823509).

1.2 Topoisomerase 1B

Nuclear human Top1B (also referred as Top1 throughout the text) is a 765 amino-acid enzyme, encoded on chromosome 20 and composed of four main domains (Fig.2): **N-terminus**, **core**, **linker**, and **C-terminus**. The N-terminus is a poorly conserved domain containing the nuclear localization signals (NLS) as well as interaction sites for other proteins (Bharti et al., 1996; Mo et al., 2000; Pommier et al., 2016). The highly conserved core domain is important for DNA interaction, even if the cleavage site (tyrosine catalytic residue -Tyr273) is located on the C-terminal domain. The core and the C-terminus are linked by the poorly conserved linker domain, which plays a major role in the controlled-rotation mechanism of the enzyme (Capranico et al., 2017; James J Champoux, 2001; D'Annessa et al., 2014).
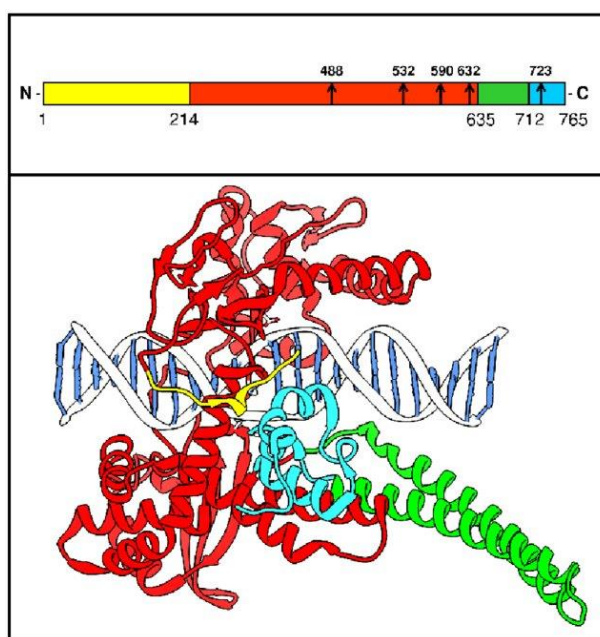
Fig.2 Topoisomerase1B structure. N-terminal domain, core, linker and C-terminal domain are represented in yellow, red, green and blue respectively. The arrows and the numbers above indicate the amino acids forming the active site. Figure from Ottaviani, A., Iacovelli, F., Fiorani, P., & Desideri, A. (2021). Natural Compounds as Therapeutic Agents: The Case of Human Topoisomerase IB. International Journal of Molecular Sciences, 22(8), 4138. Image licensed under the Creative Commons Attribution License.

Constitutively expressed throughout the cell cycle (Baker et al., 1995), Top1B relaxes topological stress by nicking one DNA strand and forming a covalent bond between the Tyr723 residue and the DNA 3′-P. The resulting DNA-enzyme covalent complex is called **Top1 cleavage complex** (**Top1cc**). After the "controlled rotation" of the cut strand around the intact one, Top1 then re-ligate the broken strands and detaches from them (Capranico et al., 2017; James J Champoux, 2001). The relegation step, during which the 3'-P end needs to be aligned with the 5'-hydroxyl (5'-OH) end, is thermodynamically favored in normal condition. This is why the reaction is transient and the cleavage complex intermediate cannot be usually detected (Seol et al., 2012). However, endogenous injuries, such as oxidized bases, mismatches, nicks, abasic sites, etc. can cause the misalignment of the 5'-OH arm. This makes the cleavage irreversible leading to DNA breaks which can threaten genome stability and cell survival. This process is exploited in medical oncology by using chemical compounds called 'poisons' as effective antitumor drugs (Capranico et al., 1997).

The described breakage-religation mechanism is fundamental during biological processes characterized by an alteration of DNA topology. For example, DNA and RNA polymerases progression imply the separation of the two strands and, consequently, the formation of positive and negative supercoils respectively upstream and downstream the two enzymes (J. J. Champoux & Dulbecco, 1972; L. F. Liu & Wang, 1987). In this context, positive supercoils represent an obstacle to these essential processes and are removed by Top1. On the other hand, negative supercoils favor the formation of non-canonical DNA structures, such as R-loops, which represent a further impediment to replication and transcription processes (Chedin et al., 2020). Once again, Top1 has the ability to relax this type of torsional stress preventing the formation of such obstacles. Curiously, considering that the opened strands of negative supercoils have a positive role in transcription initiation at the promoter level and in the firing of replication origins, it has not fully understood whether and how Top1 recognizes the different type of supercoils (Capranico et al., 2017; Di Felice & Camilloni, 2021). Always related to its relaxation activity, Top1 has been implicated also in other processes such as chromatin remodeling (Durand-Dubief et al., 2010).

In addition to the canonical activity described for Top1, there are different functions which are not related to the relaxation activity of the enzyme. For example, it has been shown that Top1 phosphorylates specific RNA splicing factors (Rossi et al., 1998) involved in splicing and other processes related to transcript maturation (Jeong, 2017; Soret et al., 2003), even if these results have not yet been replicated and the mechanism still remains to be determined. It has already been shown that, by phosphorylating these proteins, Top1 impede R-loop formation (Tuduri et al., 2009). An additional non-catalytic activity of Top1 is given by its ability to act as a scaffold protein: *in vitro* experiments demonstrated that Top1, which catalytical activity was previously inactivated, is recruited to the promoter by TFIID and stimulates transcription process by recruiting other protein factors essential for transcription initiation and elongation (Di Felice & Camilloni, 2021; Shykind et al., 1997).

1.2 Topoisomerase 1B inhibition and poisoning

Several chemical agents can interfere with Top1 action. If the compounds impede the binding or catalytic activity of the enzyme preventing Top1cc formation, they are called "**catalytic inhibitors**" or "**suppressors**". Among these agents, two main classes can be distinguished (Capranico et al., 2017; Capranico & Binaschi, 1998; Cinelli, 2019): DNA binding agents, which prevent enzyme attachment to DNA substrates, and Top1 binders, which bind to the enzyme alone avoiding DNA binding or DNA cleavage reaction. On the other hand, there are various chemical compounds which act as "**poisons**": they bind to a receptor at the DNA cleavage site, constituted by the enzyme and the DNA (Capranico et al., 1997; Capranico & Binaschi, 1998; Staker et al., 2002). Here, the poison forms hydrophobic interactions with the DNA and, at the same time, hydrogen bonds with the enzyme which stabilize the Top1cc impeding the re-ligation step (Capranico & Binaschi, 1998; Pommier et al., 2015). An important molecular feature of Top1 poisons is that, both *in vitro* and in living cells, they bind Top1cc reversibly (Covey et al., 1989; Tanizawa et al., 1994). We know that, once the drug is removed, DNA cleavage rapidly reverses due to the DNA re-ligation activity of Top1. Importantly, all clinically-effective anticancer drugs are poisons of Top1 rather than catalytic inhibitors.

Top1 poisons can be divided into two main groups (Fig.3):

- **CAMPTOTHECIN (CPT) AND ITS DERIVATES (Fig.3A)**: Camptothecin is an alkaloid derived from the *Camptotheca acuminate* tree. At physiological pH, it has an E-ring lactone (active form) which readily opens to the more soluble carboxylate form (inactive), the prevalent form at alkaline pHs (Pommier, 2006). Although it is an effective anticancer compound in animal models, CPT has a number of side effects (acute bone-marrow suppression, vomiting, diarrhea and hemorrhagic cystitis, necessity of long infusion times because its reversibility), which led to its initial dismission from clinical studies and to the development of new derivatives with the aim of reducing the side effects by increasing its water solubility and stability of the active lactone form.

  CPT derivates, Irinotecan and Topotecan, are the only Top1-targeted drugs approved by the Food and Drug administration (FDA) and European Medical Agency (EMA) for standard cancer therapy. Irinotecan can be prescribed for gastrointestinal tumors, while Topotecan is used for ovarian tumors and small cell lung cancers (SCLC). However, both compounds still have dose-limiting toxicity and short half-life because of E-ring opening.

- **NON-CAMPTOTHECIN COMPOUNDS (Fig.3B):** After discovering that Top1 was the cellular target of CPT and with the aim of overcoming drug side effects, several laboratories started searching for non-camptothecin Top1 poisons to overcome E-ring instability and CPT toxic effects. Among the new compounds, two classes (indenoisoquinolines and dibenzonaphthyridinones) are in clinical development and, apparently, they are similarly active and tolerated as CPTs in early phase clinical trials. Indenoisoquinolines, indimitecan (LMP776) and indotecan (LMP400) (Kinders et al., 2011) showed several advantages in comparison with CPTs due to their different characteristics: they have a higher chemical stability since they have no lactone groups; they form less reversible and, consequently, more stable Top1ccs (Antony et al., 2007; Tanizawa et al., 1994); they trap Top1ccs with a

11

different sequence specificity as compared with CPT (Capranico et al., 2017; Cinelli, 2019; Pommier, 2006; Tanizawa et al., 1994; Xu & Her, 2015); they have less side effects on normal tissues (Burton et al., 2018; Kummar et al., 2016).
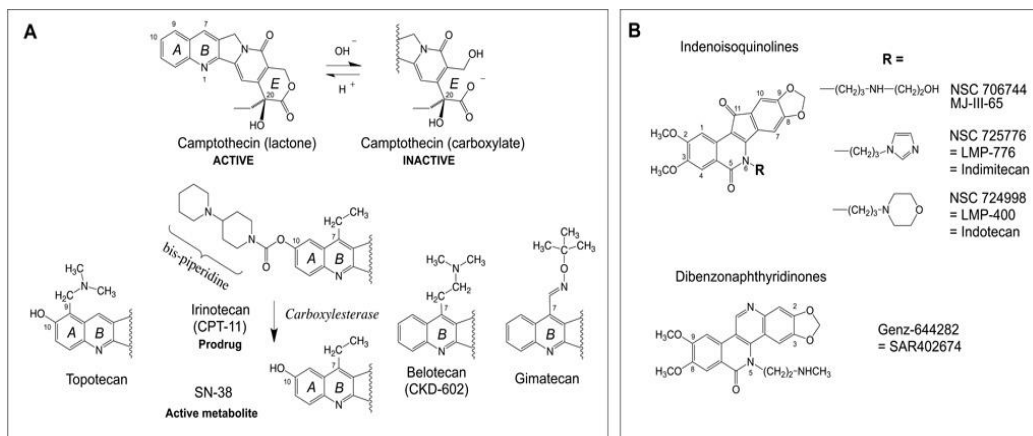
Fig.3 Camptothecins (A) and Non-camptothecin Top1 poisons (B). adapted with permission from Pommier, Y. (2013). Drugging topoisomerases: lessons and challenges. ACS chemical biology, 8(1), 82-95. Copyright 2022 American Chemical Society.

1.3 Top1 poisoning effects

As already said, Top1cc is a short-term complex which usually persists for less than a second, however when the cleavage complex is trapped and stabilized by CPT, Top1cc half-life increases to 2 minutes (Koster et al., 2007). Long-lived Top1ccs can have harmful effects such as increased DNA damage, genome instability and cell death (S. H. Chen et al., 2013; Pommier, 2013; Pommier et al., 2015). DNA damage is not caused by the drug itself but to the interference of trapped Top1cc with other biological processes. Indeed, the presence of stalled Top1ccs and the resulting DNA lesion (single strand breaks - SSBs) impair both replication and transcription processes (Ljungman & Hanawalt, 1996; Seiler et al., 2007; Stephanie Solier et al., 2013).

1.3.1. Top1 poisoning and DNA replication

When the Top1 cleavage complex is trapped by poisons, the physically-blocked Top1ccs and the associated DNA-SSB, the unresolved torsional stress ahead of replication fork and the formation of non-canonical DNA structures, all may constitute an obstacle to the advancing replication fork. As a consequence, replication inhibition, fork stalling/collapse (Hsiang et al., 1989) and increasing of single-ended double-stranded DNA breakage (se-DSBs) (Cliby et al., 2002; Nyamuswa & Silber, 1993; Ray Chaudhuri et al., 2012; Srivastava et al., 2018; Zhao et al., 2018) have been observed during the S-phase of the cell cycle. In particular, when the leading strand is replicated up to the 5′ end, the SSB associated to the TOP1cc can be converted into toxic DSB by the run-off of replication fork (Fig.4) (Strumberg et al., 2000). This is why CPT has become a common and specific tool to induce DSBs at replication forks during S phase. In addition, slow-moving replication forks increase the chances that transcription-replication conflicts occur with severe consequences for genome stability (Hamperl et al., 2018).
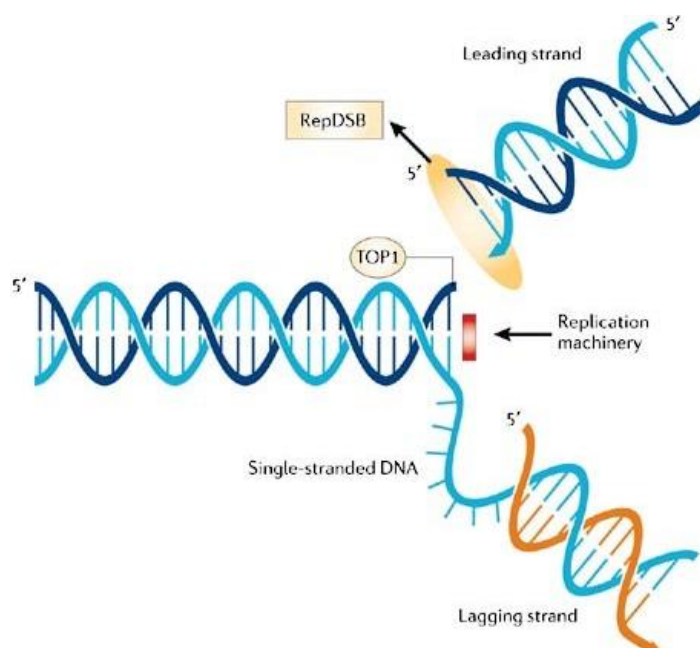
Fig.4 Conversion of Top1cc into DSB in replication context. Figure adapted from Pommier, Y. (2006). Topoisomerase I inhibitors: camptothecins and beyond. Nature Reviews Cancer, 6(10), 789-802. Image licensed by Springer Nature and Copyright Clearance Center's RightsLink® service (License n. 5236010125480).

1.3.2 Top1 poisoning and transcription

As in the case of replication, also transcription have been proposed to make TOP1ccs irreversible (Khobta et al., 2006; Wu & Liu, 1997). However, the consequent DNA damage and molecular response is not so well understood.

Top1 importance during transcription is mostly given by its relaxation activity, which is needed since RNA polymerase activity generates a high level of torsional stress. Indeed, according to the twin-supercoiled domain model (L. F. Liu & Wang, 1987; Tsao et al., 1989), as RNA polymerase moves along the template that cannot rotate around the other strand, the DNA duplex becomes negatively and positively supercoiled behind and ahead of the polymerase, respectively.

Moreover, considered that Top1 functions during transcriptions are various (Merino et al., 1993; Stéphanie Solier et al., 2011; Soret et al., 2003), CPT presence can impair also the non-catalytic activity of the enzyme. For example, it was observed that Top1cc poisoning impairs RNA splicing producing alternative transcripts (Baranello et al., 2009; Eisenreich et al., 2009; Shkreta et al., 2008; Stéphanie Solier et al., 2004).

The accumulation of negative supercoiling after Top1 poisoning locally at highly transcribed promoters (Kouzine et al., 2013) may promote the formation of non-B DNA structures such as R-loops. R-loops are non-canonical DNA structures composed of an RNA strand annealed to its DNA template and a displaced non-template strand. Their formation happens mostly during transcription as negative supercoils behind an elongating RNA Polymerase II may lead to the separation of the two DNA strands favoring RNA hybridization (Fig.5) (Chedin et al., 2020; Miglietta et al., 2020).

It is currently well known that R-loops have physiological functions: they favor transcription by protecting promoters from methylation (Grunseich et al., 2018) or by preventing transcriptional repressors binding (P. B. Chen et al., 2015); they regulate transcription termination of some genes, chromatin organization, DNA methylation at CpG islands, and

immunoglobulin class-switch recombination (Bayona-Feliu et al., 2021; Hegazy et al., 2020; Skourti-Stathaki et al., 2011). However, unbalanced levels of R-loops may have harmful consequences such as the increase of DNA double-strand breaks, genome instability and cell death (Aguilera & Gómez-González, 2017; Chédin, 2016; Sollier & Cimprich, 2015). Indeed, as mentioned before, R-loops constitute an obstacle to replication process and increase the rate of collisions between replication and transcription machineries (Chedin et al., 2020; Madzia P. Crossley et al., 2019).
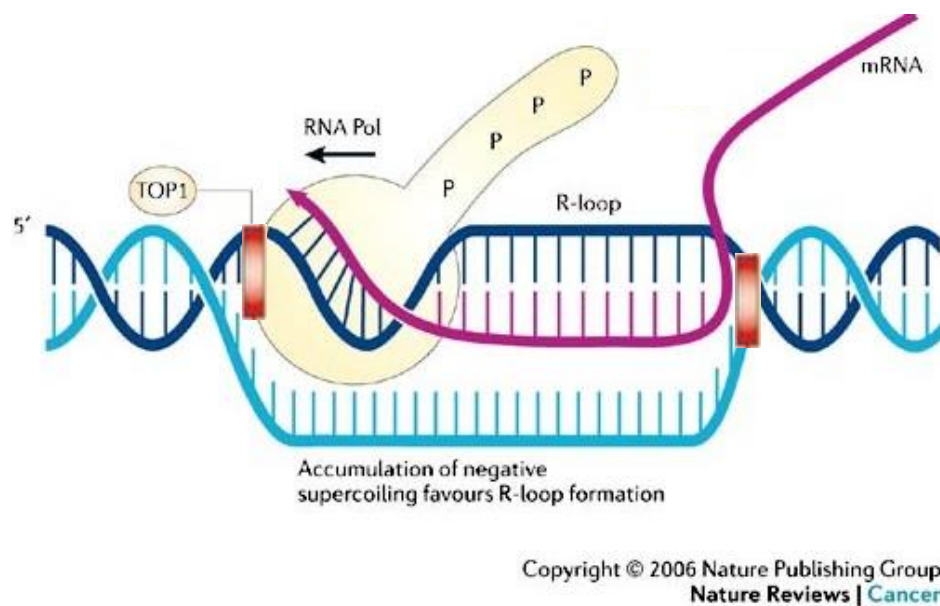
Fig.5 R-loop formation. Figure adapted from Pommier, Y. (2006). Adapted from Topoisomerase I inhibitors: camptothecins and beyond. Nature Reviews Cancer, 6(10), 789-802. Image licensed by Springer Nature and Copyright Clearance Center's RightsLink® service (License n. 5236010125480)

To maintain R-loop homeostasis, cells use different strategies which can be divided into two classes: preventing factors and removing factors. The former are recruited to the newly synthetized RNA (Domínguez-Sánchez et al., 2011; Skourti-Stathaki et al., 2011; Wahba et al., 2011) or control DNA topological changes (Aguilera & Gómez-González, 2017; Tuduri et al., 2009) while the latter directly resolve R-loop structures. Topoisomerase 1B fall into the first category, while specific nucleases such as RNase H (RNase H1 and 2 in humans)

(Cerritelli & Crouch, 2009; Wahba et al., 2011) belongs to the removing factors and are generally used to rescue R-loop formation (Domínguez-Sánchez et al., 2011).

Given the importance of Topoisomerase 1B in contrasting R-loop formation, it can be easily understood why, in case of Top1 trapping, R-loops increase interferes with replication process and leads to an increase of replication-transcription conflicts, DNA damage and genome instability. Furthermore, it has been observed that R-loops can also contrast directly with transcription and DNA damage response (Bonnet et al., 2017; Cohen et al., 2018; Cristini et al., 2019; D᾽Alessandro et al., 2018; Lang et al., 2017; Ohle et al., 2016).

1.4 Top1 mediated DNA damage cellular response

In physiological conditions, the presence of Top1cc activates several pathways (Fig.6) to resolve the protein-linked break and the consequent irreversible damage caused by the encounter with replication and transcription machineries. In this regard, the initial lesion constituted by Top1cc can be repaired by three main pathways:

- **TOP1cc REVERSAL PATHWAY**: when the 5'-OH end remains intact and aligned with the 3'-P end linked to the enzyme, the easiest thing to do is to continue with the relegation step, as explained in "Topoisomerase IB" section. Thus, this pathway mainly occurs when the harmful arriving of replication or transcription machinery is followed by its regression (pull-back) (Pommier et al., 2006). In the case of replication, regression generate a four-stranded "chickenfoot" DNA structure. The resolution of this structure has been ascribed to different elements such as RECQ helicases or homologous recombination (HR) factors (e.g. RAD51). Another possibility is the resection of reversed forks by DNA2 nuclease. However, the fate of reversed forks has not been completely unveiled (Berti et al., 2013; Quinet et al., 2017; Thangavel et al., 2015). In the case of transcription, Rad26 and TFIIS are mainly involved in RNA polymerase II (PolII) backtracking (Van Den Boom et al., 2002).

16

- **TYROSYL-DNA-PHOSPHODIESTERASE (TDP1) PATHWAY**: In this case, the first step is the ubiquitination and subsequent proteasome degradation of the trapped enzyme with a resulting short peptide covalently linked to the 3'-P end of the DNA (Desai et al., 2001; Lin et al., 2008). At this point, thanks to the intervention of some proteins of the Base Excision Repair (BER) pathway, (PARP1 and XRCC1) TDP1 is recruited to the cleavage site to hydrolyze the covalent bond between DNA and the peptide remaining after Top1 degradation by proteasome. Re-ligation is then possible essentially via the BER pathway (Mei et al., 2020).

- **ENDONUCLEASE PATHWAY**: In addition, numerous endonucleases (e.g. XPF/ERCC1, SLX1-SLX4, MUS81-EME1, Mre11/Rad50/ Nbs1 (MRN complex), FEN1, etc.) can participate in different mechanisms to remove Top1cs. In parallel with or in alternative to the TDP1 pathway (Pommier et al., 2006), they excise the DNA at a few nucleotides away from the 3'-P-TOP1 end (Lin et al., 2008; Pommier et al., 2006) converting the Top1ccs into SSBs with a gap of a few nucleotides. At this point, the break can be resolved thanks to BER enzymes which permit the filling of the gap and the rejoining of the two extremities.

If SSB is not repaired in time, as previously stated, Top1ccs can encounter with replication and/or transcription machineries leading to DSBs generation. In this case DNA lesions can be repaired by two main pathways: **homologous recombination (HR) repair**, initiated by MRN-BRCA-Rad51 activities or **nonhomologous end joining (NHEJ)**, which starts with Ku-DNA-PK intervention. More specifically, the HR pathway act by "coping" the missing information from an homologous DNA template while NHEJ repair directly ligates the two DNA ends. One or the other pathway is chosen according to the type of damage and the phase of the cells cycle (Iyama & Wilson, 2013; Mei et al., 2020; Symington & Gautier, 2011).

The DNA damage response (DDR) caused by Top1ccs triggers cell-cycle checkpoints with the aim of delaying cell cycle progression, by downregulating CDK activity. The two central checkpoint kinase cascades activated by DNA damage are the ataxia telangiectasia and Rad3-related (ATR) and ataxia telangiectasia mutated (ATM) pathways. After their

activation, ATR and ATM phosphorylate different proteins involved in damage repair and checkpoint control (Kuo & Yang, 2008; Teicher, 2008). Among these proteins, of particular importance there are:

- **H2AX HISTONE:** within few minutes from DSB formation, the H2AX histone is phosphorylated (γ-H2AX) (Furuta et al., 2003) and accumulates around the double-strand breaks forming nuclear foci. This makes γ-H2AX a sensitive and commonly-used biomarker for Top1cc-induced DNA damage;
- **RPA32:** pRPA32 stabilizes single-stranded DNA (ssDNA) during replication and repair processes forming heterotrimers with RPA70 and RPA14. Both H2AX and RPA32 are phosphorylated by the DNA-dependent protein kinase (DNAPK) in combination with ATM and ATR (Furuta et al., 2003; Shao et al., 1999; Soniat et al., 2019);
- **BLOOM'S SYNDROME PROTEIN (BLM):** After phosphorylation by ATM, BLM colocalizes with γ-H2AX to facilitate its phosphorylation (Rao et al., 2005). BLM activates HR pathway by contributing to the resection of double strand breaks. The generated single-stranded intermediate is subsequently bound by RPA and RAD51 (Patel et al., 2017).

Other ATM phosphorylated proteins are CHK2, BRCA1, TDP1 and p53, which is also a substrate of ATR together with CHK1. The phosphorylation of these proteins permits to activate the different DDR pathways and control cell cycle checkpoints, giving time for damage repair and avoiding the onset of additional damage before DNA replication or mitosis (Pommier et al., 2006).

Despite the activation of all these DDR pathways, Top1 poisons cause such a massive damage to be highly cytotoxic. Indeed, Top1cc formation, replication-dependent DNA damage, transcription and R-loops can all contribute to cell cycle blockage and apoptosis mediated by Top1 poisons (L. F. Liu et al., 1992; Morris, 1996; Zhou et al., 2002). In connection with this, the presence of higher Top1 levels in rapidly proliferating cancer cells than in healthy non-proliferating tissues makes cancer more susceptible to Top1 poisons

(Braun et al., 2008; Madden & Champoux, 1992) and, consequently, Top1 poisons an excellent tool for chemotherapeutic cancer treatment.
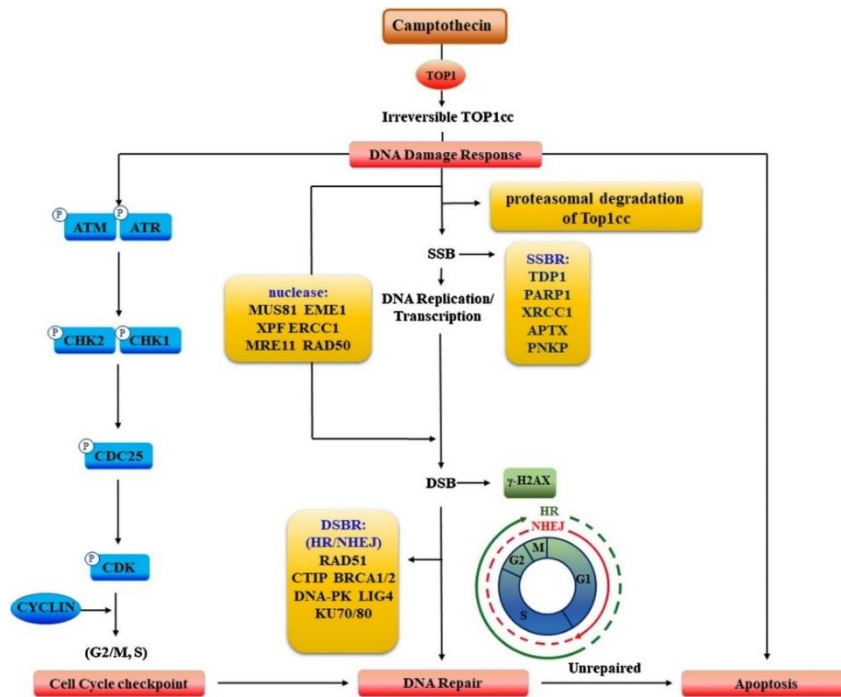
Fig.6 DNA damage response to Top1cc trapping. Figure from Mei, C., Lei, L., Tan, L. M., Xu, X. J., He, B. M., Luo, C., ... & Liu, Z. Q. (2020). The role of single strand break repair pathways in cellular responses to camptothecin induced DNA damage. Biomedicine & Pharmacotherapy, 125, 109875. Image released under a Creative Common License.

2. Top1 poisons as immunomodulators

In addition to the well cytotoxic effects, the induction of immune response by Top1 poisons is emerging as a boosting mechanism of immunotherapy efficacy (Bracci et al., 2014; Haggerty et al., 2011; Hannesdóttir et al., 2013; Wan et al., 2012). For instance, recent data showed how Top1 poisons stimulate the production of antigens in melanoma cells and the expression of class I MHC molecules and IFNβ in breast cancer cells (Haggerty et al., 2011; Wan et al., 2012). More recently, it was demonstrated that topotecan induces the production of inflammatory cytokines by stimulating the cGAS receptor (Kitai et al., 2017) and that CPT and LMP776 can also activate the innate immunity related pathway of cGAS-STING (Marinello et al., 2022). Even if the molecular basis of this immune stimulation are still being

examined, we made a small step forward by identifying micronuclei (MNi) production as an important triggering element for innate immune gene activation by Top1 poisons (Marinello et al., 2022) .

MNi are little cytoplasmatic bodies containing damaged chromosome fragments and/or whole chromosomes that were not included into the main nucleus (Fenech et al., 2016). They can likely form during mitosis from lagging chromosomes or chromatid fragments after the failure of chromosome segregation and/or cell cytokinesis (Fenech, 2020; Fenech et al., 2016; K. I. Utani et al., 2010). Indeed, although the presence of DDR pathways and cell cycle checkpoints to prevent genome instability, threatened DNA can sometimes elude cell surveillance continuing into mitosis. Progression through mitosis of damaged DNA causes mitotic defects like lagging chromosomes and ultrafine DNA bridges which can in turn lead to the formation of MNi (Wilhelm et al., 2020). Alternatively, they can form during interphase from nuclear blebbing of DNA-repair complexes or from over-amplified DNA (K. ichi Utani et al., 2011). After their formation, they can be removed by the autophagy pathway (Bartsch et al., 2017; Lan et al., 2014), reincorporated into the main nucleus contributing to chromothripsis (C. Z. Zhang et al., 2015), or can break their membrane (Hatch et al., 2013) spreading the DNA content into the cytoplasm. The presence of free DNA in the cytoplasm is a signal that triggers the activation of the cGAS-STING pathway (Harding et al., 2017; MacKenzie et al., 2017) which have a central role in innate immune response to infections, inflammation and cancer (Burdette & Vance, 2013; Dhanwani et al., 2018).

Top1 poisons induce MNi formation (Holmström & Winters, 1992; Marinello et al., 2022; K. ichi Utani et al., 2011), thus leading to immune gene activation (Marinello et al., 2022). How MNi form, as a general mechanism and as a consequence of Top1 poisoning, it is not fully established yet. We have unpublished and published data showing that MNi formation is mediated by R-loop increase (De Magis et al., 2019; Marinello et al., 2022), however, further investigation needs to be done. Understanding how Top1 poisons lead to MNi formation, will perimit a more conscious use of such chemotherapeutic drugs in an immunostimulatory context.

AIM OF THE PROJECT

MNi have recently emerged as a connection element between genome instability and innate immunity. In particular, it has been proved that some chemotherapeutic drugs, such as Top1 poisons, may stimulate the activation of innate immune genes likely by increasing the production of MNi (Marinello et al., 2022). However, it has not fully established which is the mechanism underlying their formation.

In this context, the present PhD project aimed to understand which is (are) the molecular and cellular mechanism(s) driving MNi formation after treating human cancer cells with Top1 poisons. In particular, we tried to establish if MNi production could be a cell phase specific phenomenon and whether replication, transcription and R-loop formation were involved in this process. To investigate MNi formation, we mainly conducted immunofluorescence microscopy (IF) experiments to visualize MNi and DNA damage patterns after Top1 poisons administration. Combing experiments, in parallel with IF, let us to investigate replication impairments. Finally, DRB administration and RNaseH1 overexpression were used to inhibit transcription and control R-loop cellular presence, respectively. R-loop involvement was further investigated by using DRIP-seq technique to map unbalanced R-loops forming after Top1 poisoning.

DRIP-seq experiments development for sequencing data normalization were conducted at CABIMER (Centro Andaluz de Biología Molecular y Medicina Regenerativa), where I spent six months as a visiting PhD student.

MATERIALS AND METHODS

1. Cell culture

Human cancer HeLa, HCT116 and U2OS cell lines were obtained from ATCC (American Type Culture Collection). HeLa cells were cultured in DMEM supplemented with 10% heat-inactivated fetal bovine serum (FBS). HCT116 cells were cultured in McCoy's 5A medium supplemented with 10% heat-inactivated FBS. U2OS-RH cells were obtained by transfecting U2OS with pLVX-Tight-Puro-RH-Flag and pLVX-EF1a-Tet3G-Hygro plasmids to have a Tet-On system and overexpress RNaseH1. This cells line was maintained in DMEM medium with the addition of 10% FBS, 500 µg/ml hygromycin B, 100 µg/ml penicillin-streptomycin (Pen/Strep) and 1.5 µg/ml puromycin. RNaseH1 overexpression was induced by adding 2 µg/ml doxycycline for 48h to the same medium without Pen/Strep and Puromycin.

2. Compound preparation

CPT and LMP776 were prepared in 100% dimethyl sulfoxide (DMSO) at 10 mM, while PDS was diluted at 5 mM in water. Small aliquots of 10 µL each were stored at -20°C to avoid multiple freeze-thaw cycles. Final dilutions of 10 µM were prepared in medium directly before using all compounds.

Click-iT® EdU Assay (Invitrogen) was used to identify S-phase cells by immunofluorescence or cytofluorimetry. All stack solutions were prepared following instructions provided by kit datasheet.

3. Immunofluorescence assay

Cells were seeded at a density of 200 000 cells/well in 35 mm dishes containing a 24*24 mm cover glass. After 24h, cells were treated for 1h with 10 µM of CPT/LMP776/PDS adding 2mL of solution for each dish. To detect cells in the S-phase, cells were incubated

with 10 µM of EdU solution 30' before, during the treatment and 1h afterward for a total of two and a half hours. In case of transcription inhibition, 5,6-dichloro-1-beta-D-ribofuranosylbenzimidazole (DRB) was added to cell during the same period of time of EdU and to a final concentration of 50 µM. After each step, cells were washed with PBS 1X and then arranged for the immunofluorescence or leaved to recover for additional 24h.

3.1 EdU detection

Immediately after treatment or 24h later, according to what was the main factor to be detected, cells were fixed adding 1 mL of 3.7% formaldehyde in PBS 1X to each well. After 15 minutes of incubation at room temperature (RT), cells were washed twice with 1 mL of 3% BSA in PBS 1X and permeabilized by adding 1 mL of 0.5% Triton® X-100 in PBS 1X to each well. After 20 minutes of incubation at room temperature, cells were washed with 1 mL of 3% BSA in PBS. At this point, EdU detection was performed putting each slide upside down on 100 µL of Click iT Reaction cocktail previously placed on a parafilm layer (reaction cocktail was prepared according to datasheet instructions). After 30 minutes of incubation at RT and protecting slides from light, the reaction cocktail was removed and each slide was put again in the well to perform a last washing step with 1 mL of 3% BSA in PBS.

At this point, slides were stained with different primary/secondary antibodies or directly with DAPI (see "micronuclei detection") .

3.2 γ-H2AX detection

Upon drug administration and EdU detection, cells were blocked for 30 minutes with 8% BSA in PBS 1X at RT (gently rocking) and incubated at RT with anti-γH2AX antibody (Millipore) diluted 1:1000 in 1% BSA/PBS for 2 hours. After 3 washing steps (5 minutes each), slides were incubated with secondary antibody Alexa Fluor 488 goat Anti-Mouse IgG (Life technologies) in 1% BSA/PBS for 1 hour (1:1000). After washing cells 3 times with PBS, nuclear staining and mounting was performed as described in "Micronuclei detection" section.

3.3 p53BP1 detection

After EdU detection performed at the end of drug and EdU treatment, cells were blocked for 30 minutes with 2 mL of blocking buffer (5% FBS + 0.3% Triton X-100 in PBS 1X). Then, slides were incubated for 2h with Phospho-53BP1 (Ser1778) Antibody (Cell Signaling) diluted 1:100 in blocking buffer. After three washing steps (5minutes each) with PBS 1X, slides were incubated with secondary antibody Alexa Fluor 488 goat Anti-Mouse IgG (Life technologies) in blocking buffer. After other three washing steps, nuclear staining and mounting was performed as described in "Micronuclei detection".

3.4 RPA detection

After EdU detection performed immediately after treatment, cells were blocked for 1h with 2% BSA in PBS 1X at 25°C (gently rocking). Blocked cells were incubated for 2h at 25°C with RPA70 antibody or with RPA32 antibody (Abcam) diluted respectively 1:500 and 1:175 with 0.5% tween 20 in PBS 1X. After 3 washing steps (5 minutes each) with PBS 1X, cells were incubated with secondary antibody Alexa Fluor 488 goat Anti-Rabbit IgG (Life technologies) in PBS-Tween 0.5% for 1 hour (1:1000). Slides were washed three times with PBS 1X, then nuclear staining and mounting was performed as described in "Micronuclei detection".

3.5 Micronuclei detection

At the end of EdU administration or after 24h recovery, cells were treated as described in the section "EdU detection" and, subsequently, treated as follow. Each slide was incubated upside down with 100 µL of a DAPI solution (3.3 ng/µL in water) for 30 minutes and then washed with water before being mounted with Mowiol upside down on microscope slides.

4. Cell image analysis

Fluorescence microscope Eclipse 90i (Nikon) was used to visualize slides and acquire images which were then analysed using ImageJ software.

Micronuclei analysis was conducted counting, for each captured image, the number of cells and micronuclei which were both classified as EdU+ or EdU- according to their positivity to EdU staining. Four different groups were created counting EdU+/EdU- micronuclei per 100 EdU or EdU- cells. MNi were reported as number of MNi per 100 cells normalized or not the untreated control.

For γH2AX, RPA32/RPA70 and EdU quantification, fluorescence mean value was measured for each cell and background subtracted. For p53BP1, foci number was quantified using a specific ImageJ macro. γH2AX and RPA32/RPA70 signal increase or p53BP1 foci was calculated taking distinguishing EdU+ from EdU- cells. The quantification of EdU signal was carried out only in synchronized and EdU+ cells.

5. Cytofluorimetry

Cells were seeded at a density of 1 000 000 cells/well in 100 mm dishes. After 24h from seeding, they were treated with CPT and EdU as already described in "Immunofluorescence assay" section. Immediately after EdU treatment, cells were detached from wells by using trypsin, washed with PBS 1X and fixed with 1 mL of 3.7% formaldehyde in PBS 1X. After 15 minutes at room temperature (RT), cells were washed with 5 mL of PBS 1X and permeabilized by adding 1 mL of 0.2% Triton® X-100 in PBS 1X to each falcon tube. After 10 minutes of incubation at room temperature, cells were washed with 5 mL of PBS 1X. At this point, blocking step was performed at RT for 30' with 1 ml blocking buffer (3% BSA, 0,05% Tween-20). After removing blocking buffer, EdU detection was performed by adding 100 µL of Click iT Reaction cocktail prepared according to datasheet instructions. After 30 minutes of incubation at RT, cells were stained for 1h with 500 µL of anti-γH2AX antibody (Millipore) diluted 1:100 in blocking buffer. After washing step (0.1% BSA and 0.05%

25

Tween-20 in PBS 1X), samples were incubated for 1 h with 500 µL of secondary antibody Alexa Fluor 594 in blocking buffer (1:200). After washing cells as before, nuclear staining was performed O/N with 1 µg/ml DAPI at 4°C (final concentration).

6. Cell synchronization

6.1 S-phase synchronization

Synchronization in S-phase has been performed as in (Velichko et al., 2019). In particular, cells were treated for 16h with 2mM of thymidine. At the end of the incubation, cells were washed twice with PBS 1X and release for 3h in DMEM supplemented with FBS 10%. At this point EdU, CPT, LMP776 and PDS were administrated as previously described.

6.2 G2-phase synchronization

Synchronization in late G2-phase has been performed as in (Xing et al., 2020). In particular, cells were treated for 16h with 9 µM of RO3306. At the end of the incubation, cells were washed with PBS 1X in incubator for 5 min and released for 30 min into prometaphase. At this point EdU, CPT, LMP776 and PDS were administrated as previously described.

7. Combing assay

$3*10^6$ cells were seeded in 100 mm dishes. After 24h, medium was changed with fresh medium and IdU 250 µM was added for 20'. Then, cells were washed with PBS 1X and 200 µM CldU was added for further 20'. CPT 10 µM was added for the last 10' of IdU incubation (and then washed out) or during the entire incubation of CldU. At the end, cells were washed with PBS 1X and detached with 500 µL accutase (Thermo Fisher) per dish. Cells were further washed with cold PBS 1X, pelleted and resuspended in PBS 1X at a density of $4*10^5$ cells/50 µL.

200 μL of 1% of LMP agarose were added to 200 μL of cells both pre-heated at 42°C. 100 μL per plug of the solution were transferred into a casting mould and plugs were left at RT for 25' and at 4°C for the last 5'. Four plugs for each condition were ejected into a 12 mL round-bottom tube containing 500 μL of Proteinase K (ProK) buffer (0.4 μg/ μL in TE50 (10 mM TrisHCl, pH7; 50 mM EDTA) + 1% sarkosyl). Plugs were incubated O/N at 50°C. At this point, ProK buffer was replaced by other 2 mL of ProK buffer and left for further 6 h. At the end, plugs were washed with TE50 at RT, 300 rpm speed. One plug per condition (the other were stored at 4°C in TE50) was incubated in the dark for 30', RT with 1.5 μL of YOYO-1 (Molecular probes) diluted in 100 μL of TE50. Plugs were then washed with 10 ml of TE 1X shaking at 300 rpm speed. MES 1X pH 5.7 buffer were pre-warmed at 65°C and 3mL per plug were added and incubated at 65°C for 12'. After reducing the temperature at 42°C, 3 units of β-agarose (NEB) in 100 μL of MES 1X were added and O/N incubation was performed.

After further 10' of incubation at 65°C, plugs were allowed to cool at RT. The obtained DNA solution was poured in a 2 mL Teflon reservoir where silanized coverslip were inserted and left for 15' at RT. The coverslip was then removed at 300 μm/s speed. This step was automatically performed by using a Molecular Combing System (MCS). After checking DNA fibres at fluorescence microscope (40X objective and FITC filter cube), the coverslip were dried for 2h at 60°C and then fixed on a microscope slide. Slides were incubated for 8' with 0.5 M NaOH + 1M NaCl. Five washing steps (1' each) were performed with PBS 1X. Slides were then blocked for 15' in blocking buffer solution (PBS-TRITON (0.1%) + 1%BSA). For IdU and CldU detection, slides were incubated with 1:20 mouse anti-BrdU (clone B44, Becton Dickinson) and 1:20 rat anti-BrdU (clone BU1/75, AbCys SA) for 45'. Then, 30' of incubation with Goat anti-mouse IgG1-Alexa 546 (Molecular probes) and Chicken anti-Rat-Alexa 488 (Molecular Probes) were performed. For DNA detection, slides were incubated for 30' with 1:50 Mouse anti ssDNA (poly dT) (Chemicond) and then for 30'with 1:50 Goat anti-mouse IgG2a-Alexa 647 (Molecular probes). After each incubation step, slides were washed 5 times (2' each) with PBS-Triton X-100 (0.1%). Slides were dried and mounted with 20 μL of Prolong Gold Antifade (Molecular Probes). Image acquisition was done with motorized Leica DM6000B microscope. CldU length (Kb/m) was measured

with ImageJ and fork speed was calculated multiplying measured length for the stretching factor of the MCS system (1 μm ≈ 2 kb) and dividing the resulting value for the time of CldU administration (20').

8. DRIP/qDRIP assay

DRIP assay was performed as in (García-Rubio et al., 2018) with few differences. Briefly, Genomic DNA obtained after treating HeLa or HCT116 cells with 10 μM CPT for 5, 10, 30 and 60 minutes was leaved at 30 °C for 3/4 h to permit DNA resuspension. At this point, digestion was performed O/N by adding:

-         25 μl of Buffer 2.1 NEB
-         2.5 μl of BSA NEB
-         2.5 μl HindIII (Ci =20.000 U/ml)
-         2.5 μl EcoRI (Ci =20.000 U/ml)
-         2.5 μl XbaI (Ci =20.000 U/ml)
-         5 μl BsrG1(Ci =10.000 U/ml)
-         10 μl Ssp1 (Ci =5.000 U/ml)

After purification with StrataClean Resin and Sephadex G-50 column, half of digested DNA was treated O/N at 37°C with RNase H. At the same time, 40 μl of Protein A magnetic beads per sample (Invitrogen) were incubated with 6 μl of S9.6 antibody in binding buffer 1X at 4°C. The next day, 5 μg of genomic DNA (treated or not with RNase H) were diluted in 450 μl of TE 1X with the addition of binding buffer 10X, while 1 μg was diluted in 45.5 μl of TE 1X to be used as INPUT. After adding magnetic beads to the 5 μg of DNA, immunoprecipitation was carried out at 4°C for 2h on a rotor mixer. After elution, samples were purified with Nucleo-spin Gel and PCR Clean Up Kit (Macherey-Nagel) and eluted in 150 μl TE 1X.

Enrichment over input per sample was quantified by real-time PCR using the following primers:

EGR1_Fw	GCCAAGTCCTCCCTCTCTACTG	(Salas-Armenteros et al., 2017)
EGR1_Rv	GGAAGTGGGCAGAAAGGATTG	(Salas-Armenteros et al., 2017)
SNRPN_Fw	TGCCAGGAAGCCAAATGAGT	(Salas-Armenteros et al., 2017)
SNRPN_Rv	TCCCTCTTGGCAACATCCA	(Salas-Armenteros et al., 2017)
RPL13A_Fw	GCTTCCAGCACAGGACAGGTAT	(Salas-Armenteros et al., 2017)
RPL13A_Rv	CAC CCACTACCCGAGTTCAAG	(Salas-Armenteros et al., 2017)
ACTB_Fw	GGAGCTGTCACATCCAGGGTC	(Cristini et al., 2019)
ACT_Rv	TGCTGATCCACATCTGCTGG	(Cristini et al., 2019)
SP2_Fw	GCCTAGTGCCTACCAAGTGC	(Marinello et al., 2013)
SP2_Rv	CGTGTGCATCTGAATCATCC	(Marinello et al., 2013)
APOE_Fw	CCGGTGAGAAGCGCAGTCGG	(Chedin F. personal communication)
APOE_Rv	CCCAAGCCCGACCCCGAGTA	(Chedin F. personal communication)
MYADM_Fw	CGTAGGTGCCCTAGTTGGAG	(Chedin F. personal communication)
MYADM_Rv	TCCATTCTCATTCCCAAACC	(Chedin F. personal communication)
Gemin7_Fw	TCTTCTTCCACCTGGACCAC	(Cristini et al., 2019)
Gemin7_Rv	GGGACAGAGAGAGTGCCTTG	(Cristini et al., 2019)

Tab.1 Primers for qPCR validation (human).

For DRIP-seq, two DRIP experiments were conducted in parallel and samples were pooled after the elution step. To increase the efficiency of library preparation, all samples were treated for 1h with 1 μl of RNase H at 37°C and then purified with StrataClean Resin and

Sephadex G-50 column. To concentrate the samples, they were precipitated by adding 2.5 volumes of Ethanol, 1/10 volume of Sodium Acetate 3M pH 5.3, and 1 µl of Glycogen and finally resuspended in 50 µl and then sonicated (15'' ON-30'' OFF *5 times). Library preparation and sample sequencing by Illumina paired-end (75+75 bp reads) sequencing technology was carried out by the genomic unit of CABIMER.

9. In vitro transcription assay

In vitro transcription assay was performed as described in (Hodroj et al., 2017). More detailed, 4.5 µl of T3 RNA polymerase (NEB – 50.000U/ml) were used to transcribe the plasmid pFC53 (Powell et al., 2013), which includes the *mAirn* CpG island under the control of T3 promoter. Transcription was carried out for 30 minutes at 30 °C followed by enzyme inactivation at 65°C for 10 minutes. At this point, half of transcribed plasmid was treated with 5 µl of 0.1 mg/ml RNase A (NEB) (Sample A) while the other half with 5 µl of 0.1 mg/ml RNase A and 2 µl RNase H of RNase A (NEB) (Sample B) at 37°C for 30 minutes. To remove the enzymes, Proteinase K was added for other 30' at 37°C and samples were purified with phenol:chloroform. R-loop formation was confirmed by running the samples on a 0.8% agarose gel.

Before proceeding with DRIP assay, both sample A and sample B (were split into three different sample: untreated sample (circular plasmid); ApaLI cut plasmid (linearized plasmid); HindIII cut plasmid (two-fragment plasmid). pFc53 plasmid contains the restriction sites for both the enzymes which were used according to manufacturer's instructions. At this point, ~150 ng of the plasmid were used to perform DRIP assay as previously described. For qPCR, four couple of primers were used, two designed on the R-loop forming region and two on the non R-loop region:

NRF1_Fw	TTGCCGGGAAGCTAGAGTAA	(Chedin F. personal communication)
NRF2_Rv	GCTGCCATAAGCATGAGTGA	(Chedin F. personal communication)

NRF2_Fw	TTTAGAGCTTGACGGGGAAA	Chedin F. personal communication)
NRF2_Rv	CAACAGTTGCGTAGCCTGAA	Chedin F. personal communication)
NRF3_Fw	AGGATTAGCAGAGCGAGGTATG	(Personally designed)
NRF3_Rv	GAGCGCAGATACCAAATACTGTC	(Personally designed)
RF1_Fw	CGGAATCCTACCCTCATCTG	(Personally designed)
RF1_Rv	CAGTTACCACGCAGACATCC	(Personally designed)
RF2_Fw	ACTCAGCACAACCAAGGATCA	(Personally designed)
RF2_Rv	ATTCGGAGGGTTTAGAGGGTTC	(Personally designed)

Tab.2 Primer for qPCR validation (pFC53 plasmid).

Bioinformatic analysis of DRIP-seq data

DRIP-seq libraries were quality checked using *Fastqc* and reads were trimmed using *Cutadapt* (M. Martin, 2011). Reads were aligned on human genome (hg19) using *BWA* aligner (Li & Durbin, 2009). The steps of alignment, sorting, filtering for ENCODE blacklist (Landt et al., 2012) region and duplicated reads removal were performed using Samtools (Li et al., 2009). We then performed peak calling and genomic signal computation for each library was performed using *macs2* (Y. Zhang et al., 2008). Only peaks that were present in both replicates for at least one biological condition were considered for further analysis. Read counts computation for each peak was performed by using *bedtools* (Quinlan & Hall, 2010). Differential analysis was performed with *limma* R library (Ritchie et al., 2015). DRIP-seq peak annotation was performed using DROPA(Russo et al., 2019). Plots of DRIP-seq levels over genomic features was performed using *Deeptools* (Ramírez et al., 2016).

RESULTS

Top1 poisons trigger immune gene activation in human cancer cells likely with a mechanism involving MNi and the cytoplasmic cGAS-STING pathway, as recently shown in our lab (Marinello et al., 2022). This PhD research thesis work has aimed at defining the mechanism of MNi formation following Top1 poison treatment of cells. As Top1 poisons and other unrelated chemicals (G-quadruplex binders) induce MNi in an R-loop-dependent manner (De Magis et al., 2019; Marinello et al., 2022), we have mapped R-loops in the genome of cells treated with Top1 poisons for a short time. Thus, the Results section is split into two main parts: 1) genomic R-loop mapping and 2) cell-cycle characterization of MNi formation. Bioinformatic analyses of R-loop maps have been conducted in collaboration with Marco Russo, a postdoc of our lab expert in bioinformatics and genomic analyses.

1. Part 1: *Spike-in* design and DRIP-seq analysis after CPT treatment

R-loops are known to be a source of replication stress, DNA breaks and genome instability (Aguilera & García-Muse, 2012; Hamperl & Cimprich, 2014; Okamoto et al., 2019), and R-loop-dependent MNi (De Magis et al., 2019; Marinello et al., 2022) can activate innate immune genes via the cGAS-STING pathway (Mankan et al., 2014; Marinello et al., 2022; Miglietta et al., 2021).

Top1 has a role in the modulation of R-loop levels along the genome (El Hage et al., 2010; Manzo et al., 2018), and chemical poisoning of Top1 has also been shown to increase R-loop levels (Cristini et al., 2019; Marinello et al., 2016) in a Top1-dependent manner (Marinello et al., 2016). However, there are no studies that have mapped unbalanced R-loops after Top1 poison treatment and it is still unclear the mechanism of R-loop formation. Therefore, to shed lights on the mechanism of R-loop formation following Top1 poisoning, we decided to map R-loop genome-wide after CPT treatment.

The most popular method used to detect R-loops is DNA-RNA immunoprecipitation (DRIP) and, although different variants have been proposed, DRIP-seq is still the most effective and widely used approach to map R-loops genome-wide. Briefly, the technique consists in capturing DNA-RNA hybrids by using a specific antibody called S9.6 (Boguslawski et al., 1986; Phillips et al., 2013). In almost all published studies, DRIP signal has been normalized to the total number of reads mapped from each sample. However, this normalization can introduce biases (K. Chen et al., 2016; Hu et al., 2014; Lovén et al., 2012) when comparing different samples, thus an internal standard or *spike-in* is highly recommended. Using a *spike-in* consists in adding, during sample preparation, a defined quantity of DNA-RNA hybrids from a known organism. The *spike-in* DNA will then be sequenced and used to normalize DRIP read counts and peaks in each sample (Magdalena P. Crossley et al., 2020; Šviković et al., 2019). Therefore, to map and measure R-loop levels, two different types of *spike-in* were prepared for DRIP-qPCR and DRIP-seq experiments. Firstly, we report the setup of pFC53 plasmid as a *spike-in* for DRIP-qPCR.

1.1 pFC53 plasmid as *spike-in*

The pFC53 plasmid contains the mouse Airn (mAirn) CpG island controlled by the T3 promoter (Fig.7). This region can effectively form R-loop upon *in vitro* transcription with
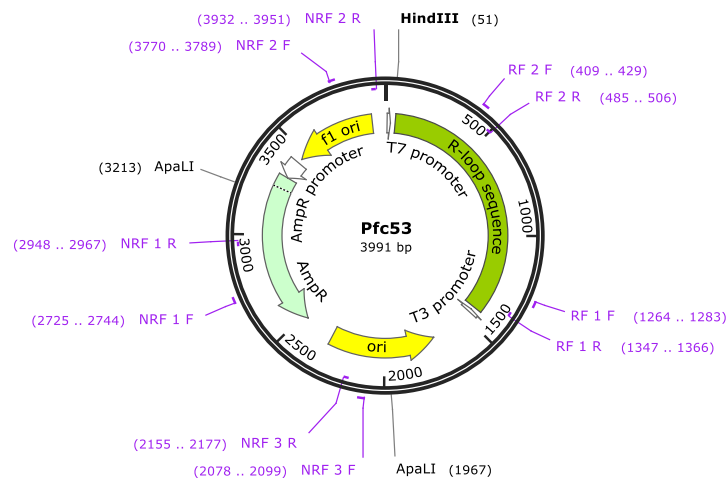
Fig.7 Graphical representation of pFC53 plasmid. *R-loop region, restriction sites and location of primers mapping are indicated.*

T3 RNA polymerase or T7 RNA polymerase (Hodroj et al., 2017). R-loop formation was validated treating the sample with RNaseA and/or RNaseH and using AFM (atomic force microscopy) images.

In Fig.8A, R-loop presence can be highlighted by the characteristic shift in mobility compared to the not transcribed sample. RNase H, but not RNase A treatment reverted the observed band-shift showing that it was specifically due to R-loops. Atomic force microscopy provided another proof of R-loop presence (Fig.8B).

A

B
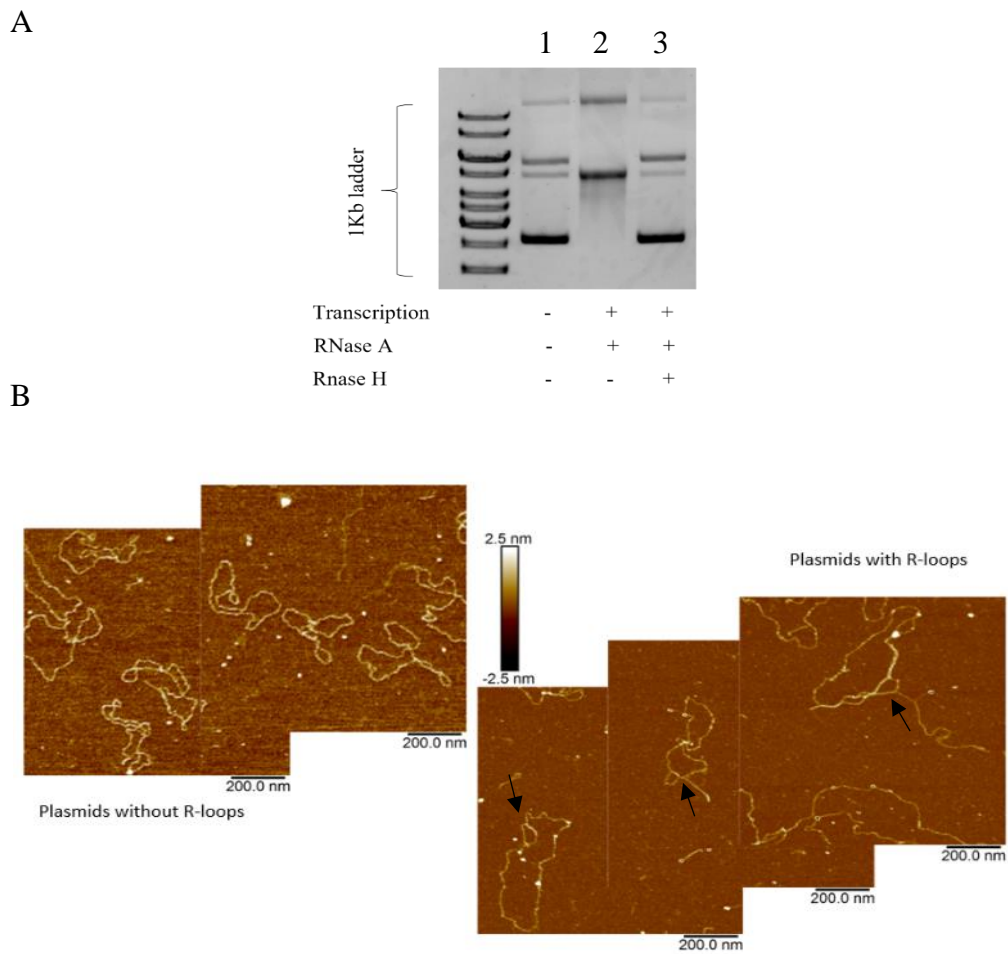
Fig.8 In vitro transcription assay (A) and atomic force microscopy images of not transcribed and transcribed plasmid. In panel (A) pFC53 plasmid (1) was transcribed and treated with RNase A only (2), or with RNase A plus RNase H (3.)

Next, to determine if transcribed plasmid would be efficiently immunoprecipitated, we performed DRIP assay using different conditions. In particular, DRIP was conducted using 150 ng of the entire plasmid or plasmid cut with ApaLI or HindIII. While HindIII linearizes the plasmid, ApaLI generates two fragments, only one containing the R-loop structure (Fig.7). To test plasmid enrichment, different couples of primers were designed in regions containing (R-loop fragment primers: RF 1; RF 2) or not containing R-loop (Non R-loop fragment primers: NRF 1; NRF 2; NRF 3) (Fig.7 and 9).

In the case of R-loop fragment primers (Fig.7 and 9A), we obtained a high plasmid recovery (immunoprecipitation (IP) fraction between 5% and 20%) for the circular and digested plasmid. The reduced recovery of digested plasmid (green and blue bar) is likely explained by the destabilization of R-loop structure after introducing a nick in the DNA (Malig et al.,
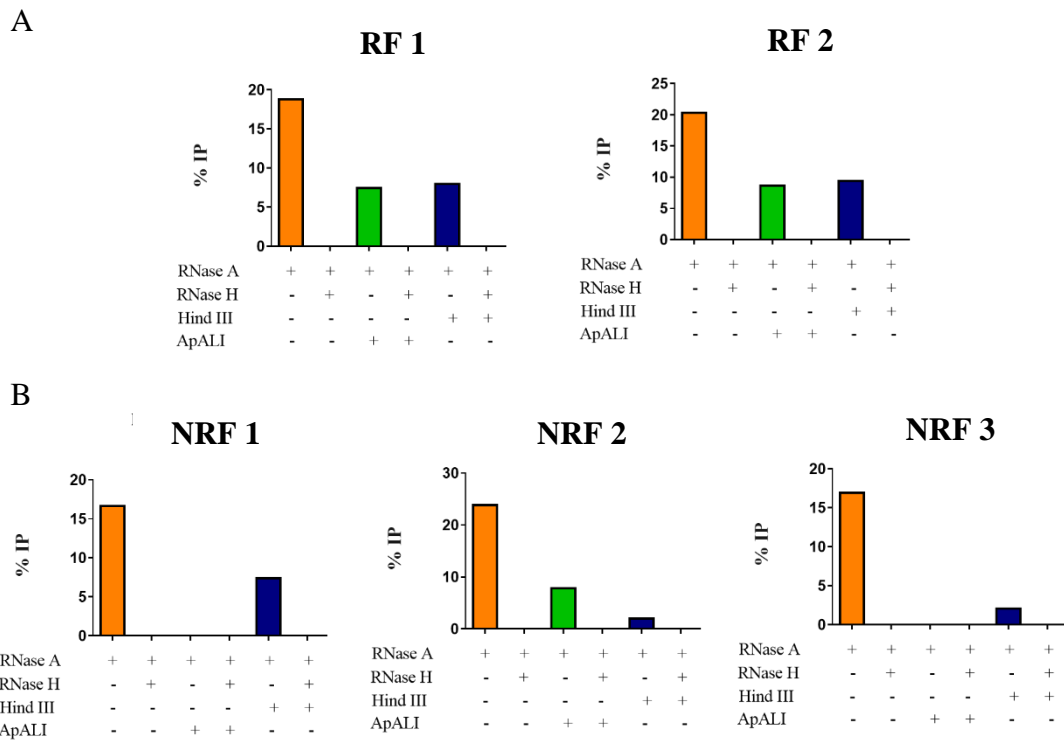
Fig.9 DRIP assay of transcribed pFC53 plasmid. Drip recovery was tested by using two couple of primers (RF1 and RF2) which map on the R-loop forming region (A) and three couple of primers (NRF1, NRF2 and NRF3) which map on the region not forming the R-loop (B)

2020; Wahba et al., 2016). If we look at the non R-loop fragment primers (Fig.7 and 9B), circular and linearized plasmids were immunoprecipitated (orange and blue bar), while we cannot observe any IP signal when the plasmid is cut with ApaLI (absent green bar). Only in case of **NRF 2** primers ApaLI digested plasmid recovery was not abolished because it maps on the R-loop containing fragment even if not directly on the mAirn region.
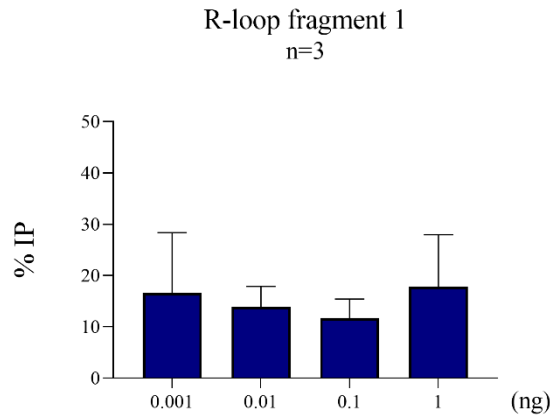
Fig.10 DRIP assay of different quantities of transcribed pFC53 plasmid. "R-loop fragment 1" primers were used to calculate the recovery rate over input.

At this point, to establish the quantity of *spike-in* to use, DRIP assay was performed using different amounts of plasmid. To have a *spike-in* as similar as possible to the main samples, 0.001 ng, 0.01 ng, 0.1 ng and 1 ng of plasmid were cut with ApaLI and added to the main samples immediately before the immunoprecipitation step. Even if the tested quantities presented similar recovery rates (Fig.10), 0.001ng and 0.1 ng were discarded because they presented unreliable Ct values of real-time PCR, comparable with negative control value. Between 0.1 and 1 ng, we chose the lowest quantity to avoid that an excessive amount of *spike-in* would compete with the main sample for S9.6 binding. Three positive genomic loci (ApoE, RPL13A and MYADM genes) and two negative loci (Gemin7 and SNRPN) were tested and the coefficient of variation (CV) was reported as a proof of the reduced variability among biological replicates after spike-in normalization (Fig.11). By comparing CV values

before and after *spike-in* normalization, we can confirm that *Spike-in* worked and that tested plasmid DNA is a good standard for DRIP-qPCR.
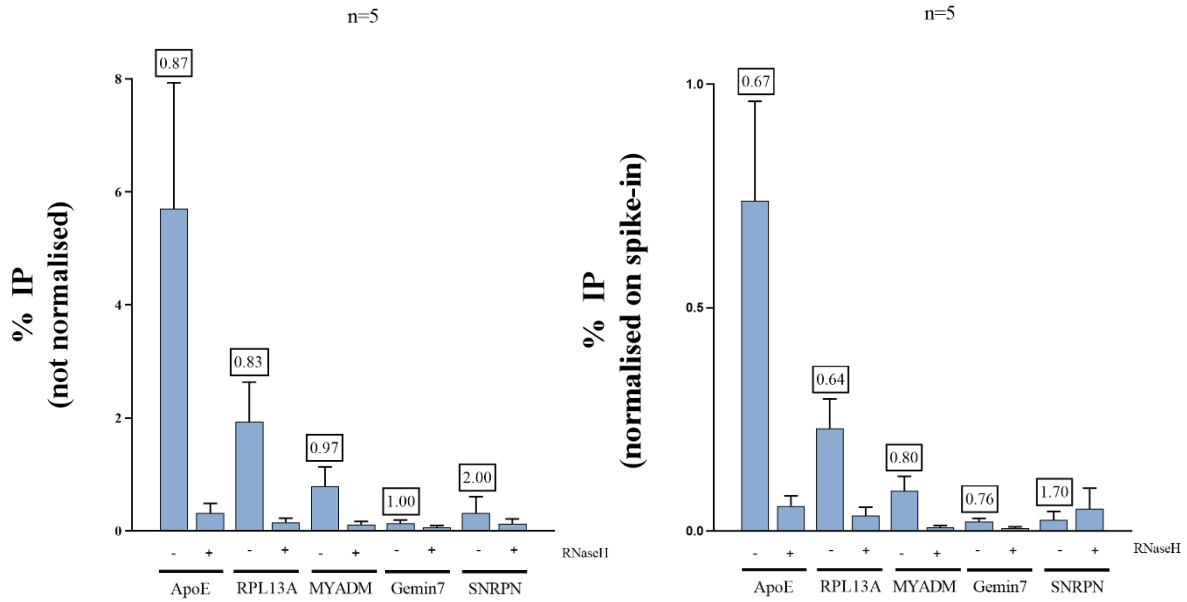
Fig.11 DRIP assay of non-treated samples after pFC53 spike-in addition. CV (coefficient of variation) value is reported in the box for each analyzed locus.

1.2 Genomic Yeast DNA as *spike-in*

To perform DRIP-seq experiments, we have employed genomic DNA from *S. cerevisiae* as *spike-in*. Yeast genomic DNA was extracted, aliquoted and stored at -80°C. To set the most proper conditions for DRIP-seq with *spike-in* usage, a DRIP experiment was conducted using HeLa cells treated for 5 minutes with CPT. Immediately before immunoprecipitation step, yeast genome was added in different quantities to find the best amount which had the following characteristics: not too high to compete with the main sample for available antibody; with a reliable Ct value to be quantified with real-time PCR. Thus, immediately before immunoprecipitation, 0.5 ng, 5 ng and 50 ng were added to the 5 µg of the main samples. Yeast genome was added to input samples using the same ratio (1:10000; 1:1000; 1:100).

PDC1 and RPL13A loci were used to evaluate the relative abundances of *spike-in* and HeLa genome, respectively. Surprisingly, from Fig.12 it seems that 0.5 ng of *spike-in* showed the highest recovery even if it was the smallest assayed quantity. Considering that the Ct values of these samples were very high and not reliable, we thought that 0.5 ng could not be adequately detected by qPCR. The two remaining quantities presented similar Ct and % of immunoprecipitation but we saw that at 5 ng the % IP of the main samples was the most similar to the sample without *spike-in*. This means that, with this amount, there was no competition between yeast and human genomic sites.
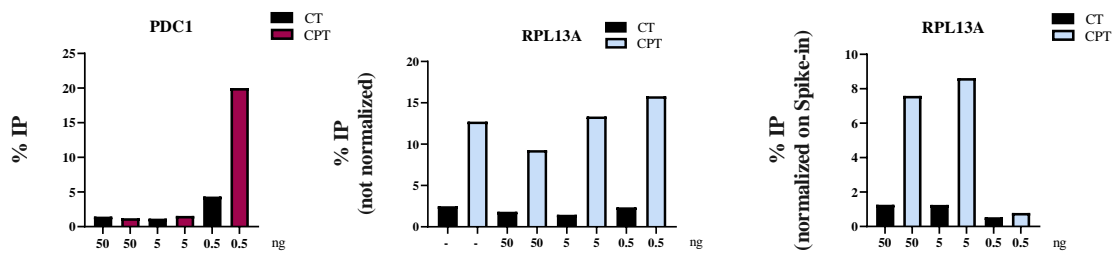
Fig.12 DRIP assay after yeast genome as spike-in. PDC1 locus for yeast genome and RPL13A for human genome were analyzed by real time PCR.

1.3 DRIP assay in HeLa and HCT116 cells after CPT treatment

To study how R-loops form after Top1 poisoning we treated HeLa cells with CPT for 5, 10, 15 and 60 minutes and DRIP assay was performed according to the protocol reported in (García-Rubio et al., 2018). Even if R-loop increase has already been shown after CPT treatment, no one was successful in determining such increase by DRIP technique. To be sure of the specificity of DRIP results, part of genomic samples was treated with RNase H before the immunoprecipitation step.
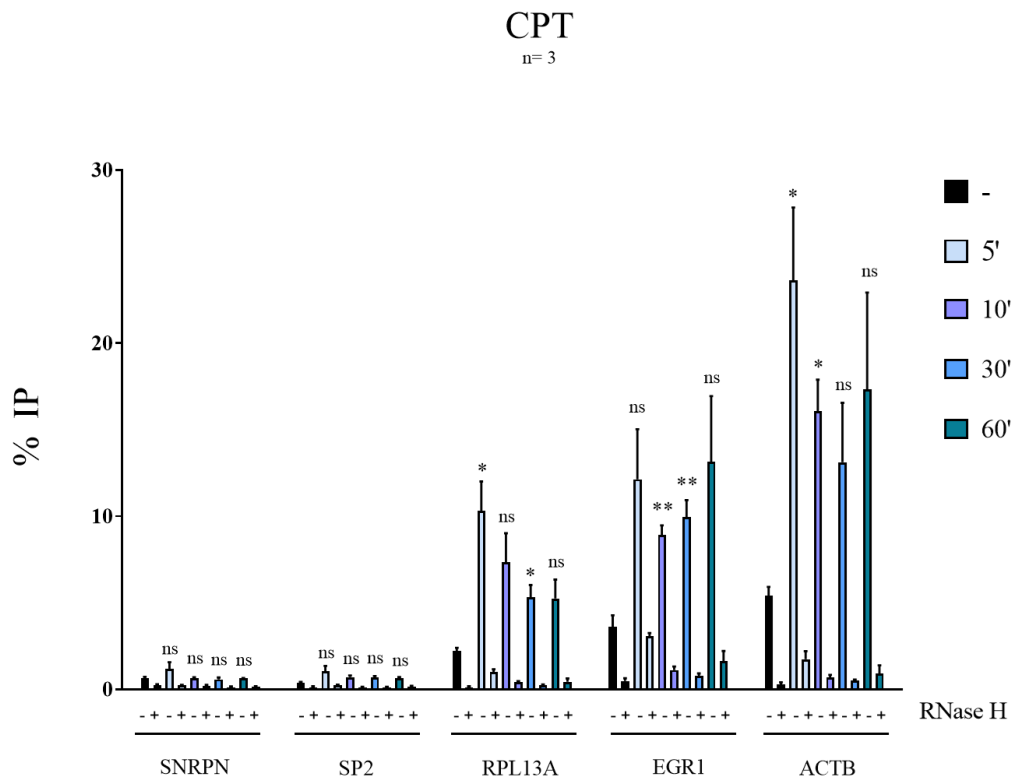
Fig.13 DRIP assay after treating HeLa cells with CPT. Statistical significance was calculated comparing treated samples with control and using Whelch's test. * P ≤ 0.05, ** P ≤ 0.01, *** P ≤ 0.001, **** P ≤ 0.0001. Each bar represents the mean value ± SEM.
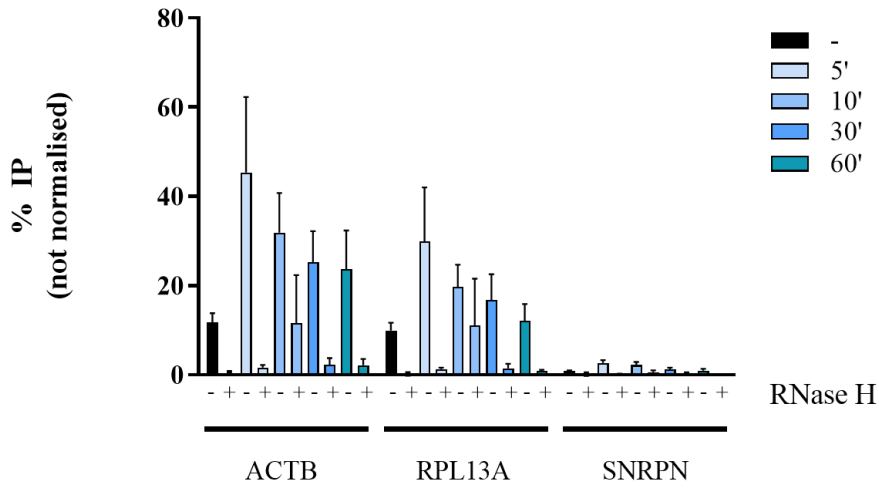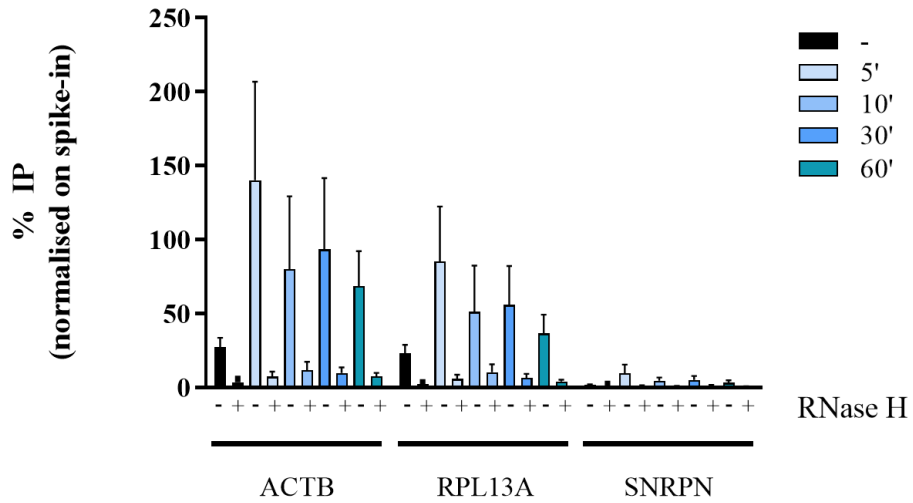
Fig.14 DRIP assay after treating HCT116 cells with CPT before (A) and after the Spike-in normalization (B).
Statistical significance was calculated comparing treated samples with control and using paired T-test. Results
were not statistically significative. Each bar represents the mean value ± SEM.

Surprisingly, we were able to observe an increase of DRIP signal confirming IF data reported in HCT116 cells (Marinello et al., 2016) and others recently obtained in HeLa cells (Marinello et al., 2022). In particular, the higher signal increase was detected after 5 minutes at positive loci (RPL13A-EGR1-ACTB) and then goes down at later times, even if it remains higher than in control sample (Fig.13). The very low % IP of the negative locus SNRPN and of RNaseH-treated samples show that we measured R-loop levels at these genomic loci. DRIP results were confirmed in human HCT116 cells. In particular, a higher increase of R-loop signal was detected after 5 minutes of CPT treatment and a decrease of R-loops was detected at later times (Fig.14) in agreement with published data (Marinello et al., 2013, 2016). Moreover, the data confirmed the validity of our *spike-in* in DRIP assay.

1.4 DRIP-seq of HCT116 cells after CPT treatment

Next, we performed two DRIP-seq experiments with the addition of yeast genomic R-loops as *spike-in* with Yeast:Human genome ratio of 1:1000, using human colon cancer HCT116 cells. R-loop maps in these cancer cells would allow a better comparison with Top1cc mapping data determined by others in the same cells (Baranello et al., 2016).

To characterize the formation of unscheduled R-loop genome-wide by Top1 poisoning, we performed DRIP-sequencing experiments after CPT treatment at different times (5 and 60 minutes). By Illumina paired-end (75+75 bp reads) sequencing technology, DRIP-seq libraries were prepared from immunoprecipitated samples (CT-IP; 5'-IP; 60'-IP), input samples (CT-IN; 5'-IN; 60'-IN) and RNaseH-treated sample (negative control: CT-H-IP; 5'-H-IP; 60'-H-IP).

Sample Name	M Reads	Mapping results		
		Human	Spike in	%Spike in
CT-IN Rep1	29.9	29,821,112	63,706	0.21
CT-IN Rep2	100.4	100,045,059	212,135	0.21
CT-IP Rep1	33.4	32,756,496	393,632	1.19
CT-IP Rep2	45	43,795,519	678,649	1.53
CT-H-IP Rep1	19.3	18,628,385	607,003	3.16
CT-H-IP Rep2	22.1	19,235,903	2,611,509	11.95
5-IN Rep1	42.5	42,325,044	93,566	0.22
5-IN Rep2	64.7	64,483,785	144,734	0.22
5-IP Rep1	25	24,645,737	227,812	0.92
5-IP Rep2	34.1	33,196,387	607,765	1.80
5-H-IP Rep1	6.3	5,899,716	409,120	6.48
5-H-IP Rep2	26.3	24,465,442	1,664,540	6.37
60-IN Rep1	49.5	49,270,972	107,814	0.22
60-IN Rep2	71.3	71,024,002	147,883	0.21
60-IP Rep1	18.7	18,180,002	266,750	1.45
60-IP Rep2	40.9	39,834,887	674,404	1.66
60-H-IP Rep1	2.7	2,545,318	183,098	6.71
60-H-IP Rep2	37.5	35,785,693	1,495,034	4.01

Fig.15 Filtered reads summary

Fig.15 shows the number of reads for each sample after they were trimmed, quality filtered and aligned as described in Material and methods section. It can be seen that input libraries generally have a higher number of human reads and a lower percentage of yeast reads (*spike-in*). On the other side, immunoprecipitated libraries have generally a lower number of reads than input samples, but they are sufficient for mapping and further analyses. As expected, RNaseH-IP libraries have the lowest number of filtered reads which consequently lead to a major amplification of *spike-in* reads. After peak calling, peaks and DRIP-seq levels were normalized using both library dimension and *spike-in* percentage.

Dot plots in Fig.16 report read counts for each called peaks of the two biological replicates, to check whether normalization can reduce technical variability in peak intensity. As shown, normalization by both total read counts (library normalization) as well as *spike-in* counts can reduce technical variability to minimum levels.
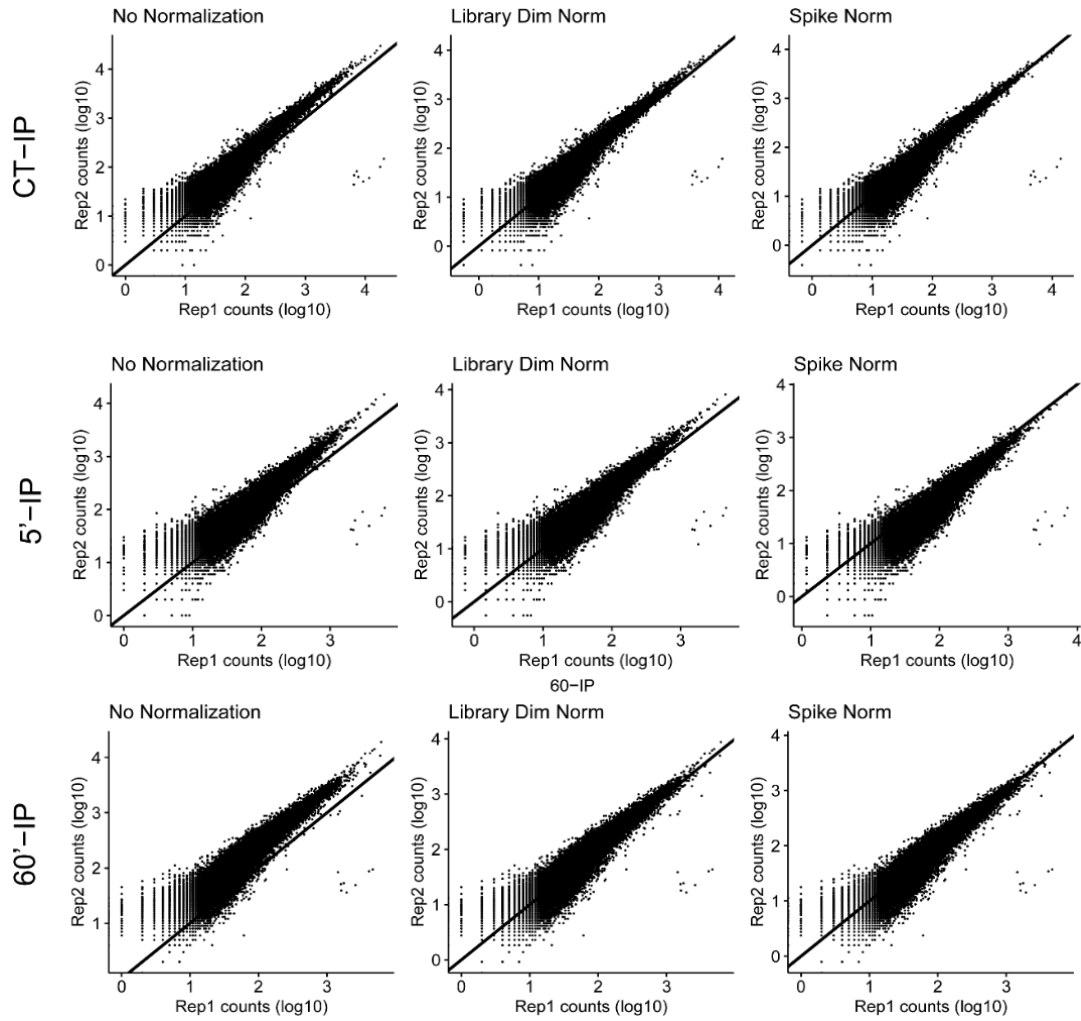
Fig.16 Immunoprecipitated sample signal without any normalization or after normalizing on library dimension alone or together with Spike-in. Each dot represents a DRIP-seq peak. X- and y- axis indicates read counts for each peak for replicate 1 and 2, respectively. Bisector lines indicate the condition in which Rep1 and rep2 counts are identical.

After normalization, Principal Component Analysis (PCA analysis) of read count levels over called peaks was performed (Fig.17). We observed two different clusters representing IP samples and RNaseH treated samples, in Fig.17A. Furthermore, Fig.17B shows how there is a clear separation between control and treated samples (PC1) but not between samples treated for 5 and 60 minutes. This means that R-loop peaks between the two time conditions

may be more similar than between treated and untreated cells. In both graphs, a residual difference between Rep1 and Rep2 experiments can be observed (PC2).
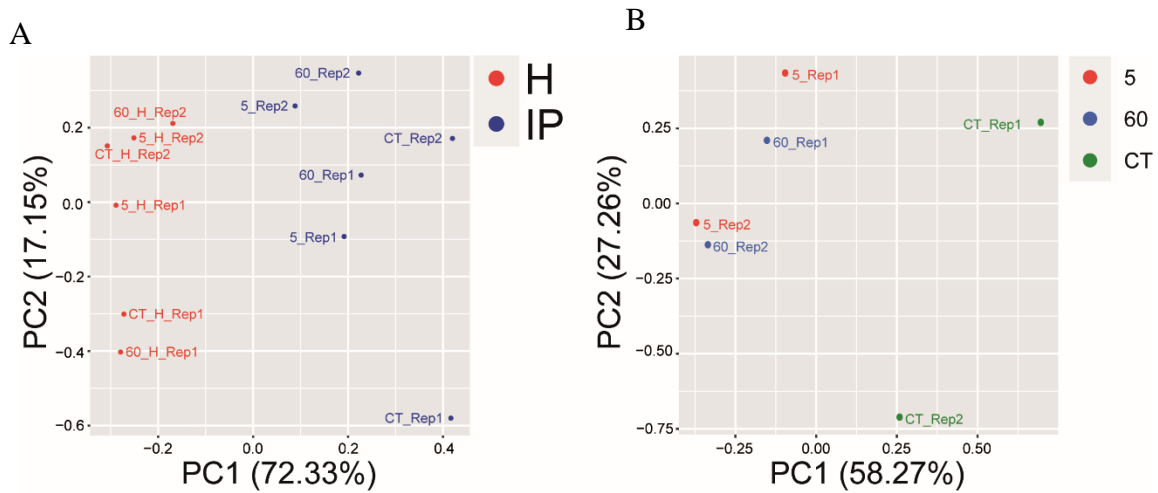
Fig.17 PCA analysis of DRIP-seq peak intensity for all libraries (immunoprecipitated samples and RNaseH negative control) (A) and of immunoprecipitated libraries only (B).

After this quality control step, a differential peak intensity analysis between IP and RNaseH conditions has been performed to remove non-specific signal appearing in RNaseH sample and, consequently, not considerable as R-loop signal. Fig.18 shows that the majority of loci found in IP samples do not present any signal in RNaseH samples, indeed only few regions (in green) were present in RNase H samples (60 of 28514 peaks).

After removing non-specific peaks, an additional differential analysis was conducted between control and treated samples. Results (Fig.19) show that, in addition to regions wherein R-loop levels remained unchanged (in green), treatment for 5' and 60' with CPT lead to both an increase (red, positive values of fold-change) and a decrease (red, negative
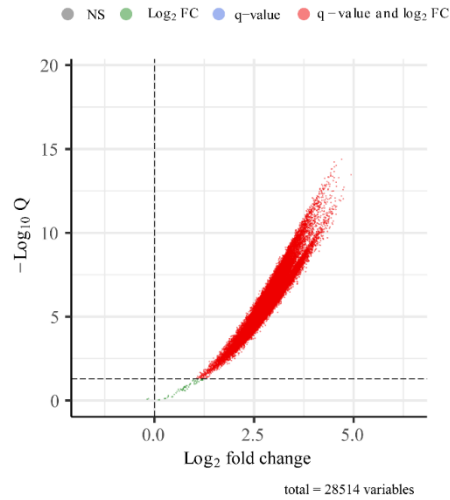
Fig.18 Differential analysis of immunoprecipitated samples versus RNaseH negative control.
Significative upregulated peaks (n=28454, red spots) have a q value < 0.05.

values of fold-change) of R-loops levels. In particular, we observed 4562 and 10645 upregulated peaks, respectively at 5' and 60', while 2573 and 4418 peaks were downregulated at the same times.

5' CPT vs CT

60' CPT vs CT
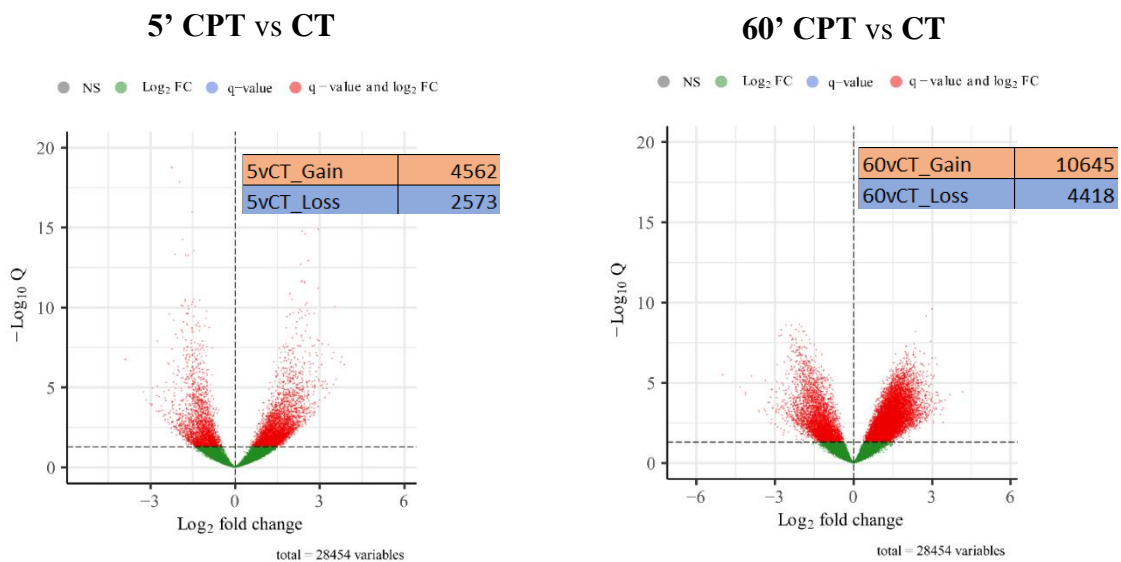
Fig.19 Differential analysis of control sample versus 5' CPT treated sample or 60' CPT treated samples.
Significative upregulated peaks (red spots) have a q value < 0.05.

1.5 CPT poisoning changes R-loop levels along the genome

As Top1 poisoning can lead to either a gain or a loss of R-loops (Fig.19), we then compared R-loop changes at the two studied times of CPT treatment, and found that genomic regions can be split into different classes depending on R-loop changes and kinetics. In particular, genomic regions can display (Fig.20):

- a **FAST** and **STABLE GAIN**: increase at 5' and 60' - **FSG**: 3,596 peaks
- a **FAST** and **TRANSIENT GAIN**: increase at 5' only - **FTG**: 966 peaks
- a **SLOW GAIN**: increase at 60' only - **SG**: 7,049 peaks
- a **FAST** and **STABLE LOSS**: decrease at 5' and 60' - **FSL**: 1,740 peaks
- a **FAST** and **TRANSIENT LOSS**: decrease at 5' only - **FTL**: 833 peaks
- a **SLOW LOSS**: decrease at 60' only - **SL**: 2678 peaks

Finally, there is also a group of regions wherein R-loop levels do not change after CPT treatments (**NO CHANGE, NC: 11,626 peaks**) (Fig.20). The NC group contains several loci wherein R-loop levels transiently increase at 5', however the increase is not statistically significant, therefore they were not included in FTG group. Overall, the number of gain peaks is higher than loss peaks, consistently with R-loop increase at short times observed in immunofluorescence experiments (Marinello et al., 2013, 2022). Interestingly, although all R-loop categories were present in all genomic area, we found that gain peaks mainly mapped at promoter and 5' UTR regions, while loss peaks were particularly enriched at gene termination and 3'UTR regions (Fig.21). To check R-loop distribution along the genome, we used DROPA peak annotation tool (Russo et al., 2019).
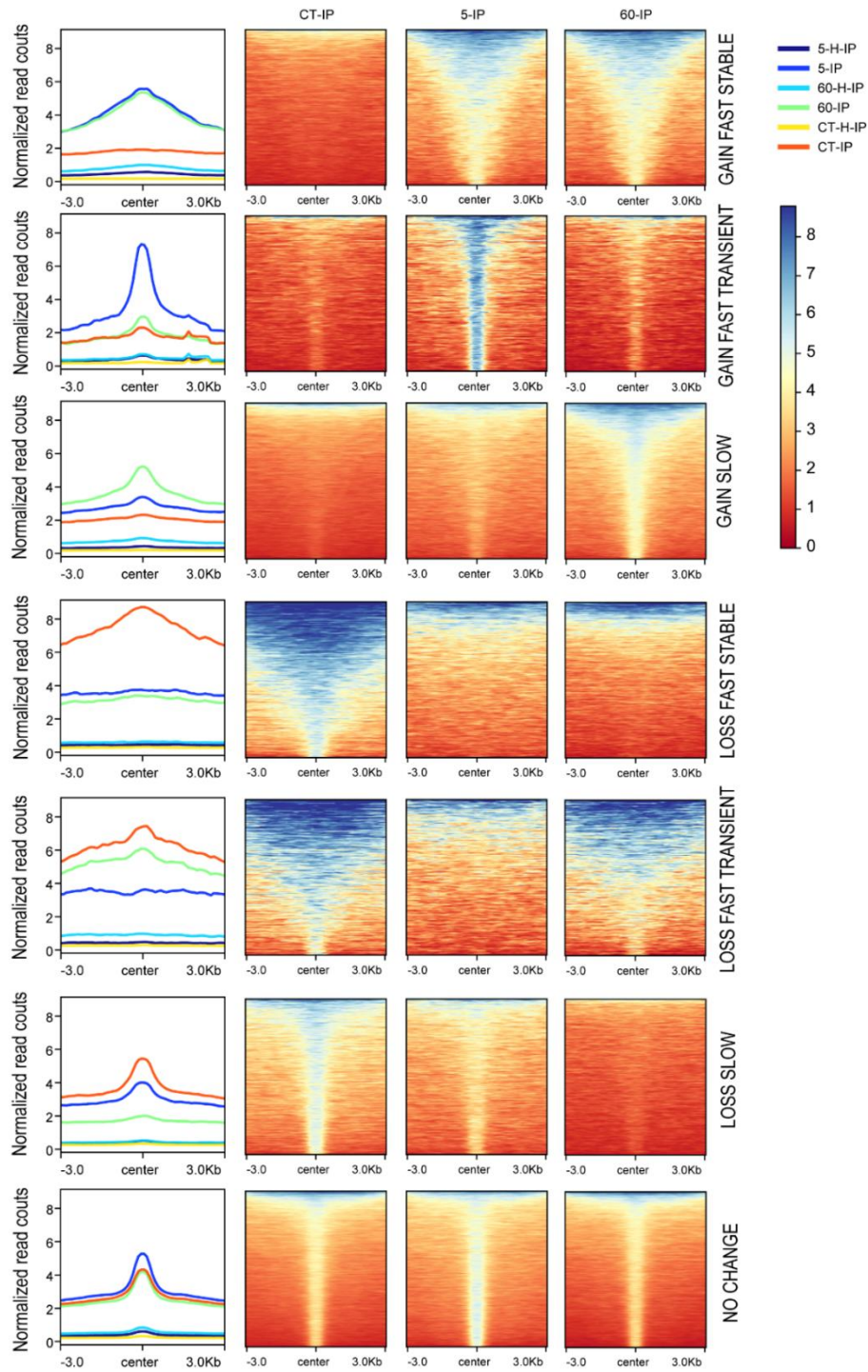
Fig.20 Heat maps showing different kinetics of R-loop gain and loss. First column represents means of DRIP seq signal in the center of each Rloop peaks (± 3 kb window, x-axis) colored as in legend. Second, third and fourth columns show intensity of DRIP-seq signal of CT-IP, 5-IP and 60-IP experiments, respectively, for each R-loop category (rows).
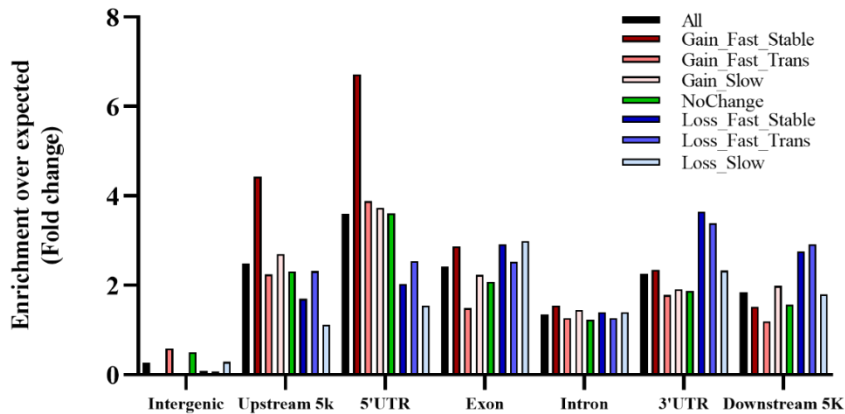
Fig.21 R-loop enrichment over genic features (x-axis) for each R-loop category, as in legend. Enrichment (y-axis) is intended as the ratio between observed R-loop peak annotation and genomic randomized peaks (n=100).

To investigate the potential role of the gene expression level in R-loop formation, we compared our data with GRO-seq data taken from (Andrysik et al., 2017). Comparing the two sequencing datasets, we observed that gain R-loop peaks, especially FSG and FTG peaks, are characterized by very high levels of active transcription compared to no change and loss peaks (Fig.22).

Then, to further address R-loop relation with transcription process, DRIP-seq data were compared with PolII sequencing data of HCT116 cell line treated with CPT for 4 minutes (Baranello et al., 2016). In this case, to see PolII occupancy related to R-loop position, we computed genomic levels of R-loop and PolII relatively to DRIP-peaks start site (RSS) for each R-loop category (Fig.23).

This analysis showed that PolII is located mainly at promoter regions, especially for R-loop gain peaks which are characterized by high transcription levels, as previously said. After CPT treatment, it is possible to observe an augment of PolII accumulation suggesting that Top1 poisons may block transcription machinery at such promoter regions. In this case, PolII signal always overlapped with R-loop peaks.
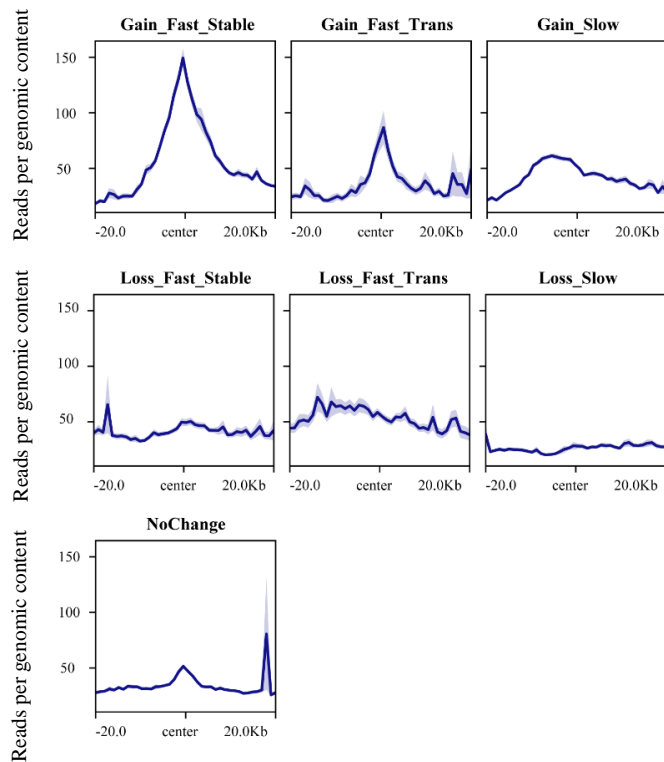
Fig.22 GRO-seq mean coverages around the centre of R-loop peaks for each R-loop category. Means of GRO seq signal were plotted in relation to the center of each Rloop peaks (± 20 kb window, x-axis).

Gene-body of gain peaks also presented a modest accumulation of PolII that increased after CPT treatment only in FSG group. In this case, PolII and R-loop signals do not coincide and, interestingly, it seems that PolII accumulates before DRIP-peaks start site. Even if further analyses are necessary to understand the biological meaning of this data, we can hypothesize that FSG R-loops forming in the gene-body may be "anterior R-loops" related to backtracked PolII (Sheridan et al., 2019; Zatreanu et al., 2019).
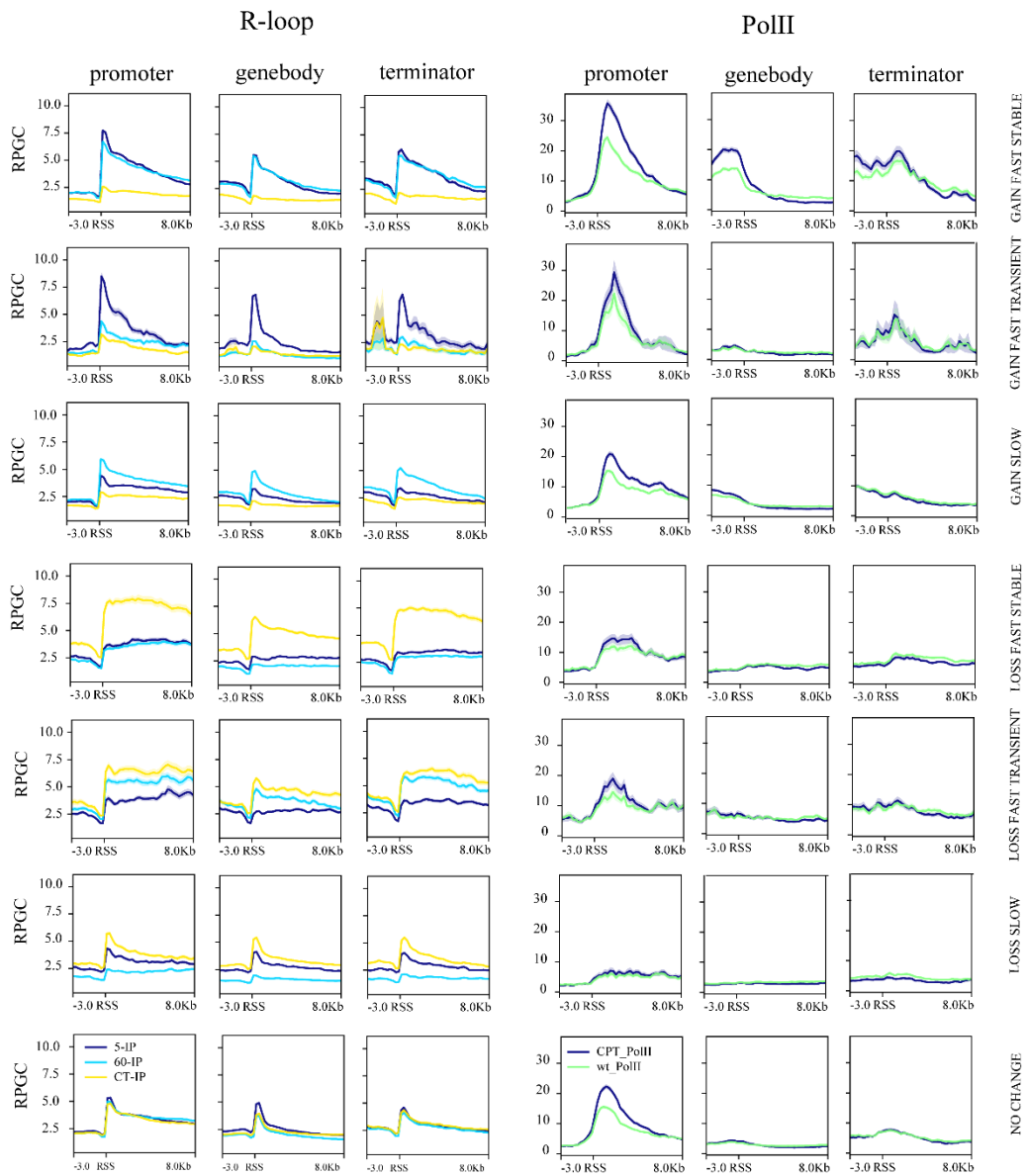
Fig.23 DRIP seq signal in the DRIP-peaks start site (RSS) (- 3 kb +8 kb window, x-axis) (left panel) and PolII-seq mean coverages around RSS for each R-loop category. RPGC= reads per genomic content.

1.6 R-loop gain regions correlate with Top1cc levels and are close to heterochromatin domains

Considering that the specific activity of CPT is to trap Top1cc on DNA, we next investigated R-loop overlap with mapped Top1 and Top1cc by comparing our results with published maps of Top1 and Top1cc in HCT116. Datasets were taken from (Baranello et al., 2016) paper where Top1 was mapped in untreated HCT116 by ChIP-seq (Top1-ChIP-seq) and Top1cc was mapped in CPT treated cells (4 minutes) by TOP1-seq, a method they developed to map catalytically-engaged TOP1.

The results (Fig.24) revealed that all peaks (gain, loss and no change) overlap with Top1 signal (Fig.24A). However, only gain peaks colocalize with Top1cc signal. In particular, in Fig.24B it can be observed a high level of colocalization between Top1cc and R-loops in FTG and FSG groups while loss categories do not overlap with Top1ccs displaying a general Top1cc level lower that NC group. The lack of overlapping between SG R-loops and Top1ccs may be due to different times of treatment, which was 4 and 60 minutes for Top1cc and R-loop detection, respectively.

Moreover, a direct comparison of Top1cc and R-loop levels revealed a solid positive correlation between the two signals. Indeed, R-loop levels following treatment with CPT for 5' are proportional to Top1cc levels (Fig.25), suggesting that CPT-induced R-loop formation can directly depend on the trapping of Top1cc.
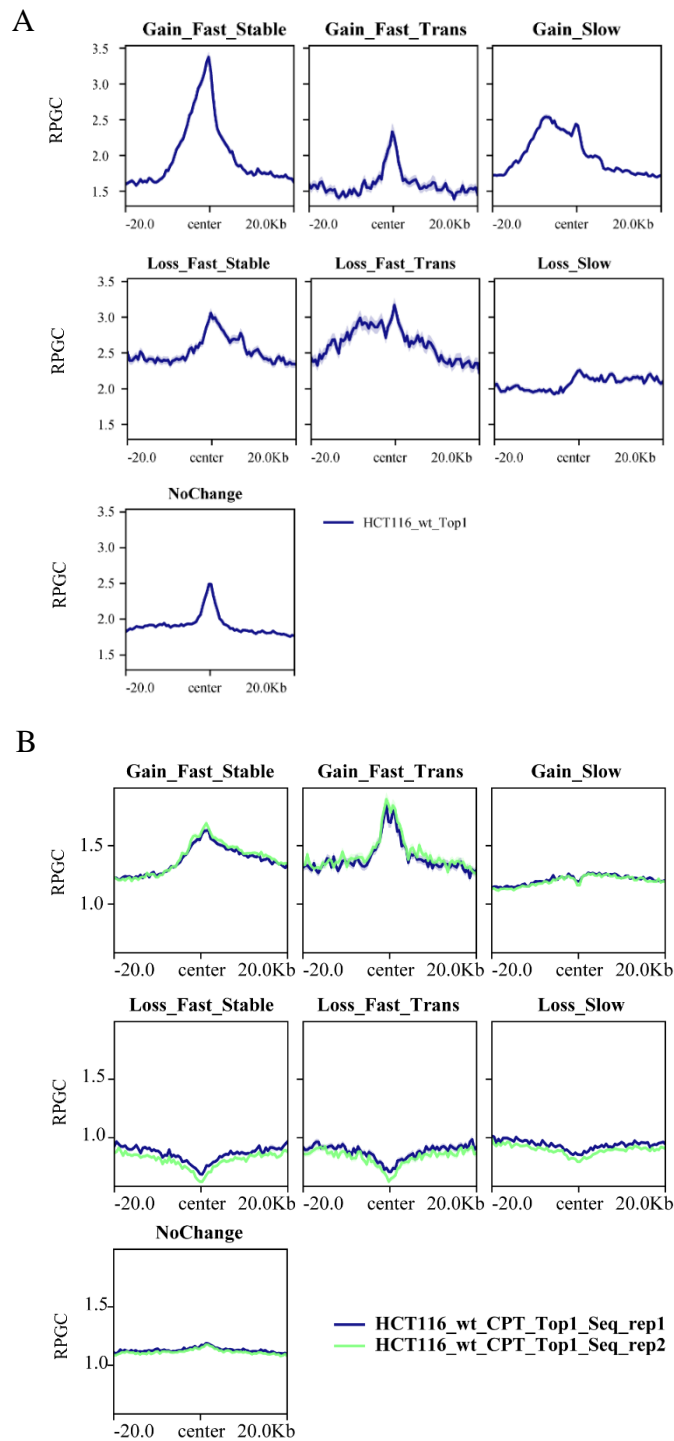
Fig.24 Top1-ChIP (A) and Top1-seq (B) mean coverages around the center of R-loop peaks for each
R-loop category. Means of Top- seq and Top1cc-seq signal were plotted in relation to center of each
Rloop peaks (± 20 kb window, x-axis). Blue and green colors of panel B represent the two biological
replicates. RPGC= reads per genomic content.

52
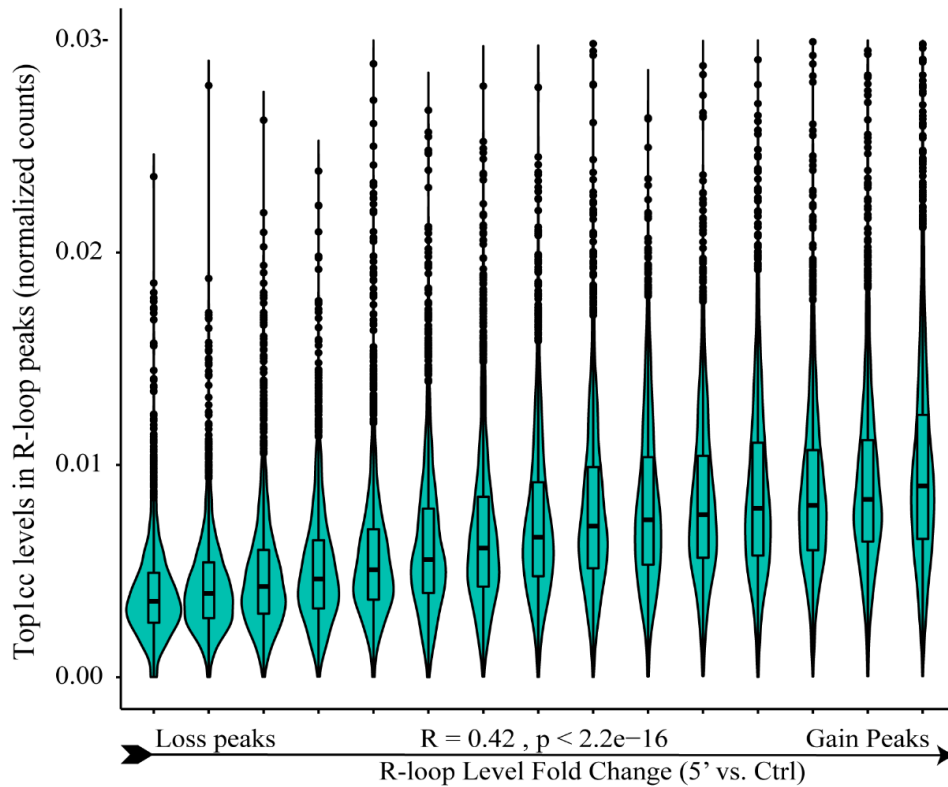
Fig.25 Correlation between Top1cc-seq levels in R-loop peaks (y axis) and R-loop fold change between 5' ***and 60'CPT treatment (x axis).*** Correlation coefficient (R) and P-value of correlation test is reported in the figure.

As chromatin boundaries and repressed chromatin spots were shown to be very close to R-loop gains in cells with silenced Top1 gene (Manzo et al., 2018), we investigated the relations of the regions with altered R-loop levels with lamina-associated domains (LADs). We found that gain peaks overlap or they are very close to LADs, while loss peaks showed the opposite trend. The analyses have been made considering the distance between R-loops and the nearest annotated LAD locus. From this analysis, we found that, compared to "No-Change", "Gain Fast" R-loops are significantly closer to LADs than "loss" groups, which instead display the longer distance (Fig.26). The data support the hypothesis that when Top1 activity is impaired, LADs may represent a physical boundary to the passive diffusion (dilution) of negative supercoils along the DNA duplex.
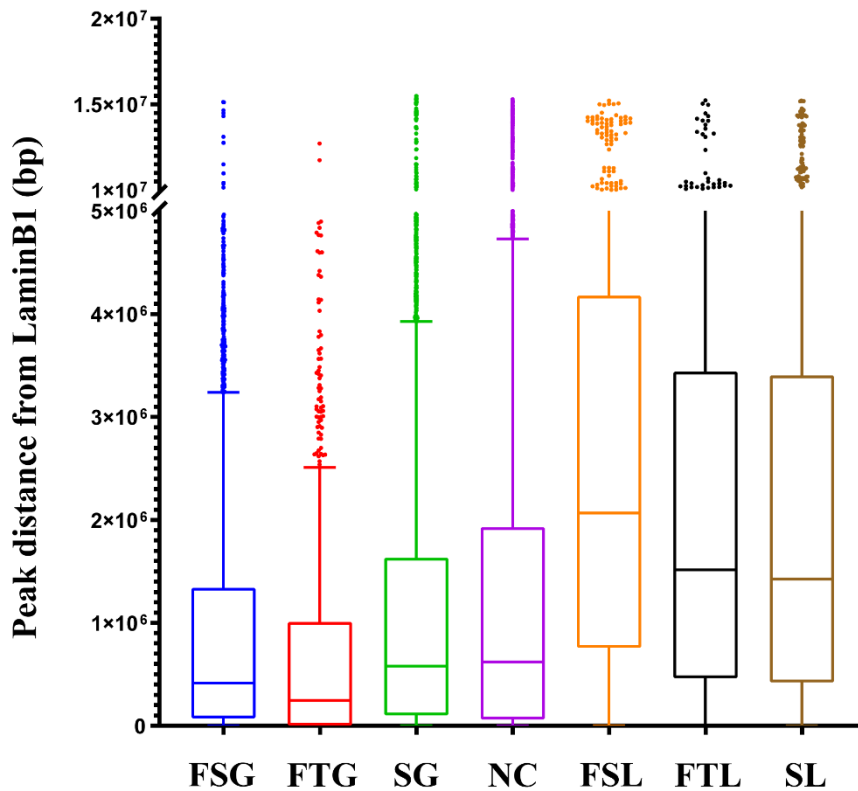
Fig.26 Distance between R-loop peaks and LADs. *For each peak category (x-axis) distance between R-loop peaks and the nearest lamina associated domain (LAD) was computed (y axis).*

1.7 R-loop decrease correlates with replication origins

Considering the importance of Top1 activity in replication process and the already known impairment of replication after Top1 poisoning, we decided to compare our DRIP data with the analysis of replication origin sites performed with Short Nascent Strand sequencing (SNS-seq) analysis (M. M. Martin et al., 2011)

From this evaluation, it turned out that loss and no change of R-loops occurs in regions highly enriched of DNA replication origins. Conversely, gain R-loops peaks do not correlate with SNS-seq signal (Fig.27). This result suggest that Top1 may contribute to replication process through R-loop structures, in agreement with published effects of Top1 silencing (Manzo et al., 2018).
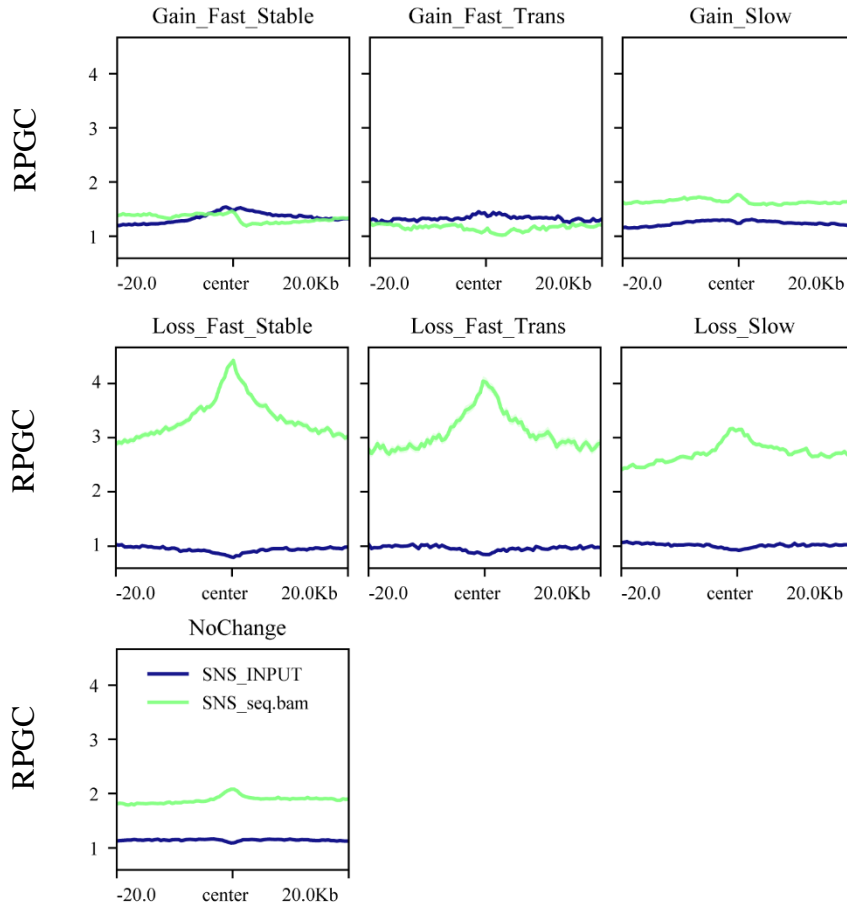
Fig.27 SNS-seq mean coverages around the center of R-loop peaks (±20 kb). *Means of SNS-seq signal were plotted in relation to center of each R-loop peaks (± 20 kb window, x-axis). RPGC= Reads per genomic content.*

2. Part 2: Cell-cycle characterization of MNi formation induced by Top1 poisons

Up to now, the presence of MNi, has been employed to evaluate the genotoxicity of chemicals. However, MNi importance has recently increased because of their ability to activate the cGAS-STIG pathway (Harding et al., 2017; MacKenzie et al., 2017; Miglietta et al., 2021). Indeed, when the micronuclear membrane breaks, DNA is poured into the cytoplasm, which rapidly recruits cGAS and induces the stimulation of innate immune genes. Despite the importance of MNi in inflammatory response activation, how they form it is not completely understood. Even less known is whether different substances can produce different type of MNi. Given the possibility for Top1 poisons to induce immune gene activation through MNi production (Marinello et al., 2022), understanding how MNi form will permit a better use of Top1 poisons in combination with immunotherapy. Therefore, to understand how MNi formation occurs after Top1 poisons, we have characterized several cell-cycle related aspects of Top1 poison-induced MNi by using immunofluorescence microscopy, cytofluorimetry and combing assay.

2.1 Top1 poisons induce the formation of EdU- but not EdU+ MNi

Previous findings of our laboratory showed that sub-cytotoxic doses of structurally-different Top1 poisons, CPT and LMP776, induce the formation of MNi in different cancer cells lines, leading to the activation of innate immune genes (Marinello et al., 2022). With the intention of understanding how MNi form and considering that low doses of poisons can cause replication inhibition and stress (Holm et al., 1989; Hsiang et al., 1989; Ray Chaudhuri et al., 2012), we aimed at determining whether MNi formation is triggered by replication stress, and therefore originated mainly in S-phase cells at the time of treatment. Hence, we labelled nascent DNA strands using the thymidine analog 5-ethynyl-2-deoxyuridine (EdU) during a 1-hour treatment of cells with Top1 poisons (Fig.28A). Then, after 24 hours from treatment, cells were analyzed with immunofluorescence microscopy for MNi formation and EdU

labelling allowed us to distinguish cells that were in S-phase during Top1 poison treatment (red cells in Fig.28B).
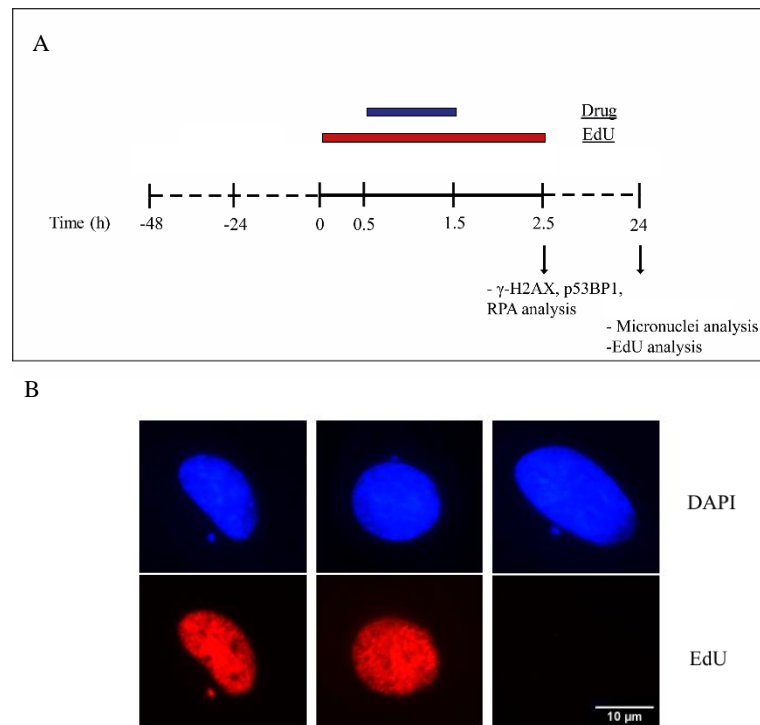
Fig.28 Experimental scheme (A) and representative images of analyzed MNi in HeLa cells (B).

HeLa cells were treated with 10 µM of CPT and LMP776 for 1 hour and EdU for 2 and a half hours under this scheme in Fig.28A and MNi were counted in EdU+ and EdU- cells. We could also distinguish and count EdU+ and EdU- MNi in the two cell populations. Pyridostatin (PDS), a G-quadruplex (G4) DNA stabilizing agent which does not target Top1, was used at the same concentration as an alternative drug producing MNi and stimulating the activation of innate immune genes (De Magis et al., 2019; Miglietta et al., 2021).

Altogether, Top1 poisons induced a slight but consistent increase of MNi with 1-hour treatments (Fig.29A). However, we noticed that EdU- MNi were increased 2.5/3-fold and 1.7/3-fold in EdU+ and EdU- cells, respectively. In contrast, EdU+ MNi decreased in EdU+ cells. In comparison, PDS (10 µM) was able to increase both EdU- and EdU+ MNi

(Fig.29B). The results suggest that Top1 poisons are somewhat different from PDS as they only increase MNi levels that do not contain EdU-labelled DNA. Interestingly, Top1 poisons and also PDS could stimulate MNi in cells that were not in S-phase at the time of treatment (EdU- cells in Fig.29) suggesting a mechanism that may extend to other phases of the cell cycle besides S-phase.
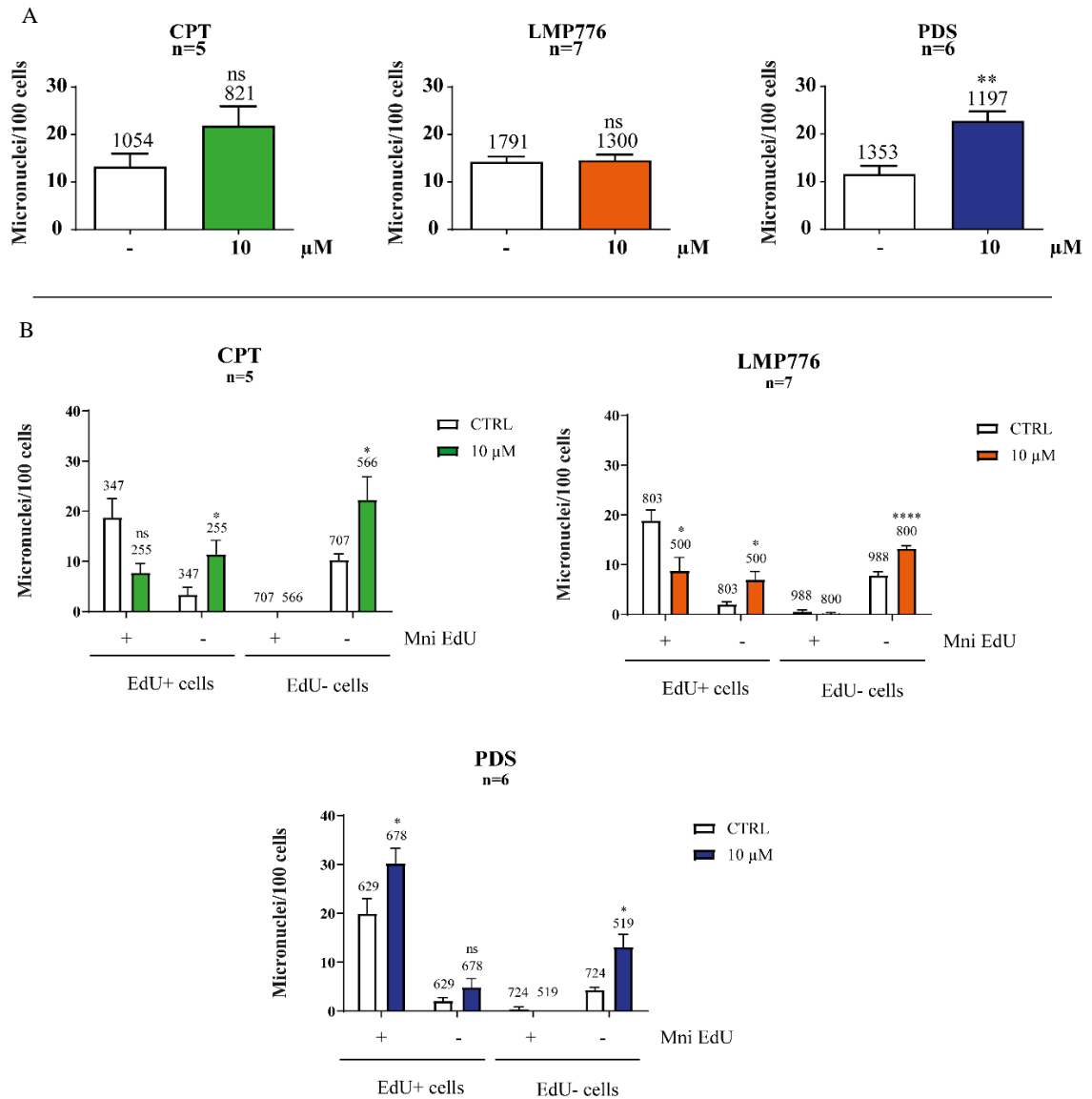
*Fig.29 Total MNi increase (A) and MNi increase in EdU+ and EdU- HeLa cells (B) after Top1 poisons and PDS treatment. Number of cells was reported over each bar. Statistical significance was calculated comparing treated samples with control and using Welch's test. * P ≤ 0.05, ** P ≤ 0.01, *** P ≤ 0.001, **** P ≤ 0.0001. Each bar represents the mean value ± SEM.*

2.2 MNi formation depends on R-loops but not on transcription

As already described in the introduction, Top1 poison increases the rate of replication-transcription conflicts and induces significant alterations of genomic distributions of R-loops (see Part 1). Thus, we tested the hypothesis that MNi increase could be related to these events. To verify transcription dependence, at the same time of drug and EdU administration, HeLa cells were treated with 50 µM of 5,6-dichloro-1-beta-D-ribofuranosylbenzimidazole (DRB) (Fig.30A), a Cdk-activating kinase inhibitor which prevents entry into the elongation phase of transcription (Darnell, 2016; Fraser et al., 1978; Mancebo et al., 1997; Y. Zhu et al., 1997). On the other side, doxycycline was used to induce RNaseH1 overexpression in U2OS-RH cells (De Magis et al., 2019) and MNi analysis was performed in induced and not induced cells (Fig.30B-30C).
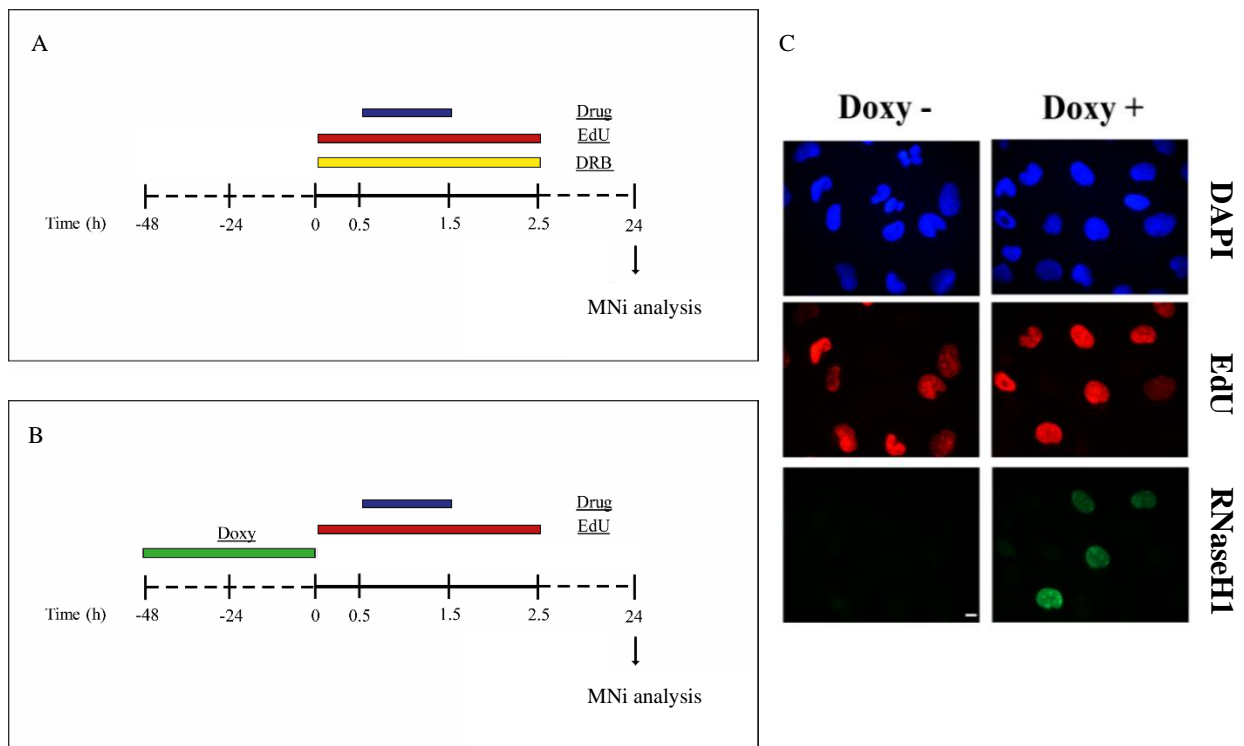
Fig.30 Experimental scheme of MNi analysis after transcription inhibition in HeLa cells with DRB treatment (A) and after RNaseH1 overexpression in U2OS-RH cells (B); Representative images of overexpressed RNaseH1 in U2OS-RH cells (C).

With regards to transcription dependence, from Fig.31 it can be noted that EdU- MNi formation is not affected by DRB treatment while there is a further decrease of EdU+ MNi. Considering that Top1 poisoning inhibits the transcriptional process, the results show that EdU+ MNi decrease observed after poisons treatment may depend on transcription impairment, whereas EdU- MNi increase do not.
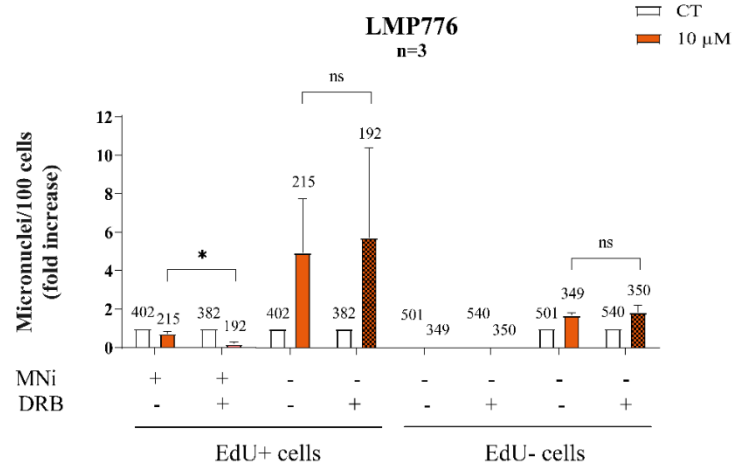
Fig.31 MNi analysis of HeLa cells treated with LMP776 after inhibiting transcription with DRB. Number of cells was reported over each bar. Each **"micronuclei/100 cells"** value was normalized over its control. EdU+ MNi over EdU- cells were not reported. Statistical significance was calculated comparing fold increase of inhibited and not inhibited samples with Welch's test. * P ≤ 0.05, ** P ≤ 0.01, *** P ≤ 0.001, **** P ≤ 0.0001. Each bar represents the mean value ± SEM.

With regards to R-loop dependence, data in Fig.32 clearly show that, even if not significative, MNi increase caused by PDS is completely dependent on R-loops. On the other side, if we look at Top1 poison-induced MNi, we can see that RNase H1 overexpression revert MNi increase but to a lesser extent than in PDS treated samples. The reduced effect is probably due to the fact that RNase H1 overexpression after doxycycline induction is variable and less than 20% of cells visibly expresses RNase H1 (Fig.30 C). As a consequence, the reported analysis include also cells which do not expresses the RNase H1. Taking this into account, it is likely that, in this system, even a low level of RNaseH1 is sufficient to resolve PDS induced R-loops and consequent MNi increase while it is not enough to entirely resolve the high R-loop levels caused by Top1 poisons (see Part 1).
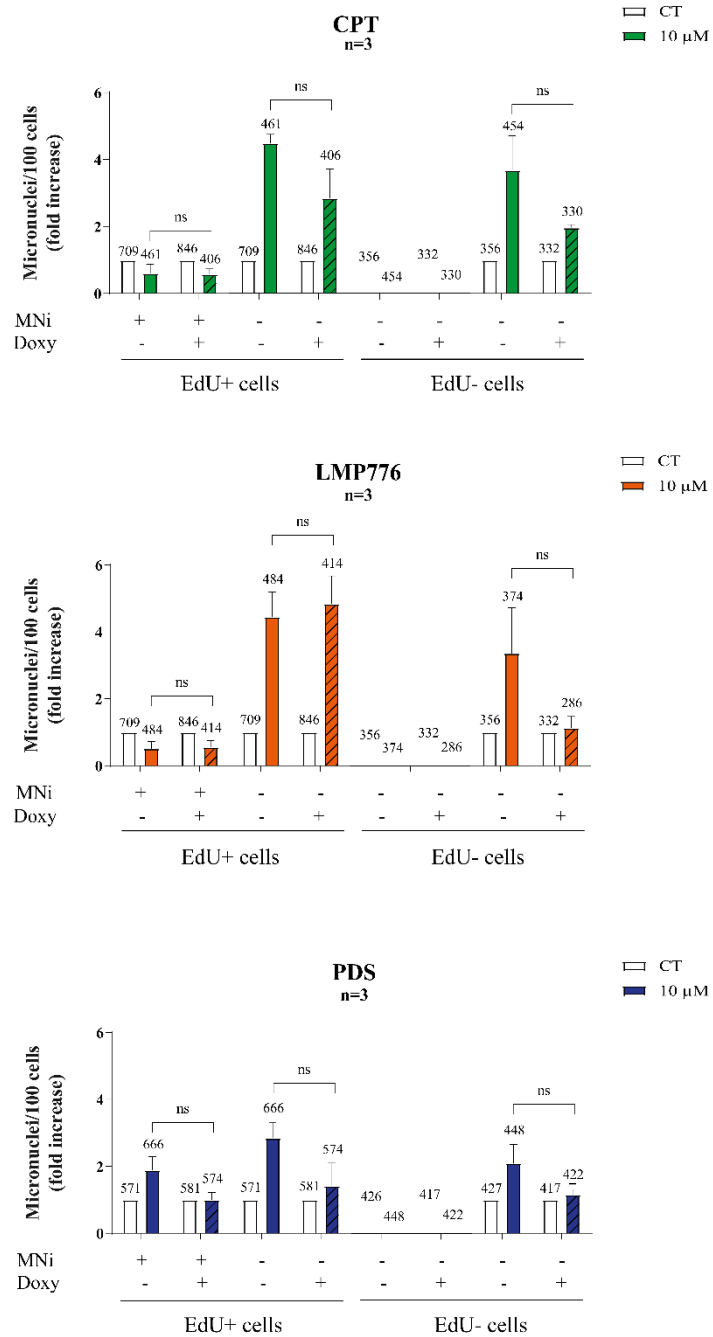
Fig.32 micronuclei analysis after treating U2OS-RH cells overexpressing or not RNase H1 with CPT,
LMP776 and PDS. *Number of cells was reported over each bar. Each **"micronuclei/100 cells"** value was*
normalized over its control. EdU+ MNi over EdU- cells were not reported. Statistical significance was
*calculated comparing fold increase of induced and not induced samples with Welch's test. * P ≤ 0.05, ***
*P ≤ 0.01, *** P ≤ 0.001, **** P ≤ 0.0001***. Each bar represents the mean value ± SEM.*

Overall, the data indicate that MNi formation depends on R-loop increase caused by either Top1 poisons and PDS.

2.3 Top1 poisons inhibit replication fork rate in HeLa cells

It is already reported that treating cancer cells with Top1 poisons affects replication fork progression (Srivastava et al., 2018; Zhao et al., 2018). Considered the formation of EdU-MNi in EdU+ cells, we wanted to verify if compromised Top1 activity could lead to the under-replication of newly synthetized DNA. Therefore, we used the combing assay in HeLa cells treated with 10 µM of CPT for 20 minutes to assess CPT effects on replication rates under our conditions. As expected, treatment slowed down replication fork velocity from a value of 1 kb/min to 700 bp/min (Fig.33). When 20 minutes of recovery were left after CPT treatment, fork speed rapidly recovered confirming that the delay was reversible and due to CPT.
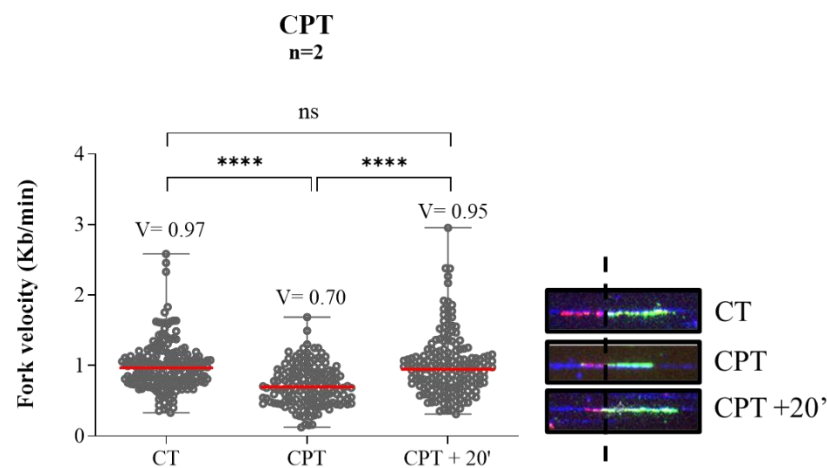
*Fig.33 Combing assay on HeLa cells treated with CPT and representative images of replication fork length with or without treatment. Statistical significance was calculated comparing treated samples with control and using Mann-Whittney test. * P ≤ 0.05, ** P ≤ 0.01, *** P ≤ 0.001, **** P ≤ 0.0001. Red line represent the median value of the samples.*

At this point, to assess if replication slowing could cause under-replication, HeLa cells were synchronized using a single thymidine block which lead to the 80 % of cells synchronized in S-phase. By immunofluorescence, EdU incorporation was measured after treating cells

for 1h with 10 µM CPT, LMP776 and PDS and leaved recover for 24h. From this analysis we saw that cells incorporate less EdU especially after treatment with CPT and LMP776 confirming the hypothesis of replication inhibition. PDS treated samples also present an overall replication impairment but to a lesser extent than the other drugs. Even if Fig.34 shows only one replicate, the result can be considered reliable because it confirms already
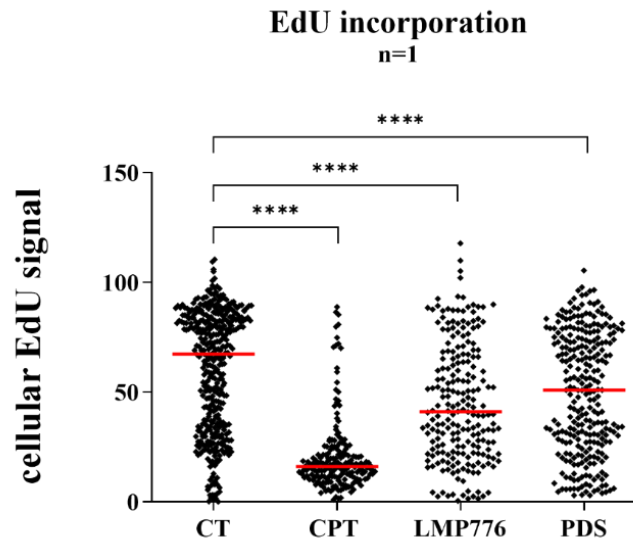
Fig.34 HeLa cells EdU incorporation after CPT, LMP776 and PDS treatment. *Statistical significance was calculated comparing treated samples with control and using Mann-Whittney test. * P ≤ 0.05, ** P ≤ 0.01, *** P ≤ 0.001, **** P ≤ 0.0001. Each point represents the fluorescence value of a single cell. Red lines represent the median value of the samples.*

published data about replication impairment after CPT treatment (Regairaz et al., 2011; Seiler et al., 2007).

2.4 Top1 poisons promote DNA damage specifically in EdU+ cells

To assess DNA cleavage levels after Top1 poisoning, we determined the levels of some DNA damage markers in immunofluorescence microscopy. We first used two antibodies against the phosphorylated forms of the H2AX histone (γ-H2AX) and p53-binding protein
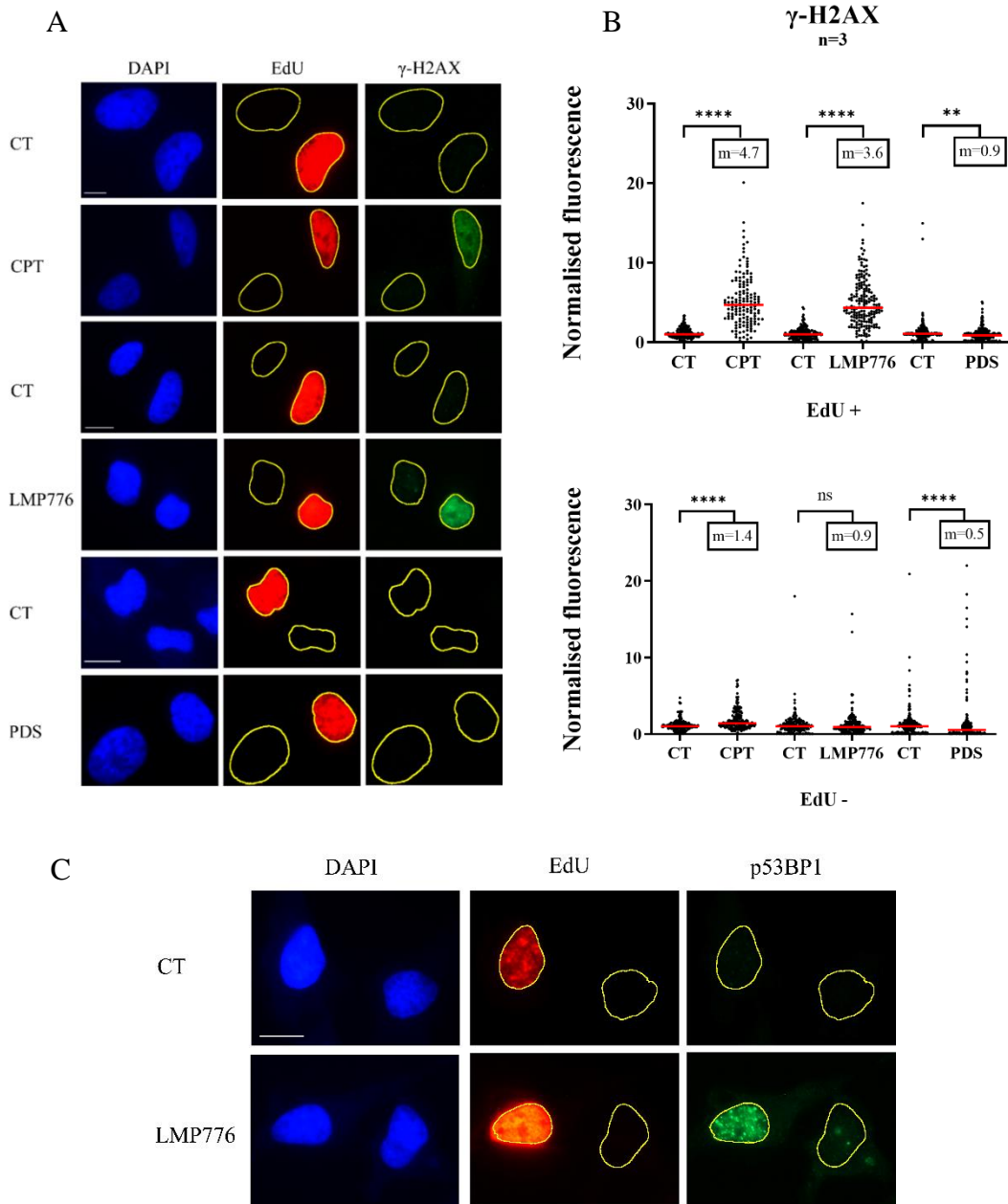
Fig.35 Representative images (A) and analysis (B) of γ-H2AX induction after CPT, LMP776 and PDS treatment; representative images of p53BP1 induction after CPT, LMP776 and PDS treatment (C). *Fluorescence values of panel B were normalized on median value of control sample. Statistical significance was calculated comparing treated samples with control and using with Mann-Whittney test. * P ≤ 0.05, ** P ≤ 0.01, *** P ≤ 0.001, **** P ≤ 0.0001. Each point represents the fluorescence value of a single cell. Red lines represent the median value of the samples also showed in the upper boxes.*

1 (p53BP1) which are markers commonly used to detect the presence of DSBs. Immunofluorescence analysis, performed immediately after drug exposure, revealed that Top1 poisons increase DNA damage signals mainly in S-phase cells. EdU- cells, instead, showed a slight, if any, increase in CPT-treated samples, while we noted a decrease of the levels of DNA damage markers for PDS and LMP776 (Fig.35).

The results were confirmed by analyzing HeLa cells stained for DAPI, EdU and γ-H2AX by cytofluorimetry. We observed that not only γ-H2AX mean value per cell increased after Top1 poisoning, but the general percentage of cells displaying DNA damage increased in EdU+ cells only (Fig.36). Thus, cytofluorimetry data further confirmed that Top1 poisons induce DNA damage specifically in S-phase cells suggesting that, unlike PDS, poisons induced DNA damage may cause MNi formation at least in S-phase cells.
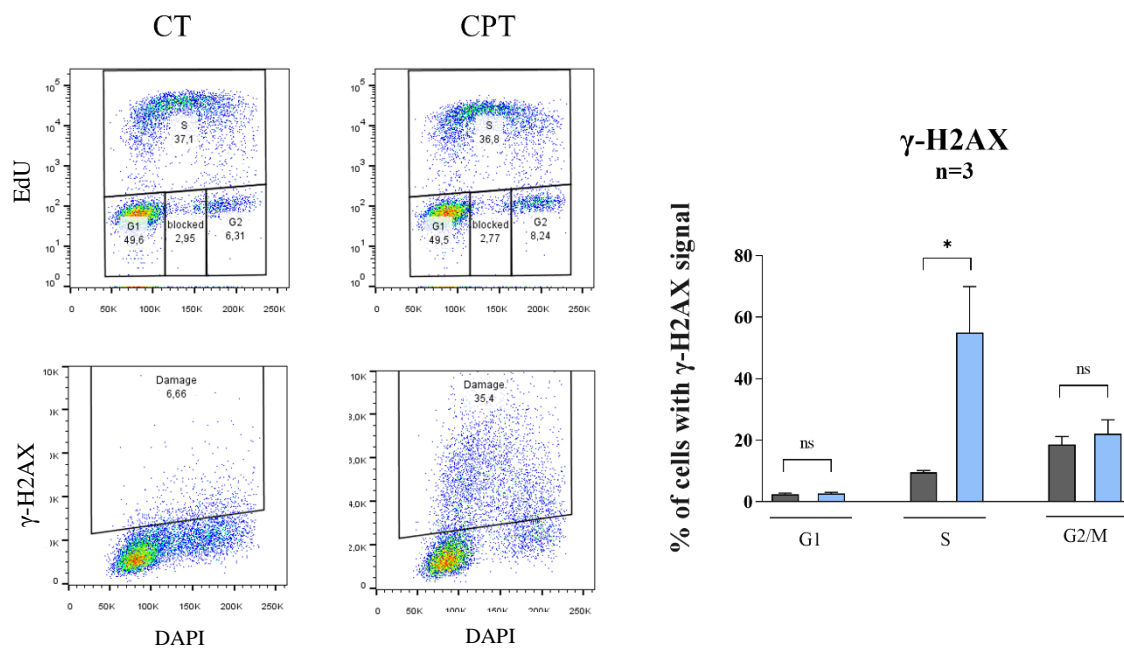
*Fig.36 Representative cytofluorimetry images (left) and analysis (right) of γ-H2AX marker in HeLa cells treated with CPT. Statistical significance was calculated comparing treated samples with control and using paired T-test. * P ≤ 0.05, ** P ≤ 0.01, *** P ≤ 0.001, **** P ≤ 0.0001. Each bar represents the median value ± SEM.*

2.6 EdU+, but not EdU-, Top1 poison-treated cells accumulate p-RPA32 foci

As already described in the introduction, Top1 poisoning produces persistent regions of ssDNA, which are bound by RPA proteins. During replication and DNA repair processes, ssDNA is coated by RPA proteins activated by phosphorylation at numerous sites of RPA32 subunit. In particular, it is already reported that CPT induce the phosphorylation of RPA32 on Ser-4/Ser-8 at seDSB (Chanut et al., 2016). Thus, we decided to investigate RPA foci as a further marker of DNA damage induced by Top1 poisons. After 1 hour treatments with LMP776, we labeled cells using two antibodies against the two largest subunits of RPA complex: RPA32, phosphorylated at Ser4/Ser8, and RPA70, which binds and stabilizes ssDNA intermediates.

Fig.37 shows that Top1 poisoning triggers RPA32 phosphorylation but mainly in EdU+ cells while RPA70 slightly reduced after LMP776 treatment. This result indicates that TOP1 poisons cause ssDNA which may accumulate at replication forks as a consequence of fork collapses due to Top1ccs and transcription-replication conflicts.
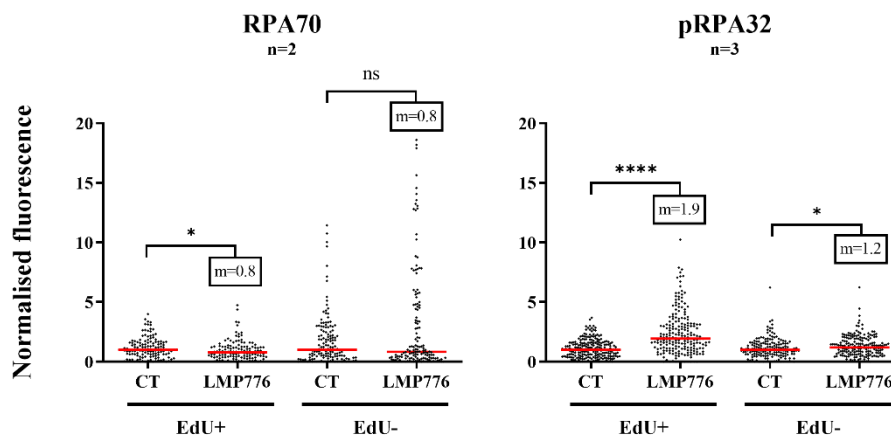
*Fig.37 Analysis of RPA70 and pRPA32 after LMP776 treatment of HeLa cells. Fluorescence values were normalized on median value of control sample. Statistical significance was calculated comparing treated samples with control and using Mann-Whittney test. * P ≤ 0.05, ** P ≤ 0.01, *** P ≤ 0.001, **** P ≤ 0.0001. Each point represents the fluorescence value of a single cell. Red lines represent the median value of the samples also showed in the upper boxes.*

2.7 Replication stress induces an asymmetric distribution of newly synthetized DNA
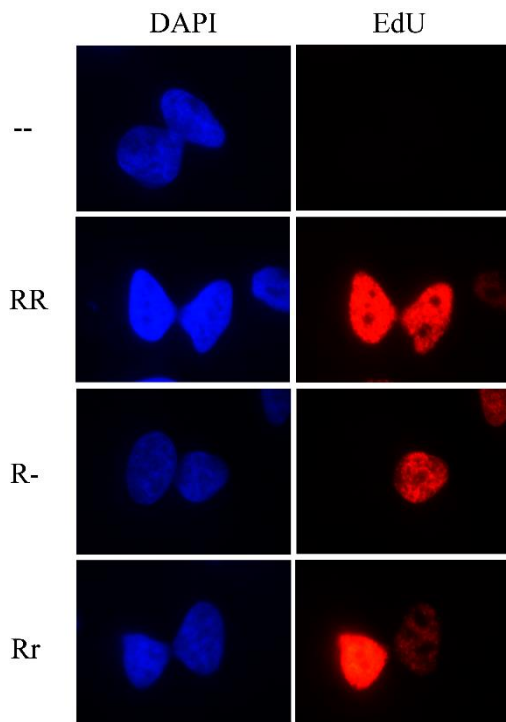
Fig.38 Representative images of EdU distribution in HeLa daughter cells.

Data reported in (Xing et al., 2020) suggest that after replication stress, cells may implement strategies to safeguards at least one of the two daughter cells. Among these strategies an asymmetric distribution of damaged DNA at mitosis step would protect cell population from genomic instability. Always in this study, a non-random distribution of MNi was observed in non-randomly segregating cells (Xing et al., 2020). This suggests that MNi formation may be involved in a cellular active mechanism to ensure cellular survival. About that, from immunofluorescence microscopy experiments performed at 24h from drug administration, we noticed that cells, immediately after mitosis exit (hereafter called daughter cells), displayed an unusual EdU distribution: only one of the two daughter cells was stained for EdU or presented a stronger signal than its sister cell. To better investigate this phenomenon, we synchronized HeLa cells at mitosis using RO3306, an ATP-competitive Cdk1 inhibitor (Vassilev et al., 2009), and analyzed cells at their first division.

Examining EdU distribution, we identified four classes of daughter cells which were called "--", "RR", "R-", "Rr" according to their EdU cellular pattern: "R" and "-" symbols were used respectively for nuclei with or without any EdU staining while "r" is used for EdU+ nuclei but with an EdU intensity 10 points lower than "R" (Fig.38). "--" and "RR" cells were considered as randomly segregating (RS) cells while "R-" and "Rr" were considered as non-randomly segregating (NRS).

Fig.39 shows a reduction in the percentage of RS cells and an increase of NRS cells especially after treatment with Top1 poisons suggesting that, during mitosis, daughter cells do not equally inherit newly synthetized DNA. Therefore, this analysis confirmed that replication stress triggered by CPT and LMPP776 really cause non-random distribution of nascent DNA between daughter cells. However, further experiments are necessary to determine MNi role in this process. In particular, we will determine if MNi distribution in daughter cells is random or whether any cellular mechanism cause a different distribution of MNi.
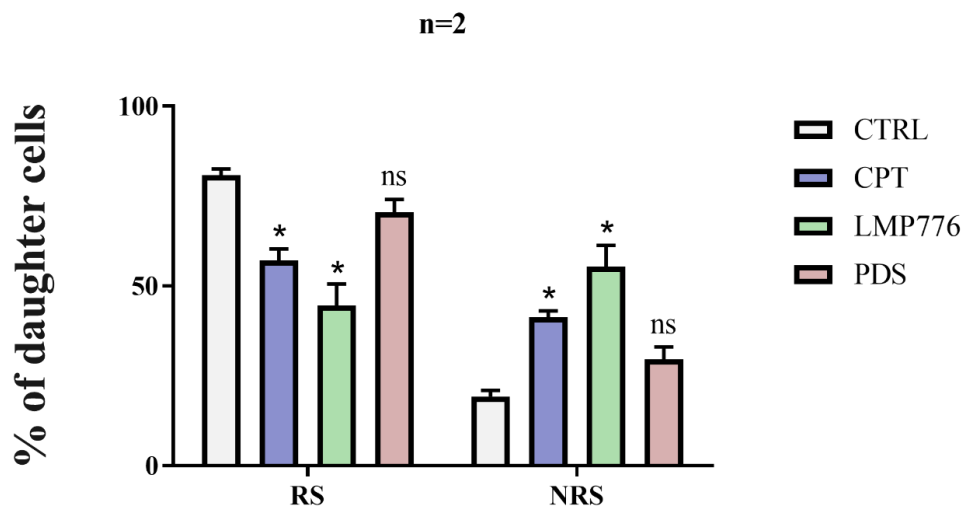
Fig.39 Daughter cells percentage after treating HeLa cells with CPT, LMP776 and PDS. *Statistical significance was calculated comparing treated samples with control and using unpaired T-test. $* P \leq 0.05$, $** P \leq 0.01$, $*** P \leq 0.001$, $**** P \leq 0.0001$. Each bar represents the mean value $\pm$ SEM.*

DISCUSSION

Cancer is still a primary cause of people death worldwide (Sung et al., 2021). In the past few years, the achievements reached by using immunotherapeutic protocols to treat cancers gave rise to a renewed interest for this approach and its combination with other strategies such as chemotherapy, radiation therapy, surgery, etc. Indeed, clinical studies show that combination immunotherapy is more effective than immunotherapy alone (Barbari et al., 2020; Drake, 2012). The combination of immunotherapy and chemotherapy is particularly interesting as anticancer drugs can have significant immunostimulatory activity (Emens & Middleton, 2015; Galluzzi et al., 2020; Saxena et al., 2020): it has been recently shown that chemotherapy efficacy is due to the involvement of the immune system (Bracci et al., 2014; Galluzzi et al., 2015; Opzoomer et al., 2019; Park et al., 2020), as many chemotherapeutics can influence the immune system acting on tumor cells and increasing their antigenicity or inducing the emission of Damage-associated molecular patterns (DAMPs) (Galluzzi et al., 2015).

In this PhD project, we mainly focused on Top1 poisons as they can induce the formation of MNi, which separate from the main nucleus after mitosis and can be a source of cytoplasmic DNA, recognized by the DNA sensor cGAS (MacKenzie et al., 2017; Miglietta et al., 2021). Thanks to the activation of the cGAS-STING pathway, Top1 poisons can activate innate immune genes in cancer cells (Marinello et al., 2022). Now, our findings shed lights on the mechanism of MNi formation in cells treated with Top1 poisons.

1. Genomic R-loop mapping

As we recently showed that R-loops can be involved in MNi formation (De Magis et al., 2019; Marinello et al., 2022), we then decided to investigate R-loop dynamics after Top1 poisoning by genome-wide mapping. For this purpose, we used DRIP and DRIP-seq techniques using the S9.6 antibody (Boguslawski et al., 1986; Phillips et al., 2013) and an internal standard (*spike-in*) to normalize DRIP and sequencing data (K. Chen et al., 2016). Taking in consideration previous settings (Magdalena P. Crossley et al., 2020; Šviković

et al., 2019), we designed two types of *spike-in* using the pFC53 plasmid, on one hand, and *S. cerevisiae* genomic DNA, on the other. By DRIP experiments we confirmed that *spike-in* normalization strongly reduced technical variability among biological replicates. Despite the functioning of the pFC53 *spike-in* in DRIP, its recovery rate resulted always very high independently from the added amount, which is probably due to the purity of *spike-in* (high amount of R-loop containing plasmid). Therefore, the tested plasmid DNA turned out to be a good standard for DRIP-qPCR but not for DRIP-seq experiments, where a too high amount of *spike-in* may lead to a poor sequencing depth of tested genomic DNA samples.

By using *spike-in*, in the first part of this PhD project we have determined genomic R-loop distributions caused by the Top1 poison CPT. Published reports showed that R-loops increase after CPT treatment (Cristini et al., 2019; Marinello et al., 2016), however, a genome-wide mapping of R-loops have not been done yet. Indeed, up to now, DRIP techniques have failed to assess levels of CPT induced R-loops (Marinello et al., 2016, 2022), as the presence of DNA nicks affect R-loop stability (Malig et al., 2020; Wahba et al., 2016) during purification of genomic DNA from CPT-treated cells. However, we were able to determine CPT-induced R-loops by using DRIP-seq protocols as already described (García-Rubio et al., 2018). We believe that differences in sample preparation may affect the final result as Top1ccs immediately revert after CPT removal, therefore requiring a cell lysis immediately upon CPT removal. Alternatively, cell types and genetic differences might affect CPT-induced R-loop stability and formation. Thus, these issues need to be addressed as a next step of this project.

Published data reports that CPT increases R-loop levels after only few minutes of treatment (Cristini et al., 2019; Marinello et al., 2013, 2016). On the other hand, a prolonged CPT exposure reverts the effect observed after 2-10 minutes, hence R-loop levels are decreased (Marinello et al., 2013, 2016). Our DRIP results in HeLa and HCT116 confirmed these findings (Fig.13 and 14): looking at different positive loci, we observed a short-term increment in R-loop signal within 5' from drug administration whereas R-loop levels were reduced after 1h although remaining higher than untreated cells (Fig.13 and 14). Genome maps have then provided a comprehensive but more complex scenario.

From differential analyses between control and treated samples, it turned out that, 5' and 60' CPT treatment lead to both an increase and a decrease of R-loops. In details, R-loop levels can change according to three different kinetics:

- R-loop gain or loss was fast and stable, occurring at 5' and persisting at 60';
- R-loop gain or loss was fast but transient because it was no more visible at 60';
- R-loop gain or loss was slow and appeared directly at 60';

If we look at the number of peaks, we realize that gain peaks are much more than loss peaks (Fig.19), in agreement with R-loop increase detected by IF assay (Marinello et al., 2013, 2022). A last group of peaks is represented by regions where R-loop levels were not affected by CPT.

First, an interesting information was achieved by comparison of R-loop maps with two Top1 datasets (Baranello et al., 2016). Here, ChIP-seq was used to map Top1 in untreated cells while a Top1-seq method was developed to map "catalytically engaged TOP1" upon CPT treatment. Thus, the two types of information were compared with our R-loop maps. The findings show that Top1 was present in, or very close to, both gain and loss R-loop peaks (Fig.24A). However, Top1ccs trapped by CPT colocalize with FSG and FTG peaks only, and not with all the other groups (Fig.24B), supporting the hypothesis that R-loop increase is due to Top1cc formation. To further support this finding, a direct comparison of Top1cc and R-loop levels revealed that as Top1cc signal increases following treatment with CPT for 5', we can observe a proportional growth of R-loop levels (Fig.25). The lack of overlapping between Top1ccs and SG peaks can be explained by the fact that Top1ccs were detected after 4 minutes CPT treatment while R-loops at SG peaks were only detected at 60 minutes from CPT administration.

Next, R-loop gains are present mainly in highly and intermediate expressed genes and preferentially at gene promoters and 5' terminal regions (Fig.21 and 22). Loss peaks were instead mainly localized at 3' terminal regions of genes (Fig.21). To explain these peak distributions, we hypothesized that R-loop increase at promoters can induce the arrest of

71

RNA pol II, which would no longer be able to continue with the transcription process. Our hypothesis was confirmed by comparing our R-loop maps with RNA Pol II sequencing datasets as reported by (Baranello et al., 2016). Here, HCT116 were treated for 4' with CPT and RNA Pol II was mapped by ChIP-seq. As expected, we detected RNA Pol II accumulation at promoter regions which increases after CPT treatment. Moreover, RNA Pol II accumulation sites colocalize with R-loop peaks (Fig.23). Arrested RNA Pol II can be a cause of R-loops stabilization at promoter while, at terminator sites, existing R-loops have the time to be rapidly resolved by multiple helicases and other removing factors since transcription has stopped or highly reduced (loss peaks).

The R-loop data are also in good agreement with redistribution of R-loops along the ACT-B gene previously reported (Cristini et al., 2019). They observed an R-loop increase in the gene-body while R-loop levels dropped at transcription start sites. Our genome-wide findings show a more detailed and general picture: upon CPT administration, gain peaks mainly localize at promoter regions while loss peaks are mostly enriched at terminator regions. Overall, gene bodies display similar level of gain and loss peaks. These limited differences may be also explained by the use of different cells, which were actively replicating in our case, while non-replicating cells were used in the other study (Cristini et al., 2019).

In a recent study (Manzo et al., 2018), R-loop genome-wide analysis in Top1-depleted cells revealed that R-loop gain peaks were very close to lamina-associated domain (LADs). Chromatin regions associated to nuclear lamina is important because it represents a physical constraint which prevents spontaneous relaxation of supercoils during transcription process (Bermejo et al., 2012). In line with data from (Manzo et al., 2018), we found that gain peaks (FSG and FTG peaks) are extremely close to LADs, while loss peaks show the opposite trend. As gain peaks are also close to arrested RNA Pol II mainly at promoter regions, their close proximity to LADs is consistent with the idea that CPT increases negative supercoils which, in turn, may favor R-loop formation/stability. Interestingly, antisense transcripts levels were increased by CPT at divergent and active CGI promoters (Marinello et al., 2013), which may correspond to an increased RNA (and R-loops) stability upstream to promoters.

72

Top1 depletion is known to cause a decrease of R-loop levels at origin of replications (Manzo et al., 2018). Therefore, by comparing our DRIP data with data obtained from reported Short Nascent Strand sequencing (SNS-seq) (M. M. Martin et al., 2011), we wanted to verify if also in case of unbalanced R-loop levels caused by CPT such a correlation occurred. We have then found that loss and no change peaks, but not gain peaks, are enriched mainly in regions with a high rate of DNA replication initiation sites. The data suggest that, in untreated cells, R-loop may contribute to replication process contributing, for example, to origin firing or, more generally, to replication initiation (Kogoma, 1997; Mazina et al., 2020; Stuckey et al., 2015).

To conclude, our work suggests that Top1 poisoning alters R-loop distribution along the genome. We found out that Top1ccs can be a direct cause of R-loop increase. If the Top1cc related nick, the consequent RNA Pol II arrest or the resolution of Top1cc causes the formation/stability of R-loops needs to be further investigated. RNA Pol II blocks at promoter regions and heterochromatin features are probably involved in this process. Therefore, regions like LADs, where supercoil dissipation is not possible, are particularly susceptible to Top1 poisoning and present high levels of R-loops. On the other side, genes characterized by loss of R-loops surprisingly overlapped with early replication origins. In control cells, high R-loop levels in this regions suggest an R-loop involvement in replication process. It would be interesting to investigate if alterations of R-loop levels at replication origins may lead to under-replication during S-phase in cancer cells (see next part of Discussion).

2. Cell-cycle characterization of MNi formation

As Top1-induced MNi formation has already been shown (Holmström & Winters, 1992; Marinello et al., 2022; K. ichi Utani et al., 2011), in the second part of this project, we have characterized cell-cycle aspects of MNi increase upon Top1 poison exposure to define the molecular mechanisms. By IF assay and using EdU to label nascent DNAs, we have analyzed MNi increase after treating cells with two structurally-different Top1 poisons (CPT and LMP776) and a Top1-unrelated compound, PDS (a G-quadruplex binder). The analyses

were performed after 24h recovery from drug removal, in order to see MNi formation at the next mitosis. By classifying cells in EdU+ and EdU-, and distinguishing also EdU+ MNi from EdU- MNi, we could observe that PDS and Top1 poisons were different as PDS caused a general increase of MNi while Top1 poisons increase EdU- MNi only, independently from EdU signal in cells. Therefore, the data suggest a some differences in the mechanisms of MNi induction by the tested compounds.

As Top1 poisons are well known to increase collisions between replication and transcription machineries (Nyamuswa & Silber, 1993; Ray Chaudhuri et al., 2012; Srivastava et al., 2018; Zhao et al., 2018), thus replication impairment might lead to an incomplete replication of DNA during treatment in S-phase cells (under-replicated or un-replicated DNA), which preferentially is then incorporated into MNi. It is already reported that under-replicated DNA can escape checkpoint surveillance mechanisms thus causing mitotic segregation defects, including MNi (Bergoglio et al., 2013; Fragkos & Naim, 2017; Minocherhomji et al., 2015) (Fragkos & Naim, 2017). We detected replication impairment due to Top1 poisons by combing assay and by quantifying EdU signal in S-phase synchronized cells. Interestingly, MNi formation seems to be independent from transcription. In addition, to assess if Top1 poisons induce MNi because of R-loop involvement, we evaluated MNi formation in a cellular system where we overexpressed RNase H1, which specifically resolve hybrid structures. With this analysis, we confirmed that Top1 poisons induced MNi in a manner dependent on R-loops.

To further investigate MNi formation mechanism, we evaluated the hypothesis that DNA damage induced by Top1 poisons may be a primary cause of MNi formation. Indeed, high levels of trapped Top1cc interfere with both transcription and replication converting the single strand breaks (SSBs) associated to Top1cc into irreversible double strand breaks (DSBs) (Khobta et al., 2006; Ljungman & Hanawalt, 1996; Seiler et al., 2007; Stephanie Solier et al., 2013; Strumberg et al., 2000; Wu & Liu, 1997). DNA damage response (DDR) and cell-cycle checkpoints are not always successful in repairing DNA damage, therefore damaged DNA can persistent in mitosis and might lead to mitotic defects and MNi (Heddle & Carrano, 1977; MacDonald et al., 2020; Wilhelm et al., 2020). In our case, IF and

cytofluorimetric experiments at 1h of treatments, highlighted that both LMP776 and CPT increase γ-H2AX and p53BP1 foci mainly in S-phase cells. In contrast, PDS did not show any significant increase of DNA damage signal. This data confirmed that DNA damage caused by CPT mostly occurs at S-phase of the cell cycle, especially at low doses (Ashour et al., 2015; Holm et al., 1989; Hsiang et al., 1989; Tomicic & Kaina, 2013). The results suggest that DNA damage may be involved in MNi formation by Top1 poisons at least in S-phase cells, somewhat in contrast with PDS.

Interestingly, we have provided evidence that Top1 poisoning produces persistent regions of ssDNA as increased levels of pRPA32 (phosphorylated Ser-4/Ser-8) foci were detected in EdU+ cells, suggesting that ssDNA accumulated during replication upon treatment with Top1 poisons, but not PDS. RPA is a protein loaded to ssDNA in response to RPA32 subunit phosphorylation during replication and repair processes forming heterotrimers with RPA70 and RPA14 (Furuta et al., 2003; Shao et al., 1999). Moreover, CPT induces the phosphorylation of RPA32 specifically at Ser-4/Ser-8 level in the presence of single-end (se)DSBs (Chanut et al., 2016). Thus, the data suggest that ssDNA induced by TOP1 poisons may accumulate at replication forks where seDSBs are likely caused by fork collapses due to Top1ccs and transcription-replication conflicts.

Altogether the findings suggest that Top1 poisons may cause mitotic segregation defects and MNi because of unresolved DNA lesions generated during S-phase cells. Under-replication has been proposed as a molecular basis for mitotic errors such as anaphase bridges (Chan et al., 2009; Fragkos & Naim, 2017), therefore Top1 poisons may cause MNi due to under-replicated regions that would lead to EdU- anaphase bridges at mitoses and consequently to EdU- MNi. Another hypothesis for the preferential generation of EdU- MNi in EdU+ cells by Top1 poisons may involve nucleases (such as Mre11) activated at collapsed replication forks (M. Zhu et al., 2018). As nucleases will degrade nascent DNAs in the attempt to restart replication, if seDSBs are then not fully and properly repaired, a DNA lesion will persist in the DNA possibly causing mitotic defects and EdU- MNi. However, as further hypotheses are possible, more experiments are needed to establish the main mechanisms.

3. Non-random segregation of nascent DNA at mitosis

MNi formation can be a way through which the cell can discard amplified genes, damaged DNA and unsolved DNA repair complexes from main nucleus (Haaf et al., 1999; Oobatake & Shimizu, 2020; K. ichi Utani et al., 2011). Thus, we wondered if Top1 related formation of MNi could be part of an active cellular response to avoid the incorporation of under-replicated or damaged DNA in the nucleus of daughter cells. More specifically, a recent work (Xing et al., 2020) linked MNi to the phenomenon of non-random segregation consequent to replication stress. Distribution of chromosomes at mitosis between the two daughter cells has historically been thought to be equal. However, recent evidence indicated the existence of an asymmetric segregation of cell components (Verbist et al., 2016; Xing et al., 2020; D. Zhang et al., 2014; Zimdahl et al., 2014). In particular, NRS can be thought as the last chance for cells to transmit the right genomic information to at least one of the two daughter cells (Xing et al., 2020). In this project, we observed that, especially after CPT and LMP776 treatment, there is an increase of cells that do not equally distribute newly synthesized DNA. Thus, MNi may be part of this active process to preserve the genome information in at least one healthy cell. However, this remains to be fully defined.

This research work has highlighted previously unknown aspects of the mechanisms of Top1 poison activity related to genome instability, altered R-loop genomic maps and production of MNi. Several aspects need to be further investigated, however our findings provide already new insights into the mechanism of Top1 poison-induced genome instability, which may be exploited for improved clinical strategies of Top1 poisons use in combination immunotherapies in cancer patients.

BIBLIOGRAPHY

Aguilera, A., & García-Muse, T. (2012). R Loops: From Transcription Byproducts to Threats to Genome Stability. *Molecular Cell*, *46*(2), 115–124. https://doi.org/10.1016/j.molcel.2012.04.009

Aguilera, A., & Gómez-González, B. (2017). DNA-RNA hybrids: The risks of DNA breakage during transcription. *Nature Structural and Molecular Biology*, *24*(5), 439–443. https://doi.org/10.1038/nsmb.3395

Andrysik, Z., Galbraith, M. D., Guarnieri, A. L., Zaccara, S., Sullivan, K. D., Pandey, A., MacBeth, M., Inga, A., & Espinosa, J. M. (2017). Identification of a core TP53 transcriptional program with highly distributed tumor suppressive activity. *Genome Research*, *27*(10), 1645–1657. https://doi.org/10.1101/gr.220533.117

Antony, S., Agama, K. K., Miao, Z. H., Takagi, K., Wright, M. H., Robles, A. I., Varticovski, L., Nagarajan, M., Morrell, A., Cushman, M., & Pommier, Y. (2007). Novel indenoisoquinolines NSC 725776 and NSC 724998 produce persistent topoisomerase I cleavage complexes and overcome multidrug resistance. *Cancer Research*, *67*(21), 10397–10405. https://doi.org/10.1158/0008-5472.CAN-07-0938

Ashour, M. E., Atteya, R., & El-Khamisy, S. F. (2015). Topoisomerase-mediated chromosomal break repair: An emerging player in many games. *Nature Reviews Cancer*, *15*(3), 137–151. https://doi.org/10.1038/nrc3892

Bailly, C., Thuru, X., & Quesnel, B. (2020). Combined cytotoxic chemotherapy and immunotherapy of cancer: modern times. *NAR Cancer*, *2*(1), 1–20. https://doi.org/10.1093/narcan/zcaa002

Baker, S. D., Wadkins, R. M., Stewart, C. F., Beck, W. T., & Danks, M. K. (1995). Cell cycle analysis of amount and distribution of nuclear DNA topoisomerase I as determined by fluorescence digital imaging microscopy. *Cytometry*, *19*(2), 134–145. https://doi.org/10.1002/cyto.990190208

Baranello, L., Bertozzi, D., Fogli, M. V., Pommier, Y., & Capranico, G. (2009). DNA topoisomerase I inhibition by camptothecin induces escape of RNA polymerase II from promoter-proximal pause site, antisense transcription and histone acetylation at the human HIF-1α gene locus. *Nucleic Acids Research*, *38*(1), 159–171.

https://doi.org/10.1093/nar/gkp817

Baranello, L., Wojtowicz, D., Cui, K., Devaiah, B. N., Chung, H. J., Chan-Salis, K. Y., Guha, R., Wilson, K., Zhang, X., Zhang, H., Piotrowski, J., Thomas, C. J., Singer, D. S., Pugh, B. F., Pommier, Y., Przytycka, T. M., Kouzine, F., Lewis, B. A., Zhao, K., & Levens, D. (2016). RNA Polymerase II Regulates Topoisomerase 1 Activity to Favor Efficient Transcription. *Cell*, *165*(2), 357–371. https://doi.org/10.1016/j.cell.2016.02.036

Barbari, C., Fontaine, T., Parajuli, P., Lamichhane, N., Jakubski, S., Lamichhane, P., & Deshmukh, R. R. (2020). Immunotherapies and combination strategies for immuno-oncology. *International Journal of Molecular Sciences*, *21*(14), 1–28. https://doi.org/10.3390/ijms21145009

Bartsch, K., Knittler, K., Borowski, C., Rudnik, S., Damme, M., Aden, K., Spehlmann, M. E., Frey, N., Saftig, P., Chalaris, A., & Rabe, B. (2017). Absence of RNase H2 triggers generation of immunogenic micronuclei removed by autophagy. *Human Molecular Genetics*, *26*(20), 3960–3972. https://doi.org/10.1093/hmg/ddx283

Bayona-Feliu, A., Barroso, S., Muñoz, S., & Aguilera, A. (2021). The SWI/SNF chromatin remodeling complex helps resolve R-loop-mediated transcription–replication conflicts. *Nature Genetics*, *53*(7), 1050–1063. https://doi.org/10.1038/s41588-021-00867-2

Bergoglio, V., Boyer, A. S., Walsh, E., Naim, V., Legube, G., Lee, M. Y. W. T., Rey, L., Rosselli, F., Cazaux, C., Eckert, K. A., & Hoffmann, J. S. (2013). DNA synthesis by pol η promotes fragile site stability by preventing under-replicated DNA in mitosis. *Journal of Cell Biology*, *201*(3), 395–408. https://doi.org/10.1083/jcb.201207066

Bermejo, R., Lai, M. S., & Foiani, M. (2012). Preventing Replication Stress to Maintain Genome Stability: Resolving Conflicts between Replication and Transcription. *Molecular Cell*, *45*(6), 710–718. https://doi.org/10.1016/j.molcel.2012.03.001

Berti, M., Chaudhuri, A. R., Thangavel, S., Gomathinayagam, S., Kenig, S., Vujanovic, M., Odreman, F., Glatter, T., Graziano, S., Mendoza-Maldonado, R., Marino, F., Lucic, B., Biasin, V., Gstaiger, M., Aebersold, R., Sidorova, J. M., Monnat, R. J., Lopes, M., & Vindigni, A. (2013). Human RECQ1 promotes restart of replication forks reversed by DNA topoisomerase I inhibition. *Nature Structural and Molecular Biology*, *20*(3), 347–354. https://doi.org/10.1038/nsmb.2501

Bharti, A. K., Olson, M. O. J., Kufe, D. W., & Rubin, E. H. (1996). Identification of a

nucleolin binding site in human topoisomerase I. *Journal of Biological Chemistry*, *271*(4), 1993–1997. https://doi.org/10.1074/jbc.271.4.1993

Boguslawski, S. J., Smith, D. E., Michalak, M. A., Mickelson, K. E., Yehle, C. O., Patterson, W. L., & Carrico, R. J. (1986). Characterization of monoclonal antibody to DNA · RNA and its application to immunodetection of hybrids. *Journal of Immunological Methods*, *89*(1), 123–130. https://doi.org/10.1016/0022-1759(86)90040-2

Bonnet, A., Grosso, A. R., Elkaoutari, A., Coleno, E., Presle, A., Sridhara, S. C., Janbon, G., Géli, V., de Almeida, S. F., & Palancade, B. (2017). Introns Protect Eukaryotic Genomes from Transcription-Associated Genetic Instability. *Molecular Cell*, *67*(4), 608-621.e6. https://doi.org/10.1016/j.molcel.2017.07.002

Bracci, L., Schiavoni, G., Sistigu, A., & Belardelli, F. (2014). Immune-based mechanisms of cytotoxic chemotherapy: Implications for the design of novel and rationale-based combined treatments against cancer. *Cell Death and Differentiation*, *21*(1), 15–25. https://doi.org/10.1038/cdd.2013.67

Braun, M. S., Richman, S. D., Quirke, P., Daly, C., Adlard, J. W., Elliott, F., Barrett, J. H., Selby, P., Meade, A. M., Stephens, R. J., Parmar, M. K. B., & Seymour, M. T. (2008). Predictive biomarkers of chemotherapy efficacy in colorectal cancer: Results from the UK MRC FOCUS trial. *Journal of Clinical Oncology*, *26*(16), 2690–2698. https://doi.org/10.1200/JCO.2007.15.5580

Bray, F., Ferlay, J., Soerjomataram, I., Siegel, R. L., Torre, L. A., & Jemal, A. (2018). Global cancer statistics 2018: GLOBOCAN estimates of incidence and mortality worldwide for 36 cancers in 185 countries. *CA: A Cancer Journal for Clinicians*, *68*(6), 394–424. https://doi.org/10.3322/caac.21492

Bray, F., Laversanne, M., Weiderpass, E., & Soerjomataram, I. (2021). The ever-increasing importance of cancer as a leading cause of premature death worldwide. *Cancer*, *127*(16), 3029–3030. https://doi.org/10.1002/cncr.33587

Burdette, D. L., & Vance, R. E. (2013). STING and the innate immune response to nucleic acids in the cytosol. *Nature Immunology*, *14*(1), 19–26. https://doi.org/10.1038/ni.2491

Burton, J. H., Mazcko, C., LeBlanc, A., Covey, J. M., Ji, J., Kinders, R. J., Parchment, R. E., Khanna, C., Paoloni, M., Lana, S., Weishaar, K., London, C., Kisseberth, W., Krick, E., Vail, D., Childress, M., Bryan, J. N., Barber, L., Ehrhart, E. J., … Pommier, Y.

(2018). NCI comparative oncology program testing of non-camptothecin indenoisoquinoline topoisomerase I inhibitors in naturally occurring canine lymphoma. *Clinical Cancer Research*, *24*(23), 5830–5840. https://doi.org/10.1158/1078-0432.CCR-18-1498

Capranico, G., & Binaschi, M. (1998). DNA sequence selectivity of topoisomerases and topoisomerase poisons. *Biochimica et Biophysica Acta - Gene Structure and Expression*, *1400*(1–3), 185–194. https://doi.org/10.1016/S0167-4781(98)00135-3

Capranico, G., Binaschi, M., Borgnetto, M. E., Zunino, F., & Palumbo, M. (1997). A protein-mediated mechanism for the DNA sequence-specific action of topoisomerase II poisons. *Trends in Pharmacological Sciences*, *18*(9), 323–329. https://doi.org/10.1016/S0165-6147(97)01095-X

Capranico, G., Marinello, J., & Chillemi, G. (2017). Type I DNA Topoisomerases. *Journal of Medicinal Chemistry*, *60*(6), 2169–2192. https://doi.org/10.1021/acs.jmedchem.6b00966

Cerritelli, S. M., & Crouch, R. J. (2009). Ribonuclease H: The enzymes in eukaryotes. *FEBS Journal*, *276*(6), 1494–1505. https://doi.org/10.1111/j.1742-4658.2009.06908.x

Champoux, J. J., & Dulbecco, R. (1972). An activity from mammalian cells that untwists superhelical DNA--a possible swivel for DNA replication (polyoma-ethidium bromide-mouse-embryo cells-dye binding assay). *Proceedings of the National Academy of Sciences of the United States of America*, *69*(1), 143–146. https://doi.org/10.1073/pnas.69.1.143

Champoux, James J. (2001). DNA T OPOISOMERASES : Structure , FunctChampoux, J. J. (2001). DNA T OPOISOMERASES : Structure , Function , 369–413.ion ,. *Annu. Rev. Biochem.*, *70*, 369–413.

Chan, K. L., Palmai-Pallag, T., Ying, S., & Hickson, I. D. (2009). Replication stress induces sister-chromatid bridging at fragile site loci in mitosis. *Nature Cell Biology*, *11*(6), 753–760. https://doi.org/10.1038/ncb1882

Chanut, P., Britton, S., Coates, J., Jackson, S. P., & Calsou, P. (2016). Coordinated nuclease activities counteract Ku at single-ended DNA double-strand breaks. *Nature Communications*, *7*. https://doi.org/10.1038/ncomms12889

Chédin, F. (2016). Nascent Connections: R-Loops and Chromatin Patterning. *Trends in*

Genetics, *32*(12), 828–838. https://doi.org/10.1016/j.tig.2016.10.002

Chedin, F., Benham, C. J., & Musier-Forsyth, K. (2020). Emerging roles for R-loop structures in the management of topological stress. *Journal of Biological Chemistry*, *295*(14), 4684–4695. https://doi.org/10.1074/jbc.REV119.006364

Chen, K., Hu, Z., Xia, Z., Zhao, D., Li, W., & Tyler, J. K. (2016). The Overlooked Fact: Fundamental Need for Spike-In Control for Virtually All Genome-Wide Analyses. *Molecular and Cellular Biology*, *36*(5), 662–667. https://doi.org/10.1128/mcb.00970-14

Chen, P. B., Chen, H. V., Acharya, D., Rando, O. J., & Fazzio, T. G. (2015). R loops regulate promoter-proximal chromatin architecture and cellular differentiation. *Nature Structural and Molecular Biology*, *22*(12), 999–1007. https://doi.org/10.1038/nsmb.3122

Chen, S. H., Chan, N. L., & Hsieh, T. S. (2013). New mechanistic and functional insights into DNA topoisomerases. *Annual Review of Biochemistry*, *82*, 139–170. https://doi.org/10.1146/annurev-biochem-061809-100002

Cinelli, M. A. (2019). Topoisomerase 1B poisons: Over a half-century of drug leads, clinical candidates, and serendipitous discoveries. *Medicinal Research Reviews*, *39*(4), 1294–1337. https://doi.org/10.1002/med.21546

Cliby, W. A., Lewis, K. A., Lilly, K. K., & Kaufmann, S. H. (2002). S phase and G2 arrests induced by topoisomerase I poisons are dependent on ATR kinase function. *Journal of Biological Chemistry*, *277*(2), 1599–1606. https://doi.org/10.1074/jbc.M106287200

Cohen, S., Puget, N., Lin, Y. L., Clouaire, T., Aguirrebengoa, M., Rocher, V., Pasero, P., Canitrot, Y., & Legube, G. (2018). Senataxin resolves RNA:DNA hybrids forming at DNA double-strand breaks to prevent translocations. *Nature Communications*, *9*(1). https://doi.org/10.1038/s41467-018-02894-w

Covey, J. M., Jaxel, C., Kohn, K. W., & Pommier, Y. (1989). Protein-linked DNA Strand Breaks Induced in Mammalian Cells by Camptothecin, an Inhibitor of Topoisomerase I. *Cancer Research*, *49*(18), 5016–5022.

Cristini, A., Ricci, G., Britton, S., Salimbeni, S., Huang, S. yin N., Marinello, J., Calsou, P., Pommier, Y., Favre, G., Capranico, G., Gromak, N., & Sordet, O. (2019). Dual Processing of R-Loops and Topoisomerase I Induces Transcription-Dependent DNA

Double-Strand Breaks. *Cell Reports*, *28*(12), 3167-3181.e6. https://doi.org/10.1016/j.celrep.2019.08.041

Crossley, Madzia P., Bocek, M., & Cimprich, K. A. (2019). R-Loops as Cellular Regulators and Genomic Threats. *Molecular Cell*, *73*(3), 398–411. https://doi.org/10.1016/j.molcel.2019.01.024

Crossley, Magdalena P., Bocek, M. J., Hamperl, S., Swigut, T., & Cimprich, K. A. (2020). QDRIP: A method to quantitatively assess RNA-DNA hybrid formation genome-wide. *Nucleic Acids Research*, *48*(14). https://doi.org/10.1093/nar/gkaa500

D'Alessandro, G., Whelan, D. R., Howard, S. M., Vitelli, V., Renaudin, X., Adamowicz, M., Iannelli, F., Jones-Weinert, C. W., Lee, M. Y., Matti, V., Lee, W. T. C., Morten, M. J., Venkitaraman, A. R., Cejka, P., Rothenberg, E., & d'Adda di Fagagna, F. (2018). BRCA2 controls DNA:RNA hybrid level at DSBs by mediating RNase H2 recruitment. *Nature Communications*, *9*(1). https://doi.org/10.1038/s41467-018-07799-2

D'Annessa, I., Coletta, A., Sutthibutpong, T., Mitchell, J., Chillemi, G., Harris, S., & Desideri, A. (2014). Simulations of DNA topoisomerase 1B bound to supercoiled DNA reveal changes in the flexibility pattern of the enzyme and a secondary protein-DNA binding site. *Nucleic Acids Research*, *42*(14), 9304–9312. https://doi.org/10.1093/nar/gku654

Darnell, E. (2016). *5 , 6-Dichloro-1-β-D-ribofuranosylbenzimidazole Inhibits Initiation of Nuclear Heterogeneous RNA Chains in HeLa Cells Author (s): Pravinkumar B . Sehgal , Eva Derman , George R . Molloy , Igor Tamm and James Published by : American Association for the A*. *194*(4263), 431–433.

De Magis, A., Manzo, S. G., Russo, M., Marinello, J., Morigi, R., Sordet, O., & Capranico, G. (2019). DNA damage and genome instability by G-quadruplex ligands are mediated by R loops in human cancer cells. *Proceedings of the National Academy of Sciences of the United States of America*, *116*(3), 816–825. https://doi.org/10.1073/pnas.1810409116

Desai, S. D., Li, T. K., Rodriguez-Bauman, A., Liu, L. F., & Rubin, E. H. (2001). Ubiquitin/26s proteasome-mediated degradation of topoisomerase I as a resistance mechanism to camptothecin in tumor cells. *Cancer Research*, *61*(15), 5926–5932.

Dhanwani, R., Takahashi, M., & Sharma, S. (2018). Cytosolic sensing of immuno-

stimulatory DNA, the enemy within. *Current Opinion in Immunology*, *50*, 82–87. https://doi.org/10.1016/j.coi.2017.11.004

Di Felice, F., & Camilloni, G. (2021). Why should dna topoisomerase i have a scaffold activity? *Biology*, *10*(3), 1–7. https://doi.org/10.3390/biology10030190

Domínguez-Sánchez, M. S., Barroso, S., Gómez-González, B., Luna, R., & Aguilera, A. (2011). Genome instability and transcription elongation impairment in human cells depleted of THO/TREX. *PLoS Genetics*, *7*(12), 19–22. https://doi.org/10.1371/journal.pgen.1002386

Drake, C. G. (2012). Combination immunotherapy approaches. *Annals of Oncology*, *23*(SUPPL.8). https://doi.org/10.1093/annonc/mds262

Durand-Dubief, M., Persson, J., Norman, U., Hartsuiker, E., & Ekwall, K. (2010). Topoisomerase I regulates open chromatin and controls gene expression in vivo. *EMBO Journal*, *29*(13), 2126–2134. https://doi.org/10.1038/emboj.2010.109

Eisenreich, A., Bogdanov, V. Y., Zakrzewicz, A., Pries, A., Antoniak, S., Poller, W., Schultheiss, H. P., & Rauch, U. (2009). Cdc2-like kinases and DNA topoisomerase I regulate alternative splicing of tissue factor in human endothelial cells. *Circulation Research*, *104*(5), 589–599. https://doi.org/10.1161/CIRCRESAHA.108.183905

El Hage, A., French, S. L., Beyer, A. L., & Tollervey, D. (2010). Loss of Topoisomerase I leads to R-loop-mediated transcriptional blocks during ribosomal RNA synthesis. *Genes and Development*, *24*(14), 1546–1558. https://doi.org/10.1101/gad.573310

Emens, L. A., & Middleton, G. (2015). The interplay of immunotherapy and chemotherapy: Harnessing potential synergies. *Cancer Immunology Research*, *3*(5), 436–443. https://doi.org/10.1158/2326-6066.CIR-15-0064

Fenech, M. (2020). Cytokinesis-block micronucleus cytome assay evolution into a more comprehensive method to measure chromosomal instability. *Genes*, *11*(10), 1–13. https://doi.org/10.3390/genes11101203

Fenech, M., Knasmueller, S., Bolognesi, C., Bonassi, S., Holland, N., Migliore, L., Palitti, F., Natarajan, A. T., & Kirsch-Volders, M. (2016). Molecular mechanisms by which in vivo exposure to exogenous chemical genotoxic agents can lead to micronucleus formation in lymphocytes in vivo and ex vivo in humans. *Mutation Research - Reviews in Mutation Research*, *770*, 12–25. https://doi.org/10.1016/j.mrrev.2016.04.008

Fragkos, M., & Naim, V. (2017). Rescue from replication stress during mitosis. *Cell Cycle*, *16*(7), 613–633. https://doi.org/10.1080/15384101.2017.1288322

Fraser, N. W., Sehgal, P. B., & Darnell, J. E. (1978). DRB-induced premature termination of late adenovirus transcription. *Nature*, *272*(5654), 590–593. https://doi.org/10.1038/272590a0

Furuta, T., Takemura, H., Liao, Z. Y., Aune, G. J., Redon, C., Sedelnikova, O. A., Pilch, D. R., Rogakou, E. P., Celeste, A., Chen, H. T., Nussenzweig, A., Aladjem, M. I., Bonner, W. M., & Pommier, Y. (2003). Phosphorylation of histone H2AX and activation of Mre11, Rad50, and Nbs1 in response to replication-dependent DNA double-strand breaks induced by mammalian DNA topoisomerase I cleavage complexes. *Journal of Biological Chemistry*, *278*(22), 20303–20312. https://doi.org/10.1074/jbc.M300198200

Galluzzi, L., Buqué, A., Kepp, O., Zitvogel, L., & Kroemer, G. (2015). Immunological Effects of Conventional Chemotherapy and Targeted Anticancer Agents. In *Cancer Cell* (Vol. 28, Issue 6, pp. 690–714). https://doi.org/10.1016/j.ccell.2015.10.012

Galluzzi, L., Humeau, J., Buqué, A., Zitvogel, L., & Kroemer, G. (2020). Immunostimulation with chemotherapy in the era of immune checkpoint inhibitors. *Nature Reviews Clinical Oncology*, *17*(12), 725–741. https://doi.org/10.1038/s41571-020-0413-z

García-Rubio, M., Barroso, S. I., & Aguilera, A. (2018). Detection of DNA-RNA Hybrids In Vivo. In M. Muzi-Falconi & G. W. Brown (Eds.), *Genome Instability: Methods and Protocols* (pp. 347–361). Springer New York. https://doi.org/10.1007/978-1-4939-7306-4_24

Grunseich, C., Wang, I. X., Watts, J. A., Burdick, J. T., Guber, R. D., Zhu, Z., Bruzel, A., Lanman, T., Chen, K., Schindler, A. B., Edwards, N., Ray-Chaudhury, A., Yao, J., Lehky, T., Piszczek, G., Crain, B., Fischbeck, K. H., & Cheung, V. G. (2018). Senataxin Mutation Reveals How R-Loops Promote Transcription by Blocking DNA Methylation at Gene Promoters. *Molecular Cell*, *69*(3), 426-437.e7. https://doi.org/10.1016/j.molcel.2017.12.030

Haaf, T., Raderschall, E., Reddy, G., Ward, D. C., Radding, C. M., & Golub, E. I. (1999). Sequestration of mammalian Rad51-recombination protein into micronuclei. *Journal*

of Cell Biology, *144*(1), 11–20. https://doi.org/10.1083/jcb.144.1.11

Haggerty, T. J., Dunn, I. S., Rose, L. B., Newton, E. E., Martin, S., Riley, J. L., & Kurnick, J. T. (2011). Topoisomerase inhibitors modulate expression of melanocytic antigens and enhance T cell recognition of tumor cells. *Cancer Immunology, Immunotherapy*, *60*(1), 133–144. https://doi.org/10.1007/s00262-010-0926-x

Hamperl, S., & Cimprich, K. A. (2014). The contribution of co-transcriptional RNA: DNA hybrid structures to DNA damage and genome instability. *DNA Repair*, *19*, 84–94. https://doi.org/10.1016/j.dnarep.2014.03.023

Hannesdóttir, L., Tymoszuk, P., Parajuli, N., Wasmer, M. H., Philipp, S., Daschil, N., Datta, S., Koller, J. B., Tripp, C. H., Stoitzner, P., Müller-Holzner, E., Wiegers, G. J., Sexl, V., Villunger, A., & Doppler, W. (2013). Lapatinib and doxorubicin enhance the Stat1-dependent antitumor immune response. *European Journal of Immunology*, *43*(10), 2718–2729. https://doi.org/10.1002/eji.201242505

Harding, S. M., Benci, J. L., Irianto, J., Discher, D. E., Minn, A. J., & Greenberg, R. A. (2017). Mitotic progression following DNA damage enables pattern recognition within micronuclei. *Nature*, *548*(7668), 466–470. https://doi.org/10.1038/nature23470

Hatch, E. M., Fischer, A. H., Deerinck, T. J., & Hetzer, M. W. (2013). Catastrophic Nuclear Envelope Collapse in Cancer Cell Micronuclei. *Cell*, *154*(1), 47. https://doi.org/10.1016/j.cell.2013.06.007

Heddle, J. A., & Carrano, A. V. (1977). The DNA content of micronuclei induced in mouse bone marrow by γ-irradiation: evidence that micronuclei arise from acentric chromosomal fragments. *Mutation Research - Fundamental and Molecular Mechanisms of Mutagenesis*, *44*(1), 63–69. https://doi.org/10.1016/0027-5107(77)90115-4

Hegazy, Y. A., Fernando, C. M., & Tran, E. J. (2020). The balancing act of R-loop biology: The good, the bad, and the ugly. *Journal of Biological Chemistry*, *295*(4), 905–913. https://doi.org/10.1074/jbc.REV119.011353

Hodroj, D., Recolin, B., Serhal, K., Martinez, S., Tsanov, N., Abou Merhi, R., & Maiorano, D. (2017). An ATR -dependent function for the Ddx19 RNA helicase in nuclear R-loop metabolism . *The EMBO Journal*, *36*(9), 1182–1198. https://doi.org/10.15252/embj.201695131

Holm, C., Covey, J. M., Kerrigan, D., & Pommier, Y. (1989). Differential Requirement of DNA Replication for the Cytotoxicity of DNA Topoisomerase I and II Inhibitors in Chinese Hamster DC3F Cells. *Cancer Research*, *49*(22), 6365–6368.

Holmström, M., & Winters, V. (1992). Micronucleus induction by camptothecin and amsacrine in bone marrow of male and female CD-1 mice. *Mutagenesis*, *7*(3), 189–193. https://doi.org/10.1093/mutage/7.3.189

Hsiang, Y. H., Lihou, M. G., & Liu, L. F. (1989). Arrest of Replication Forks by Drug-stabilized Topoisomerase I-DNA Cleavable Complexes as a Mechanism of Cell Killing by Camptothecin. *Cancer Research*, *49*(18), 5077–5082.

Hu, Z., Chen, K., Xia, Z., Chavez, M., Pal, S., Seol, J. H., Chen, C. C., Li, W., & Tyler, J. K. (2014). Nucleosome loss leads to global transcriptional up-regulation and genomic instability during yeast aging. *Genes and Development*, *28*(4), 396–408. https://doi.org/10.1101/gad.233221.113

Iyama, T., & Wilson, D. M. (2013). DNA repair mechanisms in dividing and non-dividing cells. *DNA Repair*, *12*(8), 620–636. https://doi.org/10.1016/j.dnarep.2013.04.015

Jeong, S. (2017). SR proteins: Binders, regulators, and connectors of RNA. *Molecules and Cells*, *40*(1), 1–9. https://doi.org/10.14348/molcells.2017.2319

Khobta, A., Ferri, F., Lotito, L., Montecucco, A., Rossi, R., & Capranico, G. (2006). Early effects of topoisomerase I inhibition on RNA polymerase II along transcribed genes in human cells. *Journal of Molecular Biology*, *357*(1), 127–138. https://doi.org/10.1016/j.jmb.2005.12.069

Kinders, R. J., Hollingshead, M., Lawrence, S., Ji, J., Tabb, B., Bonner, W. M., Pommier, Y., Rubinstein, L., Evrard, Y. A., & Ralph, E. (2011). *NIH Public Access*. *16*(22), 5447–5457. https://doi.org/10.1158/1078-0432.CCR-09-3076.Development

Kitai, Y., Kawasaki, T., Sueyoshi, T., Kobiyama, K., Ishii, K. J., Zou, J., Akira, S., Matsuda, T., & Kawai, T. (2017). DNA-Containing Exosomes Derived from Cancer Cells Treated with Topotecan Activate a STING-Dependent Pathway and Reinforce Antitumor Immunity. *The Journal of Immunology*, *198*(4), 1649–1659. https://doi.org/10.4049/jimmunol.1601694

Kogoma, T. (1997). Stable DNA replication: interplay between DNA replication, homologous recombination, and transcription. *Microbiology and Molecular Biology*

Reviews, *61*(2), 212–238. https://doi.org/10.1128/mmbr.61.2.212-238.1997

Koster, D. A., Palle, K., Bot, E. S. M., Bjornsti, M. A., & Dekker, N. H. (2007). Antitumour drugs impede DNA uncoiling by topoisomerase I. *Nature*, *448*(7150), 213–217. https://doi.org/10.1038/nature05938

Kouzine, F., Gupta, A., Baranello, L., Wojtowicz, D., Ben-Aissa, K., Liu, J., Przytycka, T. M., & Levens, D. (2013). Transcription-dependent dynamic supercoiling is a short-range genomic force. *Nature Structural and Molecular Biology*, *20*(3), 396–403. https://doi.org/10.1038/nsmb.2517

Kummar, S., Chen, A., Gutierrez, M., Pfister, T. D., Wang, L., Redon, C., Bonner, W. M., Yutzy, W., Zhang, Y., Kinders, R. J., Ji, J., Allen, D., Covey, J. M., Eiseman, J. L., Holleran, J. L., Beumer, J. H., Rubinstein, L., Collins, J., Tomaszewski, J., … Doroshow, J. H. (2016). Clinical and pharmacologic evaluation of two dosing schedules of indotecan (LMP400), a novel indenoisoquinoline, in patients with advanced solid tumors. *Cancer Chemotherapy and Pharmacology*, *78*(1), 73–81. https://doi.org/10.1007/s00280-016-2998-6

Kuo, L. J., & Yang, L. X. (2008). γ-H2AX- A novel biomaker for DNA double-strand breaks. *In Vivo*, *22*(3), 305–310.

Lan, Y. Y., Londoño, D., Bouley, R., Rooney, M. S., & Hacohen, N. (2014). Dnase2a deficiency uncovers lysosomal clearance of damaged nuclear DNA via autophagy. *Cell Reports*, *9*(1), 180–192. https://doi.org/10.1016/j.celrep.2014.08.074

Landt, S. G., Marinov, G. K., Kundaje, A., Kheradpour, P., Pauli, F., Batzoglou, S., Bernstein, B. E., Bickel, P., Brown, J. B., Cayting, P., Chen, Y., DeSalvo, G., Epstein, C., Fisher-Aylor, K. I., Euskirchen, G., Gerstein, M., Gertz, J., Hartemink, A. J., Hoffman, M. M., … Snyder, M. (2012). ChIP-seq guidelines and practices of the ENCODE and modENCODE consortia. *Genome Research*, *22*(9), 1813–1831. https://doi.org/10.1101/gr.136184.111

Lang, K. S., Hall, A. N., Merrikh, C. N., Ragheb, M., Tabakh, H., Pollock, A. J., Woodward, J. J., Dreifus, J. E., & Merrikh, H. (2017). Replication-Transcription Conflicts Generate R-Loops that Orchestrate Bacterial Stress Survival and Pathogenesis. *Cell*, *170*(4), 787-799.e18. https://doi.org/10.1016/j.cell.2017.07.044

Li, H., & Durbin, R. (2009). Fast and accurate short read alignment with Burrows-Wheeler

transform. *Bioinformatics*, *25*(14), 1754–1760. https://doi.org/10.1093/bioinformatics/btp324

Li, H., Handsaker, B., Wysoker, A., Fennell, T., Ruan, J., Homer, N., Marth, G., Abecasis, G., & Durbin, R. (2009). The Sequence Alignment/Map format and SAMtools. *Bioinformatics*, *25*(16), 2078–2079. https://doi.org/10.1093/bioinformatics/btp352

Lin, C. P., Ban, Y., Lyu, Y. L., Desai, S. D., & Liu, L. F. (2008). A ubiquitin-proteasome pathway for the repair of topoisomerase I-DNA covalent complexes. *Journal of Biological Chemistry*, *283*(30), 21074–21083. https://doi.org/10.1074/jbc.M803493200

Liu, L. F., D'Arpa, P., & Liu, L. F. (1992). The Involvement of Active DNA Synthesis in Camptothecin-induced G2 Arrest: Altered Regulation of p34cdc2/Cyclin B. *Cancer Research*, *52*(7), 1823–1829.

Liu, L. F., & Wang, J. C. (1987). Supercoiling of. *Proceedings of the National Academy of Sciences of the United States of America*, *84*(October), 7024–7027.

Liu, Q., Luo, X., Yi, L., Zeng, X., & Tan, C. (2021). First-Line Chemo-Immunotherapy for Extensive-Stage Small-Cell Lung Cancer: A United States-Based Cost-Effectiveness Analysis. *Frontiers in Oncology*, *11*(June), 1–8. https://doi.org/10.3389/fonc.2021.699781

Ljungman, M., & Hanawalt, P. C. (1996). The anti-cancer drug camptothecin inhibits elongation but stimulates initiation of RNA polymerase II transcription. *Carcinogenesis*, *17*(1), 31–35. https://doi.org/10.1093/carcin/17.1.31

Lovén, J., Orlando, D. A., Sigova, A. A., Lin, C. Y., Rahl, P. B., Burge, C. B., Levens, D. L., Lee, T. I., & Young, R. A. (2012). Revisiting global gene expression analysis. *Cell*, *151*(3), 476–482. https://doi.org/10.1016/j.cell.2012.10.012

MacDonald, K. M., Benguerfi, S., & Harding, S. M. (2020). Alerting the immune system to DNA damage: Micronuclei as mediators. *Essays in Biochemistry*, *64*(5), 753–764. https://doi.org/10.1042/EBC20200016

MacKenzie, K. J., Carroll, P., Martin, C. A., Murina, O., Fluteau, A., Simpson, D. J., Olova, N., Sutcliffe, H., Rainger, J. K., Leitch, A., Osborn, R. T., Wheeler, A. P., Nowotny, M., Gilbert, N., Chandra, T., Reijns, M. A. M., & Jackson, A. P. (2017). CGAS surveillance of micronuclei links genome instability to innate immunity. *Nature*,

548(7668), 461–465. https://doi.org/10.1038/nature23449

Madden, K. R., & Champoux, J. J. (1992). Overexpression of Human Topoisomerase I in Baby Hamster Kidney Cells: Hypersensitivity of Clonal Isolates to Camptothecin. *Cancer Research*, *52*(3), 525–532.

Malig, M., Hartono, S. R., Giafaglione, J. M., Sanz, L. A., & Chedin, F. (2020). Ultra-deep Coverage Single-molecule R-loop Footprinting Reveals Principles of R-loop Formation. *Journal of Molecular Biology*, *432*(7), 2271–2288. https://doi.org/10.1016/j.jmb.2020.02.014

Mancebo, H. S. Y., Lee, G., Flygare, J., Tomassini, J., Luu, P., Zhu, Y., Peng, J., Blau, C., Hazuda, D., Price, D., & Flores, O. (1997). P-TEFb kinase is required for HIV Tat transcriptional activation in vivo and in vitro. *Genes and Development*, *11*(20), 2633–2644. https://doi.org/10.1101/gad.11.20.2633

Mankan, A. K., Schmidt, T., Chauhan, D., Goldeck, M., Höning, K., Gaidt, M., Kubarenko, A. V, Andreeva, L., Hopfner, K., & Hornung, V. (2014). Cytosolic RNA:DNA hybrids activate the cGAS –STING axis . *The EMBO Journal*, *33*(24), 2937–2946. https://doi.org/10.15252/embj.201488726

Manzo, S. G., Hartono, S. R., Sanz, L. A., De Biasi, S., Cossarizza, A., Capranico, G., & Chedin, F. (2018). DNA Topoisomerase I differentially modulates R-loops across the human genome. *DNA Topoisomerase I Differentially Modulates R-Loops across the Human Genome*, 257303. https://doi.org/10.1101/257303

Marinello, J., Arleo, A., Russo, M., Delcuratolo, M., Ciccarelli, F., Pommier, Y., & Capranico, G. (2022). Topoisomerase I poison-triggered immune gene activation is markedly impaired in human small-cell lung cancers by reduced STING/cGAS gene expression. *British Journal of Cancer*. (under review)

Marinello, J., Bertoncini, S., Aloisi, I., Cristini, A., Tagliazucchi, G. M., Forcato, M., Sordet, O., & Capranico, G. (2016). Dynamic effects of topoisomerase i inhibition on R-loops and short transcripts at active promoters. *PLoS ONE*, *11*(1), 1–18. https://doi.org/10.1371/journal.pone.0147053

Marinello, J., Chillemi, G., Bueno, S., Manzo, S. G., & Capranico, G. (2013). Antisense transcripts enhanced by camptothecin at divergent CpG-island promoters associated with bursts of topoisomerase I-DNA cleavage complex and R-loop formation. *Nucleic*

Acids Research, *41*(22), 10110–10123. https://doi.org/10.1093/nar/gkt778

Martin, M. (2011). Cutadapt removes adapter sequences from high-throughput sequencing reads. *EMBnet.Journal*, *17*(1), 10. https://doi.org/10.14806/ej.17.1.200

Martin, M. M., Ryan, M., Kim, R. G., Zakas, A. L., Fu, H., Lin, C. M., Reinhold, W. C., Davis, S. R., Bilke, S., Liu, H., Doroshow, J. H., Reimers, M. A., Valenzuela, M. S., Pommier, Y., Meltzer, P. S., & Aladjem, M. I. (2011). Genome-wide depletion of replication initiation events in highly transcribed regions. *Genome Research*, *21*(11), 1822–1832. https://doi.org/10.1101/gr.124644.111

Mazina, O. M., Somarowthu, S., Kadyrova, L. Y., Baranovskiy, A. G., Tahirov, T. H., Kadyrov, F. A., & Mazin, A. V. (2020). Replication protein A binds RNA and promotes R-loop formation. *Journal of Biological Chemistry*, *295*(41), 14203–14213. https://doi.org/10.1074/jbc.RA120.013812

Mei, C., Lei, L., Tan, L. M., Xu, X. J., He, B. M., Luo, C., Yin, J. Y., Li, X., Zhang, W., Zhou, H. H., & Liu, Z. Q. (2020). The role of single strand break repair pathways in cellular responses to camptothecin induced DNA damage. *Biomedicine and Pharmacotherapy*, *125*(December 2019). https://doi.org/10.1016/j.biopha.2020.109875

Merino, A., Madden, K. R., Lane, W. S., Champoux, J. J., & Reinberg, D. (1993). DNA topoisomerase I is involved in both repression and activation of transcription. *Nature*, *365*(6443), 227–232. https://doi.org/10.1038/365227a0

Miglietta, G., Russo, M., & Capranico, G. (2020). G-quadruplex-R-loop interactions and the mechanism of anticancer G-quadruplex binders. *Nucleic Acids Research*, *48*(21), 11942–11957. https://doi.org/10.1093/nar/gkaa944

Miglietta, G., Russo, M., Duardo, R. C., & Capranico, G. (2021). G-quadruplex binders as cytostatic modulators of innate immune genes in cancer cells. *Nucleic Acids Research*, *49*(12), 6673–6686. https://doi.org/10.1093/nar/gkab500

Minocherhomji, S., Ying, S., Bjerregaard, V. A., Bursomanno, S., Aleliunaite, A., Wu, W., Mankouri, H. W., Shen, H., Liu, Y., & Hickson, I. D. (2015). Replication stress activates DNA repair synthesis in mitosis. *Nature*, *528*(7581), 286–290. https://doi.org/10.1038/nature16139

Mo, Y. Y., Wang, C., & Beck, W. T. (2000). A novel nuclear localization signal in human

DNA topoisomerase I. *Journal of Biological Chemistry*, *275*(52), 41107–41113. https://doi.org/10.1074/jbc.M003135200

Morris, E. J. (1996). Topoisomerase-I : Evidence for Cell Cycle-independent Toxicity. *Cell*, *134*(3), 757–770.

Nyamuswa, G., & Silber, R. (1993). Interaction between Replication Forks and Topoisomerase I-DNA Cleavable Complexes: Studies in a Cell-free SV40DNA Replication System. *Cancer Research*, *53*(24), 5908–5914.

Ohle, C., Tesorero, R., Schermann, G., Dobrev, N., Sinning, I., & Fischer, T. (2016). Transient RNA-DNA Hybrids Are Required for Efficient Double-Strand Break Repair. *Cell*, *167*(4), 1001-1013.e7. https://doi.org/10.1016/j.cell.2016.10.001

Okamoto, Y., Hejna, J., & Takata, M. (2019). Regulation of R-loops and genome instability in Fanconi anemia. *Journal of Biochemistry*, *165*(6), 465–470. https://doi.org/10.1093/jb/mvz019

Oobatake, Y., & Shimizu, N. (2020). Double-strand breakage in the extrachromosomal double minutes triggers their aggregation in the nucleus, micronucleation, and morphological transformation. *Genes Chromosomes and Cancer*, *59*(3), 133–143. https://doi.org/10.1002/gcc.22810

Opzoomer, J. W., Sosnowska, D., Anstee, J. E., Spicer, J. F., & Arnold, J. N. (2019). Cytotoxic chemotherapy as an immune stimulus: A molecular perspective on turning up the immunological heat on cancer. *Frontiers in Immunology*, *10*(JULY), 1–9. https://doi.org/10.3389/fimmu.2019.01654

Park, Y. H., Lal, S., Lee, J. E., Choi, Y. La, Wen, J., Ram, S., Ding, Y., Lee, S. H., Powell, E., Lee, S. K., Yu, J. H., Ching, K. A., Nam, J. Y., Kim, S. W., Nam, S. J., Kim, J. Y., Cho, S. Y., Park, S., Kim, J., … Kan, Z. (2020). Chemotherapy induces dynamic immune responses in breast cancers that impact treatment outcome. *Nature Communications*, *11*(1), 1–14. https://doi.org/10.1038/s41467-020-19933-0

Patel, D. S., Misenko, S. M., Her, J., & Bunting, S. F. (2017). BLM helicase regulates DNA repair by counteracting RAD51 loading at DNA double-strand break sites. *Journal of Cell Biology*, *216*(11), 3521–3534. https://doi.org/10.1083/jcb.201703144

Phillips, D. D., Garboczi, D. N., Singh, K., Hu, Z., Leppla, S. H., & Leysath, C. E. (2013). The sub-nanomolar binding of DNA-RNA hybrids by the single-chain Fv fragment of

antibody S9.6. *Journal of Molecular Recognition*, *26*(8), 376–381. https://doi.org/10.1002/jmr.2284

Pommier, Y. (2006). Topoisomerase I inhibitors: Camptothecins and beyond. *Nature Reviews Cancer*, *6*(10), 789–802. https://doi.org/10.1038/nrc1977

Pommier, Y. (2013). *Drugging Topoisomerases: Lessons and Challenges*.

Pommier, Y., Barcelo, J. M., Rao, V. A., Sordet, O., Jobson, A. G., Thibaut, L., Miao, Z. H., Seiler, J. A., Zhang, H., Marchand, C., Agama, K., Nitiss, J. L., & Redon, C. (2006). Repair of Topoisomerase I-Mediated DNA Damage. *Progress in Nucleic Acid Research and Molecular Biology*, *81*(06), 179–229. https://doi.org/10.1016/S0079-6603(06)81005-6

Pommier, Y., Kiselev, E., & Marchand, C. (2015). Interfacial inhibitors. *Bioorganic and Medicinal Chemistry Letters*, *25*(18), 3961–3965. https://doi.org/10.1016/j.bmcl.2015.07.032

Pommier, Y., Sun, Y., Huang, S. Y. N., & Nitiss, J. L. (2016). Roles of eukaryotic topoisomerases in transcription, replication and genomic stability. *Nature Reviews Molecular Cell Biology*, *17*(11), 703–721. https://doi.org/10.1038/nrm.2016.111

Powell, W. T., Coulson, R. L., Gonzales, M. L., Crary, F. K., Wong, S. S., Adams, S., Ach, R. A., Tsang, P., Yamada, N. A., Yasui, D. H., Chédin, F., & LaSalle, J. M. (2013). R-loop formation at Snord116 mediates topotecan inhibition of Ube3a-antisense and allele-specific chromatin decondensation. *Proceedings of the National Academy of Sciences of the United States of America*, *110*(34), 13938–13943. https://doi.org/10.1073/pnas.1305426110

Quinet, A., Lemaçon, D., & Vindigni, A. (2017). Replication Fork Reversal: Players and Guardians. *Molecular Cell*, *68*(5), 830–833. https://doi.org/10.1016/j.molcel.2017.11.022

Quinlan, A. R., & Hall, I. M. (2010). BEDTools: A flexible suite of utilities for comparing genomic features. *Bioinformatics*, *26*(6), 841–842. https://doi.org/10.1093/bioinformatics/btq033

Ramírez, F., Ryan, D. P., Grüning, B., Bhardwaj, V., Kilpert, F., Richter, A. S., Heyne, S., Dündar, F., & Manke, T. (2016). deepTools2: a next generation web server for deep-sequencing data analysis. *Nucleic Acids Research*, *44*(W1), W160–W165.

https://doi.org/10.1093/nar/gkw257

Rao, V. A., Fan, A. M., Meng, L., Doe, C. F., North, P. S., Hickson, I. D., & Pommier, Y. (2005). Phosphorylation of BLM, Dissociation from Topoisomerase IIIα, and Colocalization with γ-H2AX after Topoisomerase I-Induced Replication Damage. *Molecular and Cellular Biology*, *25*(20), 8925–8937. https://doi.org/10.1128/mcb.25.20.8925-8937.2005

Ray Chaudhuri, A., Hashimoto, Y., Herrador, R., Neelsen, K. J., Fachinetti, D., Bermejo, R., Cocito, A., Costanzo, V., & Lopes, M. (2012). Topoisomerase i poisoning results in PARP-mediated replication fork reversal. *Nature Structural and Molecular Biology*, *19*(4), 417–423. https://doi.org/10.1038/nsmb.2258

Regairaz, M., Zhang, Y. W., Fu, H., Agama, K. K., Tata, N., Agrawal, S., Aladjem, M. I., & Pommier, Y. (2011). Mus81-mediated DNA cleavage resolves replication forks stalled by topoisomerase I-DNA complexes. *Journal of Cell Biology*, *195*(5), 739–749. https://doi.org/10.1083/jcb.201104003

Ritchie, M. E., Phipson, B., Wu, D., Hu, Y., Law, C. W., Shi, W., & Smyth, G. K. (2015). *limma powers differential expression analyses for RNA-sequencing and microarray studies*. *43*(7). https://doi.org/10.1093/nar/gkv007

Rossi, F., Labourier, E., Gallouzi, I. E., Derancourt, J., Allemand, E., Divita, G., & Tazi, J. (1998). The C-terminal domain but not the tyrosine 723 of human DNA topoisomerase I active site contributes to kinase activity. *Nucleic Acids Research*, *26*(12), 2963–2970. https://doi.org/10.1093/nar/26.12.2963

Russo, M., De Lucca, B., Flati, T., Gioiosa, S., Chillemi, G., & Capranico, G. (2019). DROPA: DRIP-seq optimized peak annotator. *BMC Bioinformatics*, *20*(1), 1–7. https://doi.org/10.1186/s12859-019-3009-9

Salas-Armenteros, I., Pérez-Calero, C., Bayona-Feliu, A., Tumini, E., Luna, R., & Aguilera, A. (2017). Human THO –Sin3A interaction reveals new mechanisms to prevent R-loops that cause genome instability . *The EMBO Journal*, *36*(23), 3532–3547. https://doi.org/10.15252/embj.201797208

Saxena, P., Singh, P. K., Malik, P. S., & Singh, N. (2020). Immunotherapy Alone or in Combination with Chemotherapy as First-Line Treatment of Non-Small Cell Lung Cancer. *Current Treatment Options in Oncology*, *21*(8).

https://doi.org/10.1007/s11864-020-00768-2

Seiler, J. A., Conti, C., Syed, A., Aladjem, M. I., & Pommier, Y. (2007). The Intra-S-Phase Checkpoint Affects both DNA Replication Initiation and Elongation: Single-Cell and - DNA Fiber Analyses. *Molecular and Cellular Biology*, *27*(16), 5806–5818. https://doi.org/10.1128/mcb.02278-06

Seol, Y., Zhang, H., Pommier, Y., & Neuman, K. C. (2012). A kinetic clutch governs religation by type IB topoisomerases and determines camptothecin sensitivity. *Proceedings of the National Academy of Sciences of the United States of America*, *109*(40), 16125–16130. https://doi.org/10.1073/pnas.1206480109

Shao, R. G., Cao, C. X., Zhang, H., Kohn, K. W., Wold, M. S., & Pommier, Y. (1999). Replication-mediated DNA damage by camptothecin induces phosphorylation of RPA by DNA-dependent protein kinase and dissociates RPA:DNA-PK complexes. *EMBO Journal*, *18*(5), 1397–1406. https://doi.org/10.1093/emboj/18.5.1397

Sheridan, R. M., Fong, N., D'Alessandro, A., & Bentley, D. L. (2019). Widespread Backtracking by RNA Pol II Is a Major Effector of Gene Activation, 5′ Pause Release, Termination, and Transcription Elongation Rate. *Molecular Cell*, *73*(1), 107-118.e4. https://doi.org/10.1016/j.molcel.2018.10.031

Shkreta, L., Froehlich, U., Paquet, É. R., Toutant, J., Elela, S. A., & Chabot, B. (2008). Anticancer drugs affect the alternative splicing of Bcl-x and other human apoptotic genes. *Molecular Cancer Therapeutics*, *7*(6), 1398–1409. https://doi.org/10.1158/1535-7163.MCT-08-0192

Shykind, B. M., Kim, J., Stewart, L., Champoux, J. J., & Sharp, P. A. (1997). Topoisomerase I enhances TFIID-TFIIA complex assembly during activation of transcription. *Genes and Development*, *11*(3), 397–407. https://doi.org/10.1101/gad.11.3.397

Skourti-Stathaki, K., Proudfoot, N. J., & Gromak, N. (2011). Human Senataxin Resolves RNA/DNA Hybrids Formed at Transcriptional Pause Sites to Promote Xrn2-Dependent Termination. *Molecular Cell*, *42*(6), 794–805. https://doi.org/10.1016/j.molcel.2011.04.026

Solier, Stéphanie, Barb, J., Zeeberg, B. R., Varma, S., Ryan, M. C., Kohn, W., Weinstein, J. N., Munson, P. J., & Pommier, Y. (2011). *Genes Encoding Splicing Factors*. *70*(20), 8055–8065. https://doi.org/10.1158/0008-5472.CAN-10-2491.Genome-wide

Solier, Stéphanie, Lansiaux, A., Logette, E., Wu, J., Soret, J., Tazi, J., Bailly, C., Desoche, L., Solary, E., & Corcos, L. (2004). Topoisomerase I and II Inhibitors Control Caspase-2 Pre-Messenger RNA Splicing in Human Cells. *Molecular Cancer Research*, *2*(1), 53–61.

Solier, Stephanie, Ryan, M. C., Martin, S. E., Varma, S., Kohn, K. W., Liu, H., Zeeberg, B. R., & Pommier, Y. (2013). Transcription poisoning by topoisomerase i is controlled by gene length, splice sites, and miR-142-3p. *Cancer Research*, *73*(15), 4830–4839. https://doi.org/10.1158/0008-5472.CAN-12-3504

Sollier, J., & Cimprich, K. A. (2015). Breaking bad: R-loops and genome integrity. *Trends in Cell Biology*, *25*(9), 514–522. https://doi.org/10.1016/j.tcb.2015.05.003

Soniat, M. M., Myler, L. R., Kuo, H. C., Paull, T. T., & Finkelstein, I. J. (2019). RPA Phosphorylation Inhibits DNA Resection. *Molecular Cell*, *75*(1), 145-153.e5. https://doi.org/10.1016/j.molcel.2019.05.005

Soret, J., Gabut, M., Dupon, C., Kohlhagen, G., Stévenin, J., Pommier, Y., & Tazi, J. (2003). Altered Serine/Arginine-Rich Protein Phosphorylation and Exonic Enhancer-Dependent Splicing in Mammalian Cells Lacking Topoisomerase I. *Cancer Research*, *63*(23), 8203–8211.

Srivastava, M., Chen, Z., Zhang, H., Tang, M., Wang, C., Jung, S. Y., & Chen, J. (2018). Replisome Dynamics and Their Functional Relevance upon DNA Damage through the PCNA Interactome. *Cell Reports*, *25*(13), 3869-3883.e4. https://doi.org/10.1016/j.celrep.2018.11.099

Staker, B. L., Hjerrild, K., Feese, M. D., Behnke, C. A., Burgin, A. B., & Stewart, L. (2002). The mechanism of topoisomerase I poisoning by a camptothecin analog. *Proceedings of the National Academy of Sciences of the United States of America*, *99*(24), 15387–15392. https://doi.org/10.1073/pnas.242259599

Strumberg, D., Pilon, A. A., Smith, M., Hickey, R., Malkas, L., & Pommier, Y. (2000). Conversion of Topoisomerase I Cleavage Complexes on the Leading Strand of Ribosomal DNA into 5′-Phosphorylated DNA Double-Strand Breaks by Replication Runoff. *Molecular and Cellular Biology*, *20*(11), 3977–3987. https://doi.org/10.1128/mcb.20.11.3977-3987.2000

Stuckey, R., García-Rodríguez, N., Aguilera, A., & Wellinger, R. E. (2015). Role for

RNA:DNA hybrids in origin-independent replication priming in a eukaryotic system. *Proceedings of the National Academy of Sciences of the United States of America*, *112*(18), 5779–5784. https://doi.org/10.1073/pnas.1501769112

Sung, H., Ferlay, J., Siegel, R. L., Laversanne, M., Soerjomataram, I., Jemal, A., & Bray, F. (2021). Global Cancer Statistics 2020: GLOBOCAN Estimates of Incidence and Mortality Worldwide for 36 Cancers in 185 Countries. *CA: A Cancer Journal for Clinicians*, *71*(3), 209–249. https://doi.org/10.3322/caac.21660

Šviković, S., Crisp, A., Tan-Wong, S. M., Guilliam, T. A., Doherty, A. J., Proudfoot, N. J., Guilbaud, G., & Sale, J. E. (2019). R-loop formation during S phase is restricted by PrimPol-mediated repriming. *The EMBO Journal*, *38*(3), 1–19. https://doi.org/10.15252/embj.201899793

Symington, L. S., & Gautier, J. (2011). Double-strand break end resection and repair pathway choice. *Annual Review of Genetics*, *45*, 247–271. https://doi.org/10.1146/annurev-genet-110410-132435

Tanizawa, A., Fujimori, A., Fujimori, Y., & Pommier, Y. (1994). Comparison of topoisomerase I inhibition, DNA damage, and cytotoxicity of camptothecin derivatives presently in clinical trials. *Journal of the National Cancer Institute*, *86*(11), 836–842. https://doi.org/10.1093/jnci/86.11.836

Teicher, B. A. (2008). Next generation topoisomerase I inhibitors: Rationale and biomarker strategies. *Biochemical Pharmacology*, *75*(6), 1262–1271. https://doi.org/10.1016/j.bcp.2007.10.016

Thangavel, S., Berti, M., Levikova, M., Pinto, C., Gomathinayagam, S., Vujanovic, M., Zellweger, R., Moore, H., Lee, E. H., Hendrickson, E. A., Cejka, P., Stewart, S., Lopes, M., & Vindigni, A. (2015). DNA2 drives processing and restart of reversed replication forks in human cells. *Journal of Cell Biology*, *208*(5), 545–562. https://doi.org/10.1083/jcb.201406100

Tomicic, M. T., & Kaina, B. (2013). Topoisomerase degradation, DSB repair, p53 and IAPs in cancer cell resistance to camptothecin-like topoisomerase I inhibitors. *Biochimica et Biophysica Acta - Reviews on Cancer*, *1835*(1), 11–27. https://doi.org/10.1016/j.bbcan.2012.09.002

Tsao, Y. P., Wu, H. Y., & Liu, L. F. (1989). Transcription-driven supercoiling of DNA:

Direct biochemical evidence from in vitro studies. *Cell*, *56*(1), 111–118. https://doi.org/10.1016/0092-8674(89)90989-6

Tuduri, S., Crabbé, L., Conti, C., Tourrière, H., Holtgreve-Grez, H., Jauch, A., Pantesco, V., De Vos, J., Thomas, A., Theillet, C., Pommier, Y., Tazi, J., Coquelle, A., & Pasero, P. (2009). Topoisomerase I suppresses genomic instability by preventing interference between replication and transcription. *Nature Cell Biology*, *11*(11), 1315–1324. https://doi.org/10.1038/ncb1984

Utani, K. I., Kohno, Y., Okamoto, A., & Shimizu, N. (2010). Emergence of micronuclei and their effects on the fate of cells under replication stress. *PLoS ONE*, *5*(4). https://doi.org/10.1371/journal.pone.0010089

Utani, K. ichi, Okamoto, A., & Shimizu, N. (2011). Generation of micronuclei during interphase by coupling between cytoplasmic membrane blebbing and nuclear budding. *PLoS ONE*, *6*(11). https://doi.org/10.1371/journal.pone.0027233

Van Den Boom, V., Jaspers, N. G. J., & Vermeulen, W. (2002). When machines get stuck - Obstructed RNA polymerase II: Displacement, degradation or suicide. *BioEssays*, *24*(9), 780–784. https://doi.org/10.1002/bies.10150

Vassilev, L. T., Tovar, C., Chen, S., Knezevic, D., Sun, H., Heimbrook, D. C., Chen, L., Chent, S., & Zhao, X. (2009). Selective mitotic inhibitor functions of human reveals critical mitotic functions of human CDK1. *Pro*, *103*(28), 10660–10665.

Velichko, A. K., Petrova, N. V., Luzhin, A. V., Strelkova, O. S., Ovsyannikova, N., Kireev, I. I., Petrova, N. V., Razin, S. V., & Kantidze, O. L. (2019). Hypoosmotic stress induces R loop formation in nucleoli and ATR/ATM-dependent silencing of nucleolar transcription. *Nucleic Acids Research*, *47*(13), 6811–6825. https://doi.org/10.1093/nar/gkz436

Verbist, K. C., Guy, C. S., Milasta, S., Liedmann, S., Kamiński, M. M., Wang, R., & Green, D. R. (2016). Metabolic maintenance of cell asymmetry following division in activated T lymphocytes. *Nature*, *532*(7599), 389–393. https://doi.org/10.1038/nature17442

Wahba, L., Amon, J. D., Koshland, D., & Vuica-Ross, M. (2011). RNase H and Multiple RNA Biogenesis Factors Cooperate to Prevent RNA:DNA Hybrids from Generating Genome Instability. *Molecular Cell*, *44*(6), 978–988. https://doi.org/10.1016/j.molcel.2011.10.017

Wahba, L., Costantino, L., Tan, F. J., Zimmer, A., & Koshland, D. (2016). S1-DRIP-seq identifies high expression and polyA tracts as major contributors to R-loop formation. *Genes and Development*, *30*(11), 1327–1338. https://doi.org/10.1101/gad.280834.116

Wan, S., Pestka, S., Jubin, R. G., Lyu, Y. L., Tsai, Y. C., & Liu, L. F. (2012). Chemotherapeutics and radiation stimulate MHC class i expression through elevated interferon-beta signaling in breast cancer cells. *PLoS ONE*, *7*(3). https://doi.org/10.1371/journal.pone.0032542

Wang, J. C. (2002). Cellular roles of DNA topoisomerases: A molecular perspective. *Nature Reviews Molecular Cell Biology*, *3*(6), 430–440. https://doi.org/10.1038/nrm831

Wilhelm, T., Said, M., & Naim, V. (2020). Dna replication stress and chromosomal instability: Dangerous liaisons. *Genes*, *11*(6), 1–35. https://doi.org/10.3390/genes11060642

Wu, J., & Liu, L. F. (1997). Processing of topoisomerase I cleavable complexes into DNA damage by transcription. *Nucleic Acids Research*, *25*(21), 4181–4186. https://doi.org/10.1093/nar/25.21.4181

Xing, M., Zhang, F., Liao, H., Chen, S., Che, L., Wang, X., Bao, Z., Ji, F., Chen, G., Zhang, H., Li, W., Chen, Z., Liu, Y., Hickson, I. D., Shen, H., & Ying, S. (2020). Replication Stress Induces ATR/CHK1-Dependent Nonrandom Segregation of Damaged Chromosomes. *Molecular Cell*, *78*(4), 714-724.e5. https://doi.org/10.1016/j.molcel.2020.04.005

Xu, Y., & Her, C. (2015). Inhibition of topoisomerase (DNA) I (TOP1): DNA damage repair and anticancer therapy. *Biomolecules*, *5*(3), 1652–1670. https://doi.org/10.3390/biom5031652

Zatreanu, D., Han, Z., Mitter, R., Tumini, E., Williams, H., Gregersen, L., Dirac-Svejstrup, A. B., Roma, S., Stewart, A., Aguilera, A., & Svejstrup, J. Q. (2019). Elongation Factor TFIIS Prevents Transcription Stress and R-Loop Accumulation to Maintain Genome Stability. *Molecular Cell*, *76*(1), 57-69.e9. https://doi.org/10.1016/j.molcel.2019.07.037

Zhang, C. Z., Spektor, A., Cornils, H., Francis, J. M., Jackson, E. K., Liu, S., Meyerson, M., & Pellman, D. (2015). Chromothripsis from DNA damage in micronuclei. *Nature*, *522*(7555), 179–184. https://doi.org/10.1038/nature14493

Zhang, D., Wang, Y., & Zhang, S. (2014). Asymmetric cell division in polyploid giant cancer cells and low eukaryotic cells. *BioMed Research International*, *2014*. https://doi.org/10.1155/2014/432652

Zhang, Y., Liu, T., Meyer, C. A., Eeckhoute, J., Johnson, D. S., Bernstein, B. E., Nusbaum, C., Myers, R. M., Brown, M., Li, W., & Liu, X. S. (2008). *Open Access Model-based Analysis of ChIP-Seq (MACS)*. *9*. https://doi.org/10.1186/gb-2008-9-9-r137

Zhao, H., Zhu, M., Limbo, O., & Russell, P. (2018). RNase H eliminates R-loops that disrupt DNA replication but is nonessential for efficient DSB repair. *EMBO Reports*, *19*(5), 1–10. https://doi.org/10.15252/embr.201745335

Zhou, Y., Gwadry, F. G., Reinhold, W. C., Miller, L. D., Smith, L. H., Scherf, U., Liu, E. T., Kohn, K. W., Pommier, Y., & Weinstein, J. N. (2002). *Damage : Microarray Analysis of Dose- and Time-dependent Effects*. 1688–1695.

Zhu, M., Zhao, H., Limbo, O., & Russell, P. (2018). Mre11 complex links sister chromatids to promote repair of a collapsed replication fork. *Proceedings of the National Academy of Sciences of the United States of America*, *115*(35), 8793–8798. https://doi.org/10.1073/pnas.1808189115

Zhu, S., Zhang, T., Zheng, L., Liu, H., Song, W., Liu, D., Li, Z., & Pan, C. xian. (2021). Combination strategies to maximize the benefits of cancer immunotherapy. *Journal of Hematology and Oncology*, *14*(1), 1–33. https://doi.org/10.1186/s13045-021-01164-5

Zhu, Y., Pe'ery, T., Peng, J., Ramanathan, Y., Marshall, N., Marshall, T., Amendt, B., Mathews, M. B., & Price, D. H. (1997). Transcription elongation factor P-TEFb is required for HIV-1 Tat transactivation in vitro. *Genes and Development*, *11*(20), 2622–2632. https://doi.org/10.1101/gad.11.20.2622

Zimdahl, B., Ito, T., Blevins, A., Bajaj, J., Konuma, T., Weeks, J., Koechlein, C. S., Kwon, H. Y., Arami, O., Rizzieri, D., Broome, H. E., Chuah, C., Oehler, V. G., Sasik, R., Hardiman, G., & Reya, T. (2014). Lis1 regulates asymmetric division in hematopoietic stem cells and in leukemia. *Nature Genetics*, *46*(3), 245–252. https://doi.org/10.1038/ng.2889